学位論文

Effective nucleon-nucleon interaction in atomic nuclei

(原子核における核子間有効相互作用)

平成25年 11月　博士(理学)申請

東京大学大学院理学系研究科
物理学専攻
角田　直文

Effective nucleon-nucleon interaction in atomic nuclei

Naofumi Tsunoda

Department of Physics, University of Tokyo

November 2013

Ph.D Thesis

東京大学
THE UNIVERSITY OF TOKYO

abstract

The nuclear shell model is one of the most powerful tools to explore the various properties of the nuclei in wide region of the nuclear chart. In the shell-model studies of nuclei, effective interactions are widely used inputs. The effective interactions are derived from microscopic theories or based on fitting selected properties of nuclei in specific mass regions.

The commonly used unperturbed basis functions are given by the harmonic oscillator, reflecting the shell structure. Until recently, most shell-model calculations have been confined to a single oscillator shell like the *sd*-shell or the *pf*-shell. However, recent experiments enabled us to obtain the wide knowledge away from the stability line. Those require larger shell-model spaces than only single oscillator shell. On the other hand, the derivation of microscopic effective interactions has been limited to degenerate model spaces because of the divergences appearing in the theory. Therefore, there are both conceptual and practical limits to perform shell-model calculations with the non-degenerate model spaces.

In this work, we present a novel microscopic method to calculate effective nucleon-nucleon (*NN*) interactions for the nuclear shell model. Our method enables us to calculate the interaction defined in non-degenerate model space as well as the degenerate model space. The formalism is presented in the form of many-body perturbation theory based on the recently developed Extended Kuo-Krenciglowa (EKK) method [1, 2]. The application of EKK method to many-body problem can be interpreted as the re-definition of the unperturbed Hamiltonian and the perturbation. We show that this is exactly the re-summation of the perturbation series, avoiding the divergences appearing in the existing theories. There exist several non-trivial points in applying the EKK method to many-body problem, which we explore in detail in the thesis.

We present numerical results using effective interactions within a single oscillator shell like the *sd*-shell and the *pf*-shell, as examples so-called degenerate model space, and two major shells like the $sd f_7 p_3$-shell and the $pf g_9$-shell, as examples so-called non-degenerate model space. We also present energy levels of several nuclei which have two valence nucleons on top of a given closed-shell core. Several properties of the resultant effective interactions are also investigated. We compare the effective interaction with the phenomenological interactions, which is fitted to experimental data. We also investigate the convergence property of our perturbation theory. As a glance at the utility of our effective interactions, we apply them and perform the shell-model calculations for to selected cases where two major-shell degrees of freedom are essential.

As a conclusion, the present method works excellently in shell-model spaces that comprise several

oscillator shells, as well as in a single oscillator shell. We show in particular that the microscopic inter-shell interactions are much more attractive than has been expected by degenerate perturbation theory. We also show that our method provide us a tool to estimate the error according to the approximations. It is also shown that the consequences for shell-model studies using our effective interactions with the model space consist of two-major shell are promising though preliminary.

Table of Contents

Chapter 1

Introduction

The nuclear shell model, a sophisticated theory based on the configuration interaction method, has been one of the central theoretical tools for understanding a wealth of data from the experiments for nuclear structure.

In 1950s, Mayor and Jensen invented the nuclear shell model [3, 4, 5]. They found that the atomic nuclei have the similar shell structure to electrons in atom. The nucleons in nuclei successively fill the orbits one by one, which are the eigenstates of the mean-field potential made by the nucleons themselves. Those potentials were often approximated by harmonic oscillator potential or Woods-Saxon potential. In addition, they introduced the strong spin-orbit force, which is relatively small for atomic nuclei, as follows;

$$H = \frac{p^2}{2m} + \frac{1}{2}\omega x^2 + \alpha\, \mathbf{l} \cdot \mathbf{s}. \tag{1.1}$$

The experimental data at that time provided us the knowledge that the nuclei which have the specific numbers of protons or neutrons show the special stability, and those numbers $2, 8, 20, 28, 50, 82, 126$ are called magic numbers. The naive consideration of harmonic-oscillator potential gives us the magic numbers of $2, 8, 20, 40, 70, \cdots$, but with the inclusion of the strong spin-orbit potential, they explained the magic numbers correctly.

This nuclear shell model reproduced the properties of nuclei especially near the closed shell, with a great success. Since the closed shell nuclei are quite stable and have zero angular momentum and positive parity, the properties of nuclei with one particle or hole in addition to closed shell nuclei can be mainly explained by the motion of single particle or hole in the mean potential. This was called the independent shell model (ISM) and gave a great success in the description of the various property of those nuclei, including spin-parity of the low-lying states, life-time, magnetic moments, and so on. However when there are more than one particle with the closed-shell core, all the states with the same configuration of filling the orbits are all degenerate, which is different from the experimental observations. Therefore, obviously the inclusion of the effect of residual two-body interaction to ISM is necessary as a next step.

For example, in 1960s, Talmi and Unna analyzed the shell-model calculation with two-body interaction [6]. This method is based on the configuration interaction method. The Hamiltonian matrix elements are calculated with all the possible combinations of the configurations, using the sophisti-

cated angular-momentum algebra. Due to the rapid growth in the dimensionality of the Hilbert space with increasing degrees of freedom, we usually have to work within a reduced Hilbert space, the so-called model space. In their work, they regarded the residual two-body interaction as parameters and fitted those parameters to reproduce the experimental data the best. They analyzed the nuclei like $^{40}_{19}\text{K}_{21}$, $^{38}_{17}\text{Cl}_{21}$ as the simple example, where two particles or holes on top of the core interact each other. Their model space was, in this case, $d_{3/2}$ orbit for proton particle or hole, and $f_{7/2}$ orbit for neutron. They also discuss the Calcium isotopes, with the degrees of freedom of the neutrons in the $f_{7/2}$ only and the two-body interactions with free parameters. They succeeded to reproduce the ground state energies of Calcium isotopes in the framework of shell model [6]. In 1964, McCllen and his collaborators covered the wider range of nuclei with $20 \leq N, Z \leq 28$, using the Hamiltonians only consist of $f_{7/2}$ orbits of protons and neutrons. The experimental data of the various nuclei including spin parities and the magnetic moments were reproduced [7].

For the attempts to extend the shell-model studies, the enormous efforts have been made. The effective interaction forms an essential input to all shell-model studies. Therefore, once we know that the shell model framework works, the central problems are how large matrix we can diagonalize, and how we obtain the appropriate effective interactions. These two problems are inseparable, because the effective interactions are designed for given model spaces. The developments of computer science enable us to diagonalize the Hamiltonian matrix of larger model space. Then, the effective interactions appropriate for those model spaces were constructed, correspondingly.

For the latter point, there exist two main approaches to determine effective interactions for the nuclear shell model. One is based on the fitting of the matrix elements to reproduce the observed experimental data, like the works we mentioned above. This approach has been widely used in nuclear structure studies, and has been rather successful in reproducing properties of known nuclei and in predicting properties of nuclei not yet measured experimentally. The other approach is to derive the effective interaction using many-body theories, starting from bare *NN* interactions.

In 1966, the attempts to derive the effective interaction for the shell model were started. Kuo and Brown reported the applicability of free *NN* interaction to the ^{18}O and ^{18}F, constructing the effective interaction for the model space of *sd*-shell [8]. They treated the short-range repulsion of the *NN* interaction with Brueckner's G-matrix theory [9], and renormalized the virtual excitation to the outside of the model space perturbatively, at second order in G-matrix.

Then, the folded-diagram method appeared on this line of works. In 1971, Kuo and his collaborators constructed the effective interactions with folded-diagram method. In this method, the divergences appear in the perturbative expansion of the effective interaction are elegantly removed by factorizing out the divergent parts of the diagrammatic series. Simultaneously, the folded diagram theory include the infinite-order summation of the selected diagrams [10, 11].

On the other hand, with the development of calculational technique and the computer resources for the diagonalization, the shell-model calculation of full *sd*-shell became tractable in late 1970s. Since the microscopic methods do not have the parameters to fit the experimental data, the agreement to experimental data was not satisfactory when the shell-model calculations were performed very good

with the interaction. Then, the interactions which designed to fit the experimental data in the full *sd*-shell were considered. The interaction is called universal *sd*-shell interaction, in short, USD by Wildenthal and Brown [12, 13]. Then it became possible to reproduce the experimental data almost whole range of the *sd*-shell nuclei with a great precision. The USD interaction became one of the standard and most reliable interactions defined in *sd*-shell and is used even nowadays [14, 15]. There have been the numerous efforts to construct the effective interactions in other regions as well, and there are several effective interactions in *pf*-shell region [16, 17, 18]. This kind of interactions are often called empirical effective interactions, in contrast to the effective interaction derived via the microscopic theories.

The large-scale shell-model calculations have also been developed at the same time. As one of them, in around 2000, the Monte-Carlo shell model calculation was developed and it enabled us to diagonalize the even heavier nuclei. The effective interaction within $sdf_{7/2}p_{3/2}$-shell degrees of freedom is implemented at the same time [19]. With this interactions, they succeed to reproduce the properties of "island of inversion", which indicate the breaking the magic number of $N = 20$.

However, the main goal of effective interaction theory is still to construct and understand such sophisticated effective interactions starting from the underlying nuclear forces and so-called *ab initio* or first principle many-body methods. Most microscopic effective interactions, except for those used in no-core shell-model studies [20, 21, 22], are based on many-body perturbation theory, starting in many cases with the standard non-Hermitian Bloch-Brandow scheme [23, 24, 25, 26, 27] or with Hermitian effective Hamiltonians [28] (see for example Ref. [29] for a recent review). The situation, however, is far from being satisfactory. In spite of several developments in many-body perturbation theory, many properties of nuclei are still awaiting a proper microscopic description and understanding.

The standard approach to derive microscopic effective interactions for the shell model via many-body perturbation theory, is so-called folded diagrams [11] approach. Two widely used approaches are the Kuo-Krenciglowa (KK) [30] and the Lee-Suzuki (LS) [31] schemes. These approaches, however, are feasible only with degenerate perturbation theory and are thereby constrained to a model space consisting of typically one major oscillator shell. This poses a strong limitation on the applicability of the theory. Many unstable nuclei require at least two or more major oscillator shells for a proper theoretical description. As we mentioned above, for example, the physics on island of inversion are only described by the empirical effective interaction [19], defined for a model space consisting of the *sd*-shell and the *pf*-shell. It is therefore absolutely necessary to establish a microscopic theory that allows us to construct an effective interaction for the model spaces composed of several oscillator shells, starting from realistic nuclear forces.

We show the nuclear chart in Fig. 1.1. The black squares are stable nuclei, the dark gray squares are experimentally known but unstable nuclei. The light gray squares are experimentally unknown nuclei but theoretically predicted to exist. For the many stable nuclei, the nuclear shell model within one-major shell degrees of freedom is enough to explain the various properties of those nuclei, as we can expect from the figure. However, there are plenty of nuclei where one-major shell degrees
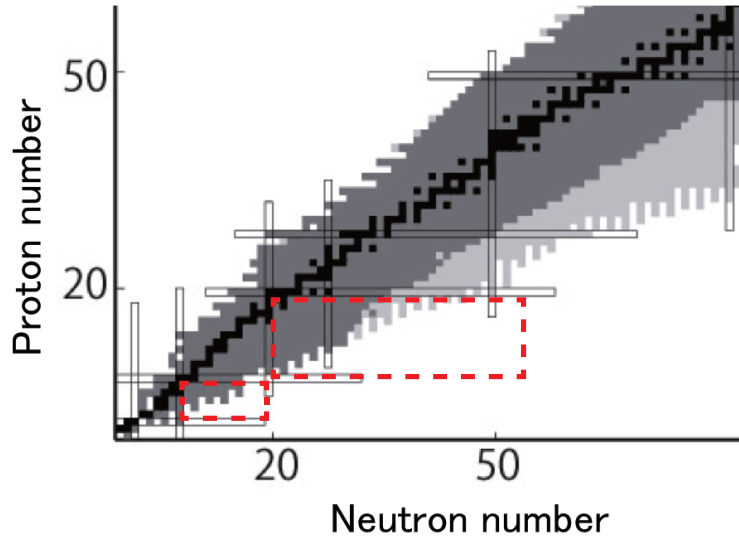
Figure 1.1: Nuclear chart. The black squares are stable nuclei, the dark gray squares are experimentally known nuclei and the light gray squares are experimentally unknown but theoretically predicted to be existing nuclei. The nuclei in the red dashed square require inter-shell interactions.

of freedom are not enough, for example the nuclei in the red dashed squares. This areas include, for example, the dripline of the light to medium-mass nuclei, and many of medium to heavy-mass nuclei. This areas also include the island of inversion.

Recently, the KK and the LS methods have been extended to the non-degenerate model spaces [1, 2]. In this work, we present the extended KK (EKK) method in many-body systems, which allows us to construct a microscopic effective interaction for several major shells. We shall see that our theory is a natural extension of the well-known folded-diagram theory of Kuo and his collaborators (see for example Refs. [30, 11]).

This thesis is structured as follows. In Chap. 2, we review the existing theories to derive the effective interaction for the shell model, starting from *NN* interaction. We briefly explain the concept of the effective interaction in a given model space, and explain Kuo-Krenciglowa method. In Chap. 3 we introduce our EKK theory for effective interactions. The formal theory of EKK method is presented in Sec. 3.1, which is mainly a summary of references [1, 2]. After Sec. 3.2 until the end of this thesis is devoted to the original works for this thesis, and the main part of them will be published in ref. [32], including some figures. We discuss in some detail the difference between the EKK method and the conventional KK approach which applies to degenerate model spaces only. In Chap. 4, we present test calculations and discussions. Here we construct effective interactions for the nuclear shell model in a single-major shell (*sd*-shell, *pf*-shell) and also in two major shells (*sdf*$_{7/2}$*p*$_{3/2}$-shell, *pfg*$_{9/2}$-shell). We then calculate energy levels of several nuclei that have two valence nucleons on top of a closed-shell core. We also show several features of the effective interaction derived via EKK method. We demonstrate that our method establishes one possible way to reliably compute microscopic effective interactions for model spaces composed of several major oscillator shells. In Chap. 5, we briefly

explore the possible application of our effective interaction. We apply our effective interactions to selected nuclei where two-major shell degrees of freedom is essential. These results are preliminary, but are promising and provide us the insight for the future direction of the work. In Chap. 6 we give a conclusion and a summary.

Chapter 2

Review of effective interaction for the shell model

In this chapter, we review the various theories of the effective interaction of the nuclear force, focusing on the renormalization scheme related to the effective interaction for the shell model.

Nuclear shell model is a configuration interaction method, which is based on usually two-body interactions and single-particle energies.

Nuclear shell model starts from the following second quantized Hamiltonian,

$$H = \sum_i \epsilon_i a_i^\dagger a_i + \sum_{ijkl} V_{ij,kl} \, a_i^\dagger a_j^\dagger a_l a_k. \tag{2.1}$$

The input parameter is the single particle energies ϵ_i and the two-body interactions $V_{ij,kl}$. Then, we calculate the Hamiltonian of many-body states, and diagonalize it to obtain the eigenenergies and the wave functions.

The creation (annihilation) operators create (annihilate) the nucleons in some discrete orbits. Usually, these orbits are defined as the eigenfunctions of the harmonic oscillator or the Woods-Saxon potential, for example. Nuclei have several tens of nucleons typically, which usually give rise to intractably large dimensions. Therefore we have to restrict ourselves to the finite small dimension, to diagonalize the Hamiltonian matrices. We define a subspace of whole Hilbert space which is called the model space, where the nucleons can move inside. We also in many cases consider a frozen-core states like ^{16}O, whose degrees of freedom are killed. As an approximation, the particles are assumed to move only outside of the core, because these degrees of freedom are enough to explain many part of the properties of the nuclei heavier than the core. This assumption enlarges the region of the calculation drastically as well.

Therefore, we have to determine the suitable parameter ϵ_i and $V_{ij,kl}$ appropriate to relevant degrees of freedom. Once we have a reliable Hamiltonian, we can calculate the Hamiltonian of many-body states and diagonalize it, to obtain the binding energies, wave functions, the strength of the transitions and the other various useful physical quantities. These parameters are often called effective interaction for the shell model calculations.

There exist two major ways to determine the effective interactions. One is determine the ϵ_i and $V_{ij,kl}$ by hand, to fit the experimental physical quantities like binding energies, spin-parities and so on. This line of researches made a great success and explained many properties of various nuclei as well as predicted the properties of experimentally unknown nuclei. The other is to *derive* the matrix elements, starting from the *NN* interaction determined by the *NN* scattering experiments. The extension of the second approach is the main purpose of this thesis.

In the derivation of the matrix elements from the *NN* interaction, there are two major problems to concur. The first is that nucleon nucleon interaction has strong short-range repulsion, unlike electromagnetic force. Therefore, naive integral to calculate matrix elements almost diverges and we need special treatments.

The other is that we need to include the indirect effects of the truncation to the model spaces, not just calculate the matrix elements of the initial *NN* interaction. This is accomplished by the perturbation theory. For degenerate perturbation theory, we have special technique called the folded-diagram method.

In this section we review the formalism to derive effective interactions defined in a model space. The process consists of two steps. First, nuclear force has strong short-range repulsion which we have to renormalize, before the perturbative expansion. In Sec. 2.1, we review the two different approaches of the renormalization of short-range repulsion, one of which is traditional and the other is modern. In Sec. 2.2, a framework to derive the effective interaction appropriate for the chosen model space is introduced. This is formulated as a similarity transformation of the Hamiltonian. The formal solutions are given in Sec. 2.3, in two different ways. One is called the Kuo-Krenciglowa method and the other is the Lee-Suzuki method. At last, in Sec. 2.4, the solution for many-body problem is presented. The folded diagram method appears as the method to give a solution.

2.1 Renormalization of short-range repulsion

2.1.1 Nuclear force and short-range repulsion

The pioneering work on nuclear force has been done by H.Yukawa in 1935 [33]. He proposed the theory of pion which account for strong and finite range attractive nature of the nuclear force. The range of the nuclear force caused by exchange of meson of finite mass m_a is given by the following Compton length,

$$\lambda_a = \frac{\hbar}{m_a c}. \tag{2.2}$$

Therefore, the range of nuclear force is determined by the lightest meson mass, pion ($m_\pi \approx 140\,\mathrm{MeV}$), corresponding range is $\lambda_\pi = 1.4$ fm. On the other hand, when the distance of two nucleons is less than λ_π, other mesons such as $\omega, \sigma, \eta \ldots$ contribute to the nuclear force.

The experiment of *NN* scattering up to several hundred MeV revealed that nuclear force is strongly repulsive at short range, typically in the range closer than 0.5 fm. This strong repulsion is called

repulsive core. In such a range, the nuclear force is considered to be affected by the internal structure of nucleons whose charge radius is approximately $\sqrt{\langle r^2 \rangle_e} = 0.8$ fm in the case of proton.

The nuclear force depends not only on distance of two particles, but also on the states of two nucleons. Here the word state indicates total spin, total isospin and angular momentum quantum numbers of two nucleons. This feature of the nuclear force gives variety of phenomena in nuclear structure physics. In late 1950s, many experiments have been done for the purpose to know the state dependence of the nuclear force using facilities of polarized nucleons.

In 1951, Taketani, Nakamura and Sasaki gave an important proposal [34]. They claimed that the long range part of nuclear force should be determined by the meson exchange mechanism and the short range part by phenomenological considerations because it includes many complicated effects at short range.

Although quantitative understanding is greatly improved, the basic philosophy of this field does not widely change from that period. At the present condition, the long range part (distance $r > 2$ fm) is determined completely by one pion exchange potential (OPEP) not only qualitatively but also quantitatively. The part where $r < 2$ fm is separated into two ranges, the intermediate range and the short range. The intermediate range part is considered to result from exchange of mesons heavier than pion, but quantitative structures are determined by phenomenological fit. The short range part is considered to result from internal structure of nucleons, but at the actual calculations of nuclear structure, phenomenological potentials are used in many cases.

Nowadays, there are plenty of experimental data to determine the nuclear force. Several potentials were made that reproduce scattering data of two-nucleons and properties of deuteron. These potentials are often called realistic nuclear force.

The Argonne potentials are example of such potentials. These are series of realistic nuclear forces, written in local operator form [35, 36]. Long range part is OPEP and intermediate and short range are determined by the phenomenological fit with experimental data of deuteron and phase shift of elastic scattering of two nucleons. Local operators are considered to include many mesons' degrees of freedom implicitly.

2.1.2 Brueckner's theory

The Brueckner's theory is the theory to renormalize the short-range repulsion of the nuclear force. When we calculate the matrix elements naively with the basis of plain waves e^{ikx} or harmonic oscillator wave functions, the short-range repulsion makes the results singular. This fact makes the nuclear many-body problem complicated. The attempt to apply the realistic *NN* interaction directly to many-body theory fails, because of this singularity of the potential. However, in the actual nuclei or nuclear matter, the distance between two nucleons are larger than the range of short-range repulsion. In other words, the wave functions of two nucleons do not have the overlap in short range, and the matrix elements result in finite even if the nuclear force have the singularity. The philosophy of the Brueckner's theory is that the combination of the singular nuclear force and the normal wave function results in

the same as the combination of the singular wave function and the renormalized nuclear force. In the other words, the simultaneous transformation of the basis states and the interaction makes the results finite and reasonable.

The G-matrix is defined by the integral equation, which is a form of Bethe-Goldstone equation,

$$G = V + V\frac{Q}{e}G, \tag{2.3}$$

where Q is the Pauli operator which exclude all the occupied states. The denominator e is defined as $e = E - E_i$, where E is the sum of self-consistent initial energies of two nucleon, and E_i is the sum of intermediate energies. This is clearly a self-consistent equation, for G is appearing left-hand side and right-hand side. Therefore, it corresponds to the summation of ladder diagrams up to infinite order in V.

The G-matrix also satisfies the following equation,

$$G\phi = V\Omega\phi = V\psi \tag{2.4}$$

where ϕ is the unperturbed wave function, Ω is the wave operator and $\psi(=\Omega\phi)$ is the correlated wave function which vanishes inside of the core radius. With the infinite summation of V in Eq. (2.3), even if the V is infinite the resultant G-matrix is finite, because the correlated wave function in Eq. (2.4) is vanished inside of the core radius.

We have to aware of one thing. When we use G-matrix as the effective interaction which do not has repulsive core, we need to consider the energy dependence in Eq. (2.3). This energy is often called starting energy and the resultant G-matrix is starting energy dependence. This feature is not convenient to calculate the effective interaction for the shell model via the perturbation theory, because we have to prepare the set of G-matrices for all the starting energies.

The newly invented $V_{\mathrm{low}k}$ interaction explained in the subsequent section does not have such a parameter dependent. In this thesis, we used the $V_{\mathrm{low}k}$ technique to renormalize the repulsive core, instead of G-matrix.

2.1.3   The low-momentum interaction $V_{\mathrm{low}k}$

The $V_{\mathrm{low}k}$ approach is more recent approach than Brueckner's G-matrix. The main merit of this new approach is that the obtained effective interaction $V_{\mathrm{low}k}$ is energy-independent, unlike G-matrix.

The $V_{\mathrm{low}k}$ potential is invented in these references [37, 38, 39, 40].

By solving the Lippmann-Schwinger equation, we obtain the following Half-On-Shell T-matrix,

$$T(k',k;k^2) = V_{NN}(k',k) + \frac{2}{\pi}\mathcal{P}\int_0^\infty \frac{V_{NN}(k',p)T(p,k;k^2)}{k^2 - p^2}p^2\mathrm{d}p \tag{2.5}$$

for a given partial wave.

In the low-momentum effective theory, the interaction and T-matrix are defined in the region of the momentum is lower than certain cutoff Λ. It is required that the low-momentum interaction leads

the same physics, that is, T-matrix. Therefore, the $V_{\text{low}k}$ potential is defined by the following equation parametrized by the cutoff parameter Λ,

$$T(k', k; k^2) = V_{\text{low}k}(k', k) + \frac{2}{\pi} \mathcal{P} \int_0^\Lambda \frac{V_{\text{low}k}(k', p)T(p, k; k^2)}{k^2 - p^2} p^2 \mathrm{d}p. \tag{2.6}$$

Because T-matrix is invariant under the cutoff Λ, The scattering standing wave function $|\chi_k\rangle$ is also invariant, and therefore expressed as the following standard equation of T-matrix,

$$|\chi_k\rangle = |k\rangle + \frac{2}{\pi} \mathcal{P} \int_0^\Lambda p^2 \mathrm{d}p \frac{1}{k^2 - p^2} T(p, k; k^2)|p\rangle \qquad (k < \Lambda). \tag{2.7}$$

Then, taking the derivative with respect to Λ in Eq. (2.6), we obtain,

$$0 = \frac{\mathrm{d}V_{\text{low}k}(k', k)}{\mathrm{d}\Lambda} + \frac{2}{\pi} \mathcal{P} \int_0^\Lambda \left(\frac{\mathrm{d}V_{\text{low}k}(k', k)}{\mathrm{d}\Lambda} \frac{T(p, k; k^2)}{k^2 - p^2} + \frac{V_{\text{low}k}(k', k)}{k^2 - p^2} \frac{\mathrm{d}T(p, k; k^2)}{\mathrm{d}\Lambda} \right) p^2 \mathrm{d}p$$
$$- \frac{2}{\pi} \frac{V_{\text{low}k}(k', \Lambda)T(\Lambda, k; k^2)}{1 - (k^2/\Lambda^2)} \tag{2.8}$$

$$\int_0^\Lambda \frac{\mathrm{d}V_{\text{low}k}(k', p)}{\mathrm{d}\Lambda} \chi_k(p) p^2 \mathrm{d}p = \frac{2}{\pi} \frac{V_{\text{low}k}(k', \Lambda)T(\Lambda, k; k^2)}{1 - (k^2/\Lambda^2)}. \tag{2.9}$$

Multiplying $\langle \tilde{\chi}_k |$ from the left and using completeness relation, finally we have the following renormalization group flow equation,

$$\frac{\mathrm{d}V_{\text{low}k}(k', k)}{\mathrm{d}\Lambda} = \frac{2}{\pi} \frac{V_{\text{low}k}(k', \Lambda)T(\Lambda, k; \Lambda^2)}{1 - (k^2/\Lambda^2)}. \tag{2.10}$$

Even if we know this RG equation exists, it is not easy to solve the differential equation directly for the actual case. For our purpose of *NN* scattering problem, we can calculate $V_{\text{low}k}$ in the other way. In the derivation of $V_{\text{low}k}$ RG equation, we impose that the T-matrix is invariant under the change of the cutoff Λ, which means the wave function in the low-momentum sector is unchanged. In the case of NN scattering problem, we can calculate the exact wave function numerically. For the numerical capability, we discretize the momentum, $k_1, k_2, \ldots, k_n$. Then the solution of Schrödinger equation is calculated by direct diagonalization of Hamiltonian matrix in momentum space,

$$H|\psi_i\rangle = E_i|\psi_i\rangle. \tag{2.11}$$

The wave functions in low-momentum sector are defined as,

$$|\chi(k_i)\rangle = |\psi(k_i)\rangle \qquad\qquad (k_i \le \Lambda) \tag{2.12}$$
$$|\chi(k_i)\rangle = 0 \qquad\qquad (k_i > \Lambda),$$

where $|\chi\rangle$ is the renormalized wave function for the low-momentum effective theory and $|\psi\rangle$ is the exact wave function. Then we can calculate the $V_{\text{low}k}$ interaction as

$$H_0 + V_{\text{low}k} = \sum_i |\chi_i\rangle E_i \langle \tilde{\chi}_i| \tag{2.13}$$

where $|\tilde{\chi}_i\rangle$ is bi-orthogonal basis which satisfies

$$\langle \tilde{\chi}_i | \chi_j \rangle = \delta_{ij}. \tag{2.14}$$

Usage of bi-orthogonal basis implies that the resultant Hamiltonian in the effective theory is non-hermitian. This is clearly the consequence of momentum cutoff. However, because of the strong repulsive property of the short range part of the nuclear force, the high-momentum component of the exact wave function $|\psi\rangle$ is generally small. In that case, we can remove the non-hermiticity by the method of Andreozzi [41], not changing all the physical observables but changing the wave function slightly. We will discuss the refinement of non-hermitian effective interaction to hermitian effective interaction again, in Sec. 2.2.3.
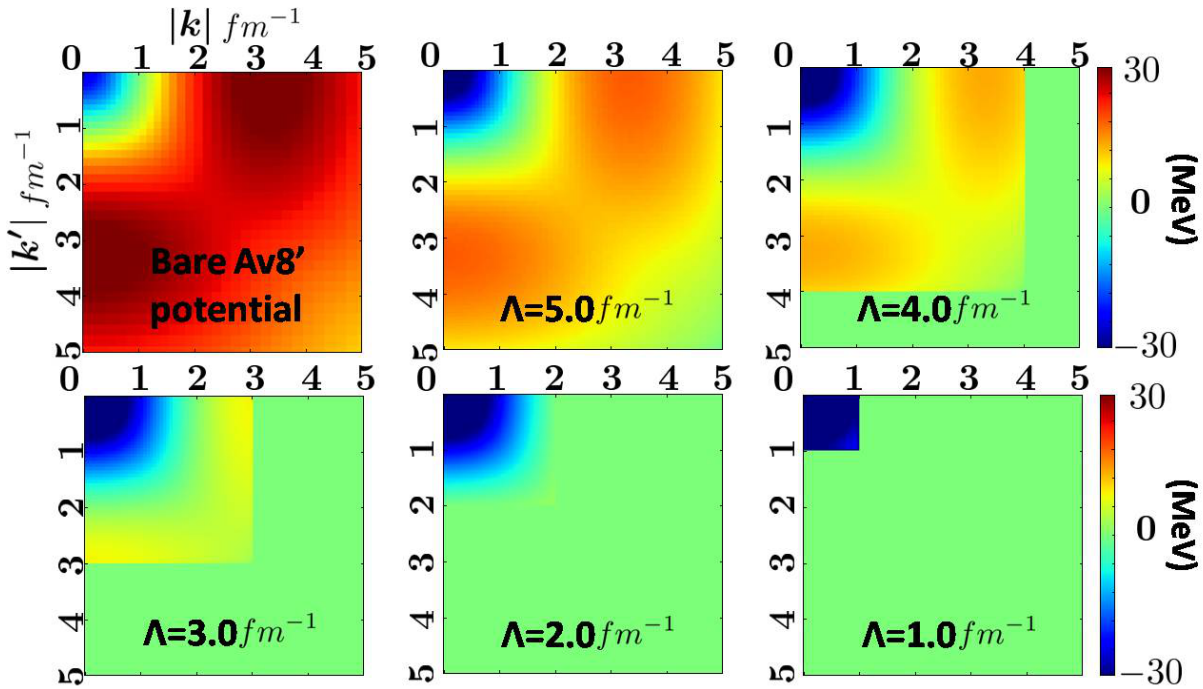

Figure 2.1: Numerical calculation of the $V_{\mathrm{low}k}$ interaction with various cutoff Λ. The original NN interaction is Argonne V8' potential, and the cutoff $\Lambda = 1.0 - 5.0 \, \mathrm{fm}^{-1}$.

Let us see the numerical example of $V_{\mathrm{low}k}$ starting from the realistic nuclear force. Figure 2.1 shows $V_{\mathrm{low}k}$ interaction with various cutoff. The interaction is shown in momentum space in 2D plot, with the cutoff $\Lambda = 5.0 - 1.0 \, \mathrm{fm}^{-1}$. The initial potential is Argonne V8' (AV8') potential, as an example [36]. The bare AV8' potential has large repulsive low to high momentum coupling. This corresponds to the repulsive core at short range. As the cutoff Λ getting smaller, The repulsion getting smaller and smaller, and we can not see it at all at $\Lambda = 2.0 \, \mathrm{fm}^{-1}$. In this sense, the interaction getting "softer" as cutoff Λ is small and therefore suitable for the perturbative calculation.

However, One should note the fact that the formalism of $V_{\mathrm{low}k}$ is only defined in 2N system. The transformation between 2N system inevitably induce the 3N or higher-body force, schematically,

$$V_{bare}(2N) \rightarrow V_{\mathrm{low}k}(NN) + V_{ind}(3N) + V_{ind}(4N) + \cdots , \tag{2.15}$$

where subscripts *ind* indicate the force induced by the renormalization. In the limit of large cutoff Λ the induced 3N force V_{ind} is zero by definition, and with the small cutoff, induced 3N becomes large. For this point, Nogga and his collaborators have done a elegant work in 2004 [42]. They calculated the $V_{\mathrm{low}k}$ potential starting from various realistic *NN* interaction, and then calculate the few nucleon system by Faddeev-Yakubovsky equations only with two-body force. They showed the Λ dependence of the binding energies of 3N or 4N system, which clearly depend on the size of induced higher-body forces. They claimed that the Λ dependence is not very large at $\Lambda \geq 1.0$ fm^{-1} region, which means the induced higher-body force is not so large in this region. They also compare the calculated binding energies of ^{3}H and ^{4}He to the experimental data and claim that the value around $\Lambda = 2.0$ fm^{-1} best reproduce the experimental value of both two nuclei. There exists the three-body force initially in nuclear force because the nucleons are composite particles consist of quarks. Therefore, the best reproduction of the experimental data means, in turn, the effects of the initial and induced three or higher-body force cancel out each other in those system.

In their work, only 3N and 4N systems are considered. Therefore, only if we believe that the higher-body force cancel exactly including all the channel dependence and strength, we can calculate the many-body system composed of more than four nucleons. However, there are some evidence that the explicit inclusion of 3N force improves the reproduction of the physical quantities far from the stability line. Combining those two facts, we may have to think about the cutoff issue again. We will come back to this point in the framework of EKK method again.

2.2 Renormalization of the medium effects

In this section, we review the second step to calculate the effective interactions for the shell model. The first step was to remove the repulsive core by changing the basis states. The resultant effective interaction do not have short-range repulsion or high-momentum component and so do the renormalized wavefunctions. Therefore, the $V_{\mathrm{low}k}$ interaction does not have singularity which prevent us performing the perturbative calculations.

In the second step, starting from the renormalized interaction, we move on the perturbation theory to calculate the effective interaction designed for suitable model spaces.

2.2.1 model space

First of all, we define the model space mathematically and clarify the notation. Suppose we describe a quantum system by the following Hamiltonian

$$H = H_0 + V, \tag{2.16}$$

where H_0 is the unperturbed Hamiltonian and V is the perturbation. In a Hilbert space of dimension D, we can write down the many-body Schrödinger equation as

$$H|\Psi_\lambda\rangle = E_\lambda|\Psi_\lambda\rangle, \quad \lambda = 1, \cdots, D. \tag{2.17}$$

In shell-model calculations, however, the dimension D of the Hamiltonian matrix increases exponentially with the particle number, limiting thereby the applicability of direct diagonalization procedures to the solution to Eq. (2.17).

In this situation, we introduce a P-space (model space) of a tractable dimension $d \leq D$ that is a subspace of the large Hilbert space of dimension D. Correspondingly, we define the projection operator P onto the P-space, and $Q = 1 - P$ onto its complement. We require that the projection operators P and Q commute with the unperturbed Hamiltonian H_0,

$$[P, H_0] = [Q, H_0] = 0. \tag{2.18}$$

As a consequence, the projection operator P and Q satisfy the following relations,

$$P^2 = P, \quad Q^2 = Q \tag{2.19}$$

$$PQ = QP = 0, \tag{2.20}$$
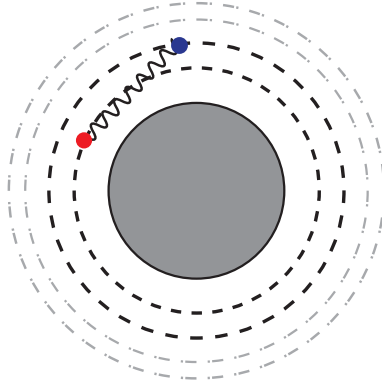
$$[P, Q] = 0. \tag{2.21}$$

Figure 2.2: The model space is presented schematically. The black dashed line is the model space and the gray dashed line is the particle states outside the model space. The circle indicate the inert core, for example, ^{16}O.

Figure 2.2 shows the schematic image of the model space. The gray circle is the inert core, and the black dash lines are the model space, and the gray dash-doted lines are in the Q-space. The two particles move only inside the model space. Two particles interact only inside the model space. The presence of the core and the orbits outside the model space should be considered to affect the V_{eff} defined in P-space, and be not included to shell-model calculation as explicit degrees of freedom.

2.2.2 Energy-dependent approach

We start our explanation by introducing an energy-dependent effective Hamiltonian. By using the projection operators P and Q, we can express Eq. (2.17) in the following partitioned form ($\lambda =$

$1, \cdots, D$):

$$\begin{pmatrix} PHP & PVQ \\ QVP & QHQ \end{pmatrix} \begin{pmatrix} |\phi_\lambda\rangle \\ |\rho_\lambda\rangle \end{pmatrix} = E_\lambda \begin{pmatrix} |\phi_\lambda\rangle \\ |\rho_\lambda\rangle \end{pmatrix}, \qquad (2.22)$$

where $|\phi_\lambda\rangle = P|\Psi_\lambda\rangle$ is the projection of the true eigenstate $|\Psi_\lambda\rangle$ onto the P-space. The Q-space component is written as $|\rho_\lambda\rangle = |\Psi_\lambda\rangle - |\phi_\lambda\rangle$. Then we obtain

$$|\rho_\lambda\rangle = (E_\lambda - QHQ)^{-1} QVP|\phi_\lambda\rangle \qquad (2.23)$$

$$|\phi_\lambda\rangle = (E_\lambda - PHP)^{-1} PVQ|\rho_\lambda\rangle. \qquad (2.24)$$

Substituting these equations, we can decouple the equations to P-space and Q-space respectively as follows,

$$\left(PHP - \frac{1}{E_\lambda - QHQ} QVP \right) |\phi_\lambda\rangle = E_\lambda |\phi_\lambda\rangle \qquad (2.25)$$

$$\left(QHQ - \frac{1}{E_\lambda - PHP} PVQ \right) |\rho_\lambda\rangle = E_\lambda |\rho_\lambda\rangle. \qquad (2.26)$$

The first equation is exactly the secure equation defined purely in P-space and the second one is in Q-space. For our purpose of obtaining the effective theory defined in P-space, we adapt Eq. (2.25) and introduce the following Bloch-Horowitz effective Hamiltonian H_{BH} defined purely in the P-space,

$$H_{\mathrm{BH}}(E) = PHP + PVQ \frac{1}{E - QHQ} QVP. \qquad (2.27)$$

Then Eq. (2.17) reads,

$$H_{\mathrm{BH}}(E_\lambda)|\phi_\lambda\rangle = E_\lambda |\phi_\lambda\rangle, \quad \lambda = 1, \cdots, D. \qquad (2.28)$$

Note that Eq. (2.28) requires a self-consistent solution, because $H_{\mathrm{BH}}(E_\lambda)$ depends on the eigenenergy E_λ. In the previous section, we saw the case of $V_{\mathrm{low}k}$ in which we know the exact solution but still we needed to calculate the effective interaction. In the present case, however, we do not know the exact solution generally, because the Hamiltonian in the full space is supposed to have the intractably large dimension. Therefore, the energy-dependence of the effective interaction is not a desirable property for the shell-model calculation, and therefore we adopt the energy-independent approach below.

2.2.3 Energy-independent approach

Next we introduce the energy-independent effective Hamiltonian in the P-space. We first choose d eigenstates $\{|\Psi_i\rangle, i = 1, \cdots, d\}$ among D solutions of Eq. (2.17), with $d \leq D$. Then we require that $|\phi_i\rangle = P|\Psi_i\rangle$, the P-space component of the chosen d eigenstates, be described by the d-dimensional effective Hamiltonian H_{eff} as

$$H_{\mathrm{eff}}|\phi_i\rangle = E_i |\phi_i\rangle, \quad i = 1, \cdots, d. \qquad (2.29)$$

This energy-independent effective Hamiltonian is most concisely described as

$$H_{\mathrm{eff}} = \sum_{i=1}^{d} |\phi_i\rangle E_i \langle \tilde{\phi}_i|, \qquad (2.30)$$

which is equivalent to Eq. (2.13), appearing in the derivation of $V_{\text{low}k}$. In the derivation of $V_{\text{low}k}$, P-space can be interpreted as the low-momentum space whose initial and final momentum $k, k' \leq \Lambda$ and Q-space is high-momentum space. However, Eq. (2.30) is also just a formal solution because we do not know the exact solution $|\Psi_i\rangle$ and its projection to P-space $|\phi_i\rangle$. Now we need to obtain the effective interaction V_{eff} without solving the original Schrödinger equation by the direct diagonalization.

To derive the energy-independent effective Hamiltonian H_{eff}, let us consider the following similarity transformation of the Hamiltonian H:

$$\mathcal{H} = e^{-\omega}He^{\omega}, \quad Q\omega P = \omega. \tag{2.31}$$

By construction, the transformed Hamiltonian, $\mathcal{H}$, gives the same eigenenergies as the original Hamiltonian H. The corresponding eigenstates $|\Psi_i\rangle$, however, are transformed into $e^{-\omega}|\Psi_i\rangle$. We require therefore that the second relation in Eq. (2.31),

$$Q\omega P = \omega, \tag{2.32}$$

satisfies

$$Pe^{-\omega}|\Psi_i\rangle = P(1 - \omega)|\Psi_i\rangle = |\phi_i\rangle, \tag{2.33}$$

that is, the transformation does not change the P-space component $|\phi_i\rangle$ of the eigenstates. Here we used the fact that $\omega^2 = 0$. With this transformation, the P-space components of any wave-function is unchanged.

Then, Our next step includes the determination of ω. The most convenient way to determine ω is by using the following equation

$$0 = Q\mathcal{H}P = QVP - \omega PHP + QHQ\omega - \omega PVQ\omega, \tag{2.34}$$

which decouples the P-space part in the transformed Schrödinger equation. Comparing to Eq. (2.27), starting from this transformed Hamiltonian $\mathcal{H}$, the Bloch-Horowitz Hamiltonian is just $P\mathcal{H}P$. This means that the P-space part of the transformed Hamiltonian, $P\mathcal{H}P$, is exactly H_{eff} in Eq. (2.29). Then the effective Hamiltonian and the effective interaction can be written as

$$\begin{aligned}
H_{\text{eff}} &= P\mathcal{H}P \\
&= Pe^{-\omega}He^{\omega}P \\
&= P(1 - \omega)H(1 + \omega)P \\
&= PHP + PV\omega P \\
&= PHP + PVQ\omega \tag{2.35} \\
V_{\text{eff}} &= PVP + PVQ\omega. \tag{2.36}
\end{aligned}$$

We note here that H_{eff} is energy-independent. Furthermore, the derivation of H_{eff} requires the determination of ω in order to satisfy Eq. (2.34).

As we discussed in Sec. 2.1.3, the resultant effective interaction is non-Hermitian. In the language of ω, the similarity transformation Eq. (2.31) is not an unitary transformation because ω is not Hermite. Now we see the way to remove this non-Hermite part of the effective Hamiltonian. Let us consider the following operator defined in P-space $(P + \omega^\dagger\omega)$ and we obtain

$$(P + \omega^\dagger\omega)H_{\text{eff}} = H_{\text{eff}}^\dagger(P + \omega^\dagger\omega). \tag{2.37}$$

By means of Cholesky decomposition, it can be rewritten by the lower-triangular matrix L and its adjoint $L^\dagger$,

$$P + \omega^\dagger\omega = LL^\dagger. \tag{2.38}$$

Then we get the following,

$$L^{-1}H_{\text{eff}}^\dagger L = L^\dagger H_{\text{eff}}(L^\dagger)^{-1} = \left(L^{-1}H_{\text{eff}}^\dagger L\right)^\dagger \tag{2.39}$$

This implies that the Hermitian effective interaction with the same eigenvalues as the original H_{eff},

$$H_{\text{eff}}^{her} = L^\dagger H_{\text{eff}}(L^\dagger)^{-1}. \tag{2.40}$$

The combined transformation $U = e^\omega(L^\dagger)^{-1}$ is an unitary transformation.

The unitary transformation does not change all the eigenvalues, therefore, the phase shifts and the other physical quantities, but changes the wave function. Since the operator L is $L = P + O(\omega)$, if ω is small the non-Hermiticity is also small and therefore the change of wave function is small. For our problem of $V_{\text{low}k}$ potential, the Q-space high-momentum component of the exact wave function is small and so ω is small. For the problem of shell model effective interactions, we find the same observation. For example, if we consider the case of ^{18}O, two neutrons are placed in the orbits outside the ^{16}O core. The lowest orbits are of course sd-shell and for low-lying states, the occupation probability of pf-shell or higher-shell is almost negligible. This suggests the transformation from non-Hermite effective interaction to Hermite effective interaction does not affect the wave function and other physics, in the case that we calculate the effective interaction for the shell model.

In summary, we consider the similarity transformation Eq. (2.31) with the minimal transformation condition, which changes neither selected d eigenvalues nor the P-space component of the wavefunctions. Then we impose decoupling condition shown in Eq. (2.34), to decouple the P-space physics from the Q-space. The resultant effective interaction H_{eff} is slightly non-Hermitian and we further transform it to Hermite Hamiltonian by using the operator obtained by means of Cholesky decomposition of the operator defined in P-space, shown in Eq. (2.38).

In the next section, we will see the solution of Eq. (2.34). Since this is the non-linear equation of ω, there exists no unique solution, and we have several ways to obtain the solutions.

2.3 Formal theory of effective interaction

The decoupling equation Eq. (2.34), being nonlinear, can be solved by iterative methods, to give H_{eff} and V_{eff} of Eq. (2.36). Although the decoupling equation Eq. (2.34) itself is valid in the general cases,

the following solutions need the condition of degenerate unperturbed eigenvalues in P-space. We first explain the KK method [30] for the degenerate model space. Then we explain the LS method [31] for the degenerate model space. Both methods eliminate the energy-dependence of $H_{\mathrm{BH}}(E)$ of Eq. (2.27) by introducing the so-called $\hat{Q}$-box and its energy derivatives, resulting in an energy-independent effective interaction H_{eff}.

2.3.1   Kuo-Krenciglowa (KK) method

In the KK method, we assume a degenerate model space,

$$PH_0P = \epsilon_0 P. \tag{2.41}$$

Then Eq. (2.34) reads

$$(\epsilon_0 - QHQ)\omega = QVP - \omega PVP - \omega PVQ\omega. \tag{2.42}$$

The KK method provides us a one possible way to solve this decoupling equation. Multiplying $(\epsilon_0 - QHQ)$ from the left,

$$
\begin{aligned}
\omega &= \frac{1}{\epsilon_0 - QHQ}\left(QVP - \omega\left(PVP + PVQ\omega\right)\right) \\
&= \frac{1}{\epsilon_0 - QHQ}\left(QVP - \omega V_{\mathrm{eff}}\right),
\end{aligned} \tag{2.43}
$$

using the expression of V_{eff} in Eq. (2.36). Then we obtain the the following iterative form:

$$\omega^{(n)} = \frac{1}{\epsilon_0 - QHQ}\left(QVP - \omega^{(n)}V_{\mathrm{eff}}^{(n-1)}\right), \tag{2.44}$$

where $\omega^{(n)}$ and $V_{\mathrm{eff}}^{(n)} = PVP + PVQ\omega^{(n)}$ stand for ω and V_{eff} in the n-th step, respectively.

Now we introduce the important operator called $\hat{Q}$-box as follows:

$$
\begin{aligned}
\hat{Q}(E) &= PVP + PVQ\frac{1}{E - QHQ}QVP, \\
\hat{Q}_k(E) &= \frac{1}{k!}\frac{\mathrm{d}^k\hat{Q}(E)}{\mathrm{d}E^k}.
\end{aligned} \tag{2.45}
$$

The $\hat{Q}$-box is clearly defined as an operator act in P-space. Intuitively this quantity stands for the interacting matrix which the P-space wavefunction having energy E makes excited to Q-space, and propagate in Q-space, and then makes it back to P-space again.

Then we immediately arrive at the following iterative formula for $V_{\mathrm{eff}}^{(n)}$:

$$V_{\mathrm{eff}}^{(n)} = \hat{Q}(\epsilon_0) + \sum_{k=1}^{\infty}\hat{Q}_k(\epsilon_0)\{V_{\mathrm{eff}}^{(n-1)}\}^k. \tag{2.46}$$

In the limit of $n \to \infty$, Eq. (2.46) gives $V_{\mathrm{eff}} = V_{\mathrm{eff}}^{(\infty)}$, if the iteration converges. The first term of Eq. (2.46) is $\hat{Q}$-box itself, which means the effective interaction include the effect of virtual excitation

to Q-space degrees of freedom. In addition, to obtain exact solution of V_{eff}, we need to include multiple scatterings to Q-space, that is, the P-space state has to be excited to Q-space once, come back to P-space and excite to Q-space again. The infinite summation can be considered as the multiple scattering to Q-space. The more concrete interpretation of the Eq. (2.46) is given in the framework of time-dependent perturbation theory (See Sec. 2.4.2).

We stress here again that the above KK method can only be applied, by construction, to a system with a degenerate unperturbed model space that satisfies $PH_0P = \epsilon_0 P$. It cannot be applied, for instance, to obtain the effective interaction for the model space composed of the sd-shell and the pf-shell.

2.3.2 Lee-Suzuki (LS) method

In this section, we see another way to solve the decoupling equation Eq. (2.34). Starting from the Eq. (2.34) in the following form, we obtain

$$(\epsilon_0 - QHQ)\omega = QVP - \omega PVP - \omega PVQ\omega$$

$$\omega = \frac{1}{\epsilon_0 - QHQ}QVP - \frac{1}{\epsilon_0 - QHQ}\omega V_{\text{eff}}. \tag{2.47}$$

In LS method, we transform the V_{eff} in a different way as KK method, using the above expression of ω as follows:

$$\begin{aligned} V_{\text{eff}} &= PVP + PVQ\omega \\ &= PVP + PVQ\left(\frac{1}{\epsilon_0 - QHQ}QVP - \frac{1}{\epsilon_0 - QHQ}\omega V_{\text{eff}}\right) \\ &= \hat{Q}(\epsilon_0) - PVQ\frac{1}{\epsilon_0 - QHQ}\omega V_{\text{eff}} \end{aligned} \tag{2.48}$$

therefore, $\hat{Q}$-box can be rewritten by means of V_{eff},

$$\begin{aligned} \hat{Q}(\epsilon_0) &= \left(1 + PVQ\frac{1}{\epsilon_0 - QHQ}\omega\right)V_{\text{eff}} \\ V_{\text{eff}} &= \frac{1}{1 + PVQ\dfrac{1}{\epsilon_0 - QHQ}\omega}\hat{Q}(\epsilon_0) \end{aligned} \tag{2.49}$$

To obtain the numerical solution, we apply the following iteration scheme according to Eqs. (2.47) and (2.49),

$$V_{\text{eff}}^{(n)} = \frac{1}{1 + PVQ\dfrac{1}{\epsilon_0 - QHQ}\omega_n}\hat{Q}(\epsilon_0) \tag{2.50}$$

$$\omega_n = \frac{1}{\epsilon_0 - QHQ}QVP - \frac{1}{\epsilon_0 - QHQ}\omega_{n-1}V_{\text{eff}}^{(n-1)}. \tag{2.51}$$

By substituting ω_n to the expression of $V_{\text{eff}}^{(n)}$ successively, finally we obtain the iterative formula written in terms of $\hat{Q}$-box and V_{eff},

$$V_{\text{eff}}^{(n)} = \frac{1}{1 - \hat{Q}_1 - \sum_{m=2}^{n-1} \hat{Q}_m \prod_{i=n-m+1}^{n-1} V_{\text{eff}}^{(i)}} \hat{Q}(\epsilon_0). \tag{2.52}$$

The main merit of this iterative formula is that V_{eff} appears in the denominator, in contrast to KK method. Therefore, the divergence of V_{eff} never happens. Therefore, the LS method reproduce the lowest d eigenstates and will never affected by the intruder states. However, it is difficult to interpret Eq. (2.52) with the time-dependent perturbation theory.

2.4 Many-body theory of effective interaction

For the purpose of obtaining the effective interaction for the shell model, we need to apply the formal theory of the effective interaction in Sec. 2.3 to nuclear many-body systems. In Sec. 2.4.2, we explain the standard Kuo-Krenciglowa (KK) theory in a many-body system. Its diagrammatic expression can be established both in time-dependent [11] and time-independent [23] perturbation theory, and is conveniently summarized by the $\hat{Q}$-box expansion in terms of the so-called folded diagrams [11]. In this thesis, we discuss the time-dependent version of the derivation of the effective interactions.

2.4.1 Model space in many-body system

Our quantum many-body system is described by the following second quantized form,

$$\begin{aligned} H &= H_0 + V \\ &= \sum \epsilon_\alpha a_\alpha^\dagger a_\alpha + \frac{1}{2} \sum V_{\alpha\beta,\gamma\delta} a_\alpha^\dagger a_\beta^\dagger a_\delta a_\gamma, \end{aligned} \tag{2.53}$$

where H_0 is the unperturbed Hamiltonian and V is the two-body interaction. We limit ourselves, for the sake of simplicity, up to two-body interactions only, although the theory can be extended to include three-body or more complicated nuclear forces.

For specifying single-particle states, we use indices a, b, c, d for valence single-particle states (active single-particle states), and p and h for passive particle and hole single-particle states, respectively. In a generic case, we use Greek indices.

In a many-body system, the P-space is defined using the valence single-particle states that make up the P-space. Let us take as an example the nucleus ^{18}O, where we treat ^{16}O as a closed-shell core. In this case we can define the P-space by specifying the valence states to be determined by the single-particle states of the sd-shell. The P-space is then composed by the ^{16}O closed-shell core plus two neutrons in the sd-shell.

Explicitly, P-space taken as the d-dimensional subspace of the whole Hilbert space, which have two nucleons on top of the core,

$$P = \sum_i^d |\phi_i\rangle\langle\phi_i| \tag{2.54}$$

$$|\phi_i\rangle = \sum a_\lambda^\dagger a_\gamma^\dagger |c\rangle. \tag{2.55}$$

Hereafter we write the wavefunctions within P-space with small letters, and the capital letters usually indicate the wavefunction defined in the whole Hilbert space.

In the following, we derive H_{eff} (and V_{eff}) in Eq. (2.36) with the above Hamiltonian Eq. (2.53), which gives

$$H_{\text{eff}}|\phi_i\rangle = E_i|\phi_i\rangle, \quad i = 1, \cdots, d, \tag{2.56}$$

for the many-body system.

2.4.2   Kuo-Krenciglowa (KK) method

In this section, we revisit the KK method in the framework of the many-body perturbation theory. The theory is applied to degenerate P-space. As a consequence, Eq. (2.46) is lead in the framework of the time-dependent perturbation theory. In the degenerate perturbation theory, the naive perturbative treatments lead obvious divergences, originating from the zero energy denominator.

Actually, the iterative solution of the Eq. (2.46) shows that the KK method is more than a naive perturbation theory.

We start our discussion from the following Schrödinger equation written in Schrödinger picture,

$$H|\Psi_n\rangle = E_n|\Psi_n\rangle \tag{2.57}$$

with n being $n = 1, 2, \cdots, N$ where N is the dimension of the Hamiltonian matrix. The Hamiltonian consist of unperturbed H_0 and perturbation H_1,

$$H = H_0 + H_1. \tag{2.58}$$

To formulate the time-dependent perturbation theory, we move to the interaction picture. In interaction picture, the wave functions, the perturbative part of the Hamiltonian H_1 and the operator depend on the time t explicitly,

$$
\begin{aligned}
H_1^I(t) &= e^{-iH_0t} H_1 e^{iH_0t} \\
|\Psi^I(t)\rangle &= e^{-iH_0t}|\Psi^I(t)\rangle \\
\hat{O}^I(t) &= e^{-iH_0t} \hat{O} e^{iH_0t},
\end{aligned}
\tag{2.59}
$$

where the superscripts I indicate the operators and wavefunctions are written in interaction picture. In the following, we usually omit the superscripts.

Using the expressions of the interaction picture, the time-development operator is defined as the operator to develop the wave functions at the time t' to that of time t, that is,

$$|\Psi(t)\rangle = U(t, t')|\Psi(t')\rangle \tag{2.60}$$

and with the Dyson equation the time-development operator is written down as the following perturbative form,

$$U(t, t') = \lim_{\epsilon \to 0} \lim_{t' \to -\infty(1-i\epsilon)} \sum_{n=0}^{\infty} \frac{(-i)^n}{n!} \int_{t'}^{t} dt_1 \int_{t'}^{t} dt_2 \cdots \int_{t'}^{t} dt_n T[H_1(t_1)H_1(t_2) \cdots H_1(t_n)]. \tag{2.61}$$

Applying Eq. (2.59) with the notation in Eq. (2.53), the creation and annihilation operators of nucleons in interaction picture are written down simply as

$$a_i(t) = e^{-i\epsilon_i t} a_i$$
$$a_i^\dagger(t) = e^{i\epsilon_i t} a_i^\dagger. \tag{2.62}$$

Since the time-development is factorized out in this expression, one can evaluate time-development operator shown in Eq. (2.61) as a diagrammatic form in a usual manner.

Now we consider the states defined in the P-space, called parent states. First we chose the D-solutions of Eq. (2.57). Then consider a projection from the eigenvector $|\Psi_\lambda\rangle$ to $|\rho_\lambda\rangle$, $|\rho_\lambda\rangle$ being a member of P-space wave function. Therefore, the parent states $|\rho_\lambda\rangle$ can be expanded with basis space of P-space,

$$|\rho_\lambda\rangle = \sum_{\alpha=1}^{d} C_\alpha^{(\lambda)} |\psi_\alpha\rangle. \tag{2.63}$$

Taking the true eigenstates $|\Psi_\lambda\rangle$ linearly independent, we can choose the projection such that $|\rho_\lambda\rangle$ satisfies the following orthogonality conditions,

$$\langle \rho_\lambda | P\Psi_\mu \rangle = 0 \qquad (\lambda \neq \mu = 1, 2, \cdots, D). \tag{2.64}$$

Note that the parent states $|\rho_\lambda\rangle$ are only a mathematical tool, because $|\rho_\lambda\rangle$ can be calculated only knowing the effective Hamiltonian H_{eff}. This projection is not available until we know the final result H_{eff}. Therefore, the final results should not depend on the knowledge of $|\rho_\lambda\rangle$. We demonstrate the results actually does not include $|\rho_\lambda\rangle$ explicitly.

Using the orthogonality condition Eq. (2.64), the parent states correspond to true eigenstates by the following equation,

$$\frac{|\Psi_\lambda\rangle}{\langle \rho_\lambda | \Psi_\lambda \rangle} = \lim_{\epsilon \to 0} \lim_{t' \to -\infty(1-i\epsilon)} \frac{U(0, t')|\rho_\lambda\rangle}{\langle \rho_\lambda | U(0, t') |\rho_\lambda\rangle} \tag{2.65}$$

and therefore,

$$H \frac{U(0, -\infty)|\rho_\lambda\rangle}{\langle \rho_\lambda | U(0, -\infty) |\rho_\lambda\rangle} = E_\lambda \frac{U(0, -\infty)|\rho_\lambda\rangle}{\langle \rho_\lambda | U(0, -\infty) |\rho_\lambda\rangle}. \tag{2.66}$$

This imaginary time development leads us to a d lowest eigenenergies E_λ with true eigenstates of $|\Psi_\lambda\rangle$ with non-zero overlap to P-space. In the actual calculation, however, for we only calculate the effective interactions approximately, we might not necessarily obtain the lowest D eigenvalues.

Equation (2.65) can be expressed by the basis states in P-space $|\psi_\lambda\rangle$ instead of $|\rho_\lambda\rangle$, using the expansion in Eq. (2.63) as follows,

$$\sum_{\alpha=1}^{D} C_\alpha^{(\lambda)} H \frac{U(0,-\infty)|\psi_\lambda\rangle}{\langle\rho_\lambda|U(0,-\infty)|\rho_\lambda\rangle} = \sum_{\beta=1}^{D} C_\beta^{(\lambda)} E_\lambda \frac{U(0,-\infty)|\psi_\lambda\rangle}{\langle\rho_\lambda|U(0,-\infty)|\rho_\lambda\rangle}. \tag{2.67}$$

Therefore, $HU(0,-\infty)$ is nearly the effective interaction H_{eff} defined in P-space. However, the perturbative expansion of $HU(0,-\infty)$ leads a divergence immediately, because of the zero energy denominators.

The important point of KK method is the removal of those divergences. We will see that we can factorize the divergent parts of Eq. (2.67), and cancel them out. We use the familiar factorization theorem whose proof will be presented in Appendix B. The factorization theorem tells us that a diagram consist of several disconnected pieces can be evaluated by the product of those individual pieces. We factorize the numerator and denominators in Eq. (2.67), focusing on the states consist of two-particle plus the inert core.

Let us start from the numerator. The factor $U(0,-\infty)|\psi_\alpha\rangle$ includes all the contributions of the time development of two particles plus the core states. Then, we can factorize the contribution which has no connection to any of the valence states as follows:

$$U(0,-\infty)|\psi_\alpha\rangle = U_V(0,-\infty)a_i^\dagger a_j^\dagger|c\rangle \times U(0,-\infty)|c\rangle, \tag{2.68}$$

where the subscript V indicates the fact that the diagram has at least one connected valence line. The first factor indicates the contributions of the process starting from two particles plus core and the second factor is considered to be insertion of bubble diagrams and the contribution terminate at $t = 0$ as a states with equal numbers of particles and holes. We can express this consideration explicitly using the factorization theorem again,

$$U(0,-\infty)|c\rangle = U_Q(0,-\infty)|c\rangle \times \langle c|U(0,-\infty)|c\rangle, \tag{2.69}$$

where the subscript Q means the diagram terminate as the state of Q-space at $t = 0$.

The first term of Eq. (2.68) $U_V(0,-\infty)|\psi_\alpha\rangle$ experiences the similar decomposition as Eq. (2.69). As final states of the time development by $U_V(0,-\infty)$, the states results in the states within P-space and the states within Q-space at the time $t = 0$, that is,

$$U_V(0,-\infty)|\psi_\alpha\rangle = |\chi_P\rangle + |\chi_Q\rangle. \tag{2.70}$$

where $|\chi_P\rangle$ is the term which terminates at $t = 0$ as P-space state and $|\chi_Q\rangle$ terminates as Q-space state.

For further decomposition, we introduce two things. One is $\hat{Q}$-box and the other is folded diagrams. The $\hat{Q}$-box is defined as

$$
\begin{aligned}
\hat{Q}(E) &= PVP + PVQ\frac{1}{E - QHQ}QVP \\
&= PVP + PVQ\frac{1}{E - QH_0Q}QVP + PVQ\frac{1}{E - QH_0Q}QVQ\frac{1}{E - QH_0Q}QVP + \cdots \quad (2.71)
\end{aligned}
$$

which is already appeared in the formal theory of KK method and LS method (See Eq. (2.45)). The $\hat{Q}$-box is the summation of all the contributions of the irreducible diagrams. Here the term irreducible means that the diagrams cannot be divided into two pieces by cutting the P-space states by horizontal lines. Therefore, in the evaluation of $\hat{Q}$-box, we do not face to the divergence caused by the zero energy-denominator, if the P-space is degenerate and the unperturbed Q-space energy is different from that of P-space.

Next, we move to the folded diagrams. Let us consider a diagram which includes two vertices at $t = t_1$ and $t = t_2$, with $0 > t_1 > t_2$. When the state before $t = t_2$ and after $t = t_2$ are the same, clearly we face to the zero denominator. This divergence can be factorized as follows:

$$
\begin{array}{cc}
t_1 \\
t_2
\end{array}
\quad = \quad
t_1
\quad \times \quad
t_2
\quad - \quad
t_1 \quad^{t_2} . \tag{2.72}
$$

In the left hand side, $0 > t_1 > t_2$, and in the right hand side, the first term does not have the restriction of ordering and the second term is the corresponding subtraction of $0 > t_2 > t_1$. Suppose the railed line is in Q-space and the other is in P-space. Since P-space is degenerate, the left hand side is obviously divergent. In the right hand side, the divergence only appears in the second factor in the first term. In this sense, Eq. (2.72) shows a minimal example of factorization of the divergence. Our purpose of implementing the factorization theorem and folded diagram procedure is that we factorize the divergence and cancel them so that we obtain the finite physical results.

Now we come back to the factorization of Eq. (2.70). Both the first and second term include the divergences. The first term $|\chi_P\rangle$, which terminates at $t = 0$ as P-space state, is expressed as

$$
|\chi_P\rangle = \quad \Big| \quad + \quad \bullet \quad + \quad \bullet\!\!\bullet \quad + \quad \bullet\!\!\bullet\!\!\bullet \quad + \cdots \tag{2.73}
$$

where filled circles represent the $\hat{Q}$-box and the line is the two-body states within P-space. Since we are considering of the degenerate P-space, this leads a clear divergence. On the other hand, the

second term $|\chi_Q\rangle$, which terminates as Q-space at $t = 0$, is written as follows,

$$|\chi_Q\rangle = \text{[diagram]} + \text{[diagram]} + \text{[diagram]} + \cdots$$

$$= \left(\text{[diagram]} - \text{[diagram]} \int \text{[diagram]} + \text{[diagram]} \int \text{[diagram]} \int \text{[diagram]} - \cdots \right) \tag{2.74}$$

$$\times \left(\text{[diagram]} + \text{[diagram]} + \text{[diagram]} + \text{[diagram]} + \cdots \right)$$

where integral represent the folding procedure. The railed lines represent the states within Q-space. The folded diagrams here are defined as the contribution of the end of the former $\hat{Q}$-box is placed after the beginning latter $\hat{Q}$-box. Note that the second factor is the exactly $|\chi_P\rangle$. Equivalently we can write down the above as follows,

$$U_V(0, -\infty)|\psi_\alpha\rangle = \sum_{\beta=1}^{D} U_{VQ}(0, -\infty)|\psi_\beta\rangle\langle\psi_\beta|U_V(0, -\infty)|\psi_\alpha\rangle. \tag{2.75}$$

where U_{VQ} represent the contributions of the first factor in Eq. (2.74). The point is that the divergence is only appearing in the second factor in Eq. (2.75).

Combining Eqs. (2.68), (2.70), (2.74), (2.75) together,

$$U(0, -\infty)|\psi_\alpha\rangle = U_Q(0, -\infty)|c\rangle\langle c|U(0, -\infty)|c\rangle \times \sum_{\beta=1}^{d} U_{VQ}(0, -\infty)|\psi_\beta\rangle\langle\psi_\beta|U_V(0, -\infty)|\psi_\alpha\rangle \tag{2.76}$$

Then, Eq. (2.67) reads,

$$\sum_{\gamma=1}^{d} b_\gamma^\lambda HU_Q(0, -\infty)|c\rangle U_{VQ}(0, -\infty)|\psi_\gamma\rangle = \sum_{\delta=1}^{d} b_\delta^\lambda E_\lambda U_Q(0, -\infty)|c\rangle U_{VQ}(0, -\infty)|\psi_\gamma\rangle \tag{2.77}$$

where $b_\gamma^{(\lambda)}$ is defined as

$$b_\gamma^{(\lambda)} = \sum_{\alpha=1}^{d} C_\alpha^{(\lambda)} \frac{\langle\psi_\gamma|U_V(0, -\infty)|\psi_\alpha\rangle\langle c|U(0, -\infty)|c\rangle}{\langle\rho_\lambda|U(0, -\infty)|\rho_\lambda\rangle} \tag{2.78}$$

Note that there are divergences in the numerator and the denominator and they are canceled out. Then, the coefficient $b_\gamma^{(\lambda)}$ is finite.

Now we define an operator U_L as follows,

$$U_L(0, -\infty)|\psi_\alpha\rangle \equiv U_{VQ}(0, -\infty)|\psi_\alpha\rangle U_Q(0, -\infty)|c\rangle, \tag{2.79}$$

meaning that the contribution is linked diagrams.

Using the fact that

$$\langle \psi_\beta | U_{VQ}(0, -\infty) | \psi_\alpha \rangle = \delta_{\alpha\beta}, \tag{2.80}$$

and multiplying $\langle \psi_\sigma |$ from the left we obtain,

$$\sum_{\gamma=1}^{d} b_\gamma^{(\lambda)} \langle \psi_\sigma | H U_L(0, -\infty) | \psi_\lambda \rangle = E_\lambda | \psi_\sigma \rangle. \tag{2.81}$$

Then we obtain the following secular equation defined only within P-space,

$$P H_{\text{eff}} P | \Psi_\lambda \rangle = E_\lambda P | \Psi_\lambda \rangle \tag{2.82}$$

where H_{eff} is determined by

$$H_{\text{eff}} = \langle \psi_\sigma | H U_L(0, -\infty) | \psi_\lambda \rangle. \tag{2.83}$$

From Eq. (2.82), we can extract the core degrees of freedom. If the final interaction does not finish with valence particles, it gives the energy of the core. Therefore, defining $H_0(V)$ and $H_1(V)$ as those related to valence particles, we can extract the energy of the core as follows,

$$P H_{\text{eff}} P | \Psi_\alpha \rangle = (E_\alpha - E_C) P | \Psi_\alpha \rangle \tag{2.84}$$

where

$$H_{\text{eff}} = \langle \psi_\sigma | (H_0(V) + H_1(V)) U_L(0, -\infty) | \psi_\lambda \rangle. \tag{2.85}$$

The presence of $H_0(V)$ and $H_1(V)$ means the diagram must terminate with valence particles at the time $t = 0$. Then we have succeeded to extract the energy of the core. The next problem is how to calculate the $\langle \psi_\beta | U_{VQ}(0, -\infty) | \psi_\alpha \rangle$ in a practical way. This factor corresponds to the first factor of Eq. (2.74) and is calculated by the evaluation of $\hat{Q}$-box and its folded diagram.

In summary, the effective interaction V_{eff} can be calculated as follows,

$$V_{\text{eff}} = \hat{Q}(\epsilon_0) - \hat{Q}'(\epsilon_0) \int \hat{Q}(\epsilon_0) + \hat{Q}'(\epsilon_0) \int \hat{Q}(\epsilon_0) \int \hat{Q}(\epsilon_0) \cdots, \tag{2.86}$$

where the integrals represent the folding procedures, and $\hat{Q}'$ represents $\hat{Q}$-box contributions which have at least two *NN* interaction vertices. Note that, in order to have a degenerate P-space energy, ϵ_0, the single-particle energies in Eq. (2.53) for valence single-particle states, ϵ_a, $\epsilon_b, \ldots$ are completely degenerate. Equation (2.86) is the basis of the perturbative expansion of V_{eff} in the folded diagram theory (see for example Ref. [11] for more details).

There are two points to be noted here. First, because we cannot evaluate the $\hat{Q}$-box defined in Eq. (2.45) exactly (which implies including all terms to infinite order), we use the perturbative

expansion in Eq. (2.71), which we can currently evaluate up to the third order in the *NN* interaction. Second, the valence-linked diagram theorem states that we need to retain only the valence-linked part (See Fig. 2.3), i.e., unlinked parts can be proved to cancel among themselves [11, 23]. At the same time, the eigenvalue E_i in Eq. (2.56) changes its meaning; it is no longer the total energy of the system, but is now the total energy measured from the true ground state energy of the core.

In actual calculations, however, we do not calculate V_{eff} order by order using Eq. (2.86). Since the contribution of folded diagrams can be calculated by energy derivatives when the model space is degenerate (see Appendix B), we can translate Eq. (2.86) into the following equation

$$V_{\text{eff}} = \hat{Q}(\epsilon_0) + \sum_{k=1}^{\infty} \hat{Q}_k(\epsilon_0)\{V_{\text{eff}}\}^k, \tag{2.87}$$

The above expression clearly shows that the iterative solution of Eq. (2.46) reaches at V_{eff} in the limit of $n \to \infty$ if it converges [11].

We can summarize the KK method as follows; we calculate the valence-linked $\hat{Q}$-box diagrams (usually up to second or third order) and the corresponding energy derivatives at the degenerate P-space energy ϵ_0, and carry out the iteration of Eq. (2.46) starting from $V_{\text{eff}}^{(0)} = V$. This procedure ultimately gives $V_{\text{eff}} = V_{\text{eff}}^{(\infty)}$.
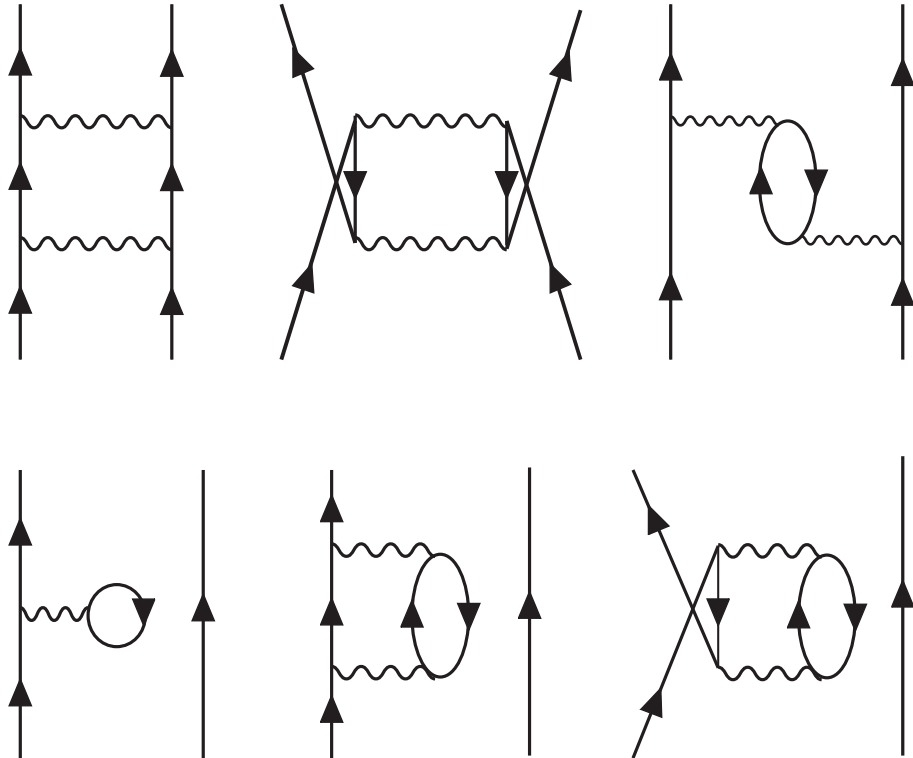

Figure 2.3: Valence-linked $\hat{Q}$-box diagrams up to second order in *V*.

At the end, we stress again that the above KK method can yield V_{eff} only for a degenerate model space. Suppose we are working with the harmonic oscillator shell model of ^{18}O, treating ^{16}O as the

core. If we take the P-space composed only of the degenerate sd-shell, the above KK method works well as shown by many applications (see for example Ref. [29]). If, on the other hand, we take an enlarged P-space defined by the non-degenerate $sd f_{7/2} p_{3/2}$-shell, the KK method breaks down. A naive calculation of V_{eff} by Eq. (2.86) easily leads to divergences of the $\hat{Q}$-box, as we shall see later.

Chapter 3

Extended Kuo-Krenciglowa method

In this chapter, we explain how the Extended Kuo-Krenciglowa (EKK) method is implemented. As we stressed repeatedly, there has not been existing a microscopic method to derive the effective interaction in arbitrary non-degenerate model space. Focusing on the difference between KK method, we will explore the new method which is able to be applied to not only degenerate but non-degenerate model space. In Sec. 3.1, formal theory of EKK method is presented, which is mainly a summary of references [1, 2].

After Sec. 3.2 is the original work for this thesis. In Sec. 3.2, EKK method in many-body systems is presented. The formulation based on the folded-diagram method. Based on the second-quantized form and the time-dependent perturbation theory, the folded-diagram theory formulated in KK method can be applied also in this case with some modifications. However, there are a few non-trivial point in the formulation and application of the folded diagrams in EKK method. Those things are discussed in Appendix A and Appendix B more precisely.

As we will explain in Sec. 3.1 and Sec. 3.2, in EKK method an arbitrary parameter E with the dimension of energy is introduced. Section 3.3 is devoted to explain the properties and the usage of the parameter E. The numerical results are not presented in this chapter and will be presented in Chap. 4.

3.1 Formal extended Kuo-Krenciglowa (EKK) method

The EKK method is designed to construct an effective Hamiltonian H_{eff} for non-degenerate model spaces [1, 2].

For the completeness, we start from repeating the discussion for the KK method. The similarity transformation of the Hamiltonian is as follows,

$$\mathcal{H} = e^{-\omega} H e^{\omega} \tag{3.1}$$

where the operator ω satisfies the following relation,

$$Q\omega P = \omega \tag{3.2}$$

Then we impose the decoupling condition for the transformed Hamiltonian $\mathcal{H}$,

$$0 = Q\mathcal{H}P = QVP - \omega PHP + QHQ\omega - \omega PVQ\omega, \tag{3.3}$$

which decouples the P-space Schrödinger equation to Q-space.

Now we rewrite Eq. (3.3) as

$$(E - QHQ)\omega = QVP - \omega P\tilde{H}P - \omega PVQ\omega, \tag{3.4}$$

where

$$\tilde{H} = H - E \tag{3.5}$$

is a shifted Hamiltonian obtained by the introduction of the energy parameter E. Equation (3.4) plays the same role in the EKK method as Eq. (2.42) does in the KK method. The difference is that we introduce a parameter E and replace PVP by $P\tilde{H}P$. By solving Eq. (3.4) iteratively as in the KK method, we obtain the following iterative scheme to calculate the effective Hamiltonian H_{eff} instead of V_{eff},

$$\tilde{H}_{\text{eff}}^{(n)} = \tilde{H}_{\text{BH}}(E) + \sum_{k=1}^{\infty} \hat{Q}_k(E)\{\tilde{H}_{\text{eff}}^{(n-1)}\}^k, \tag{3.6}$$

where

$$\tilde{H}_{\text{eff}} = H_{\text{eff}} - E, \quad \tilde{H}_{\text{BH}}(E) = H_{\text{BH}}(E) - E, \tag{3.7}$$

and $\tilde{H}_{\text{eff}}^{(n)}$ stands for $\tilde{H}_{\text{eff}}$ at the n-th step. The effective Hamiltonian H_{eff} is obtained as $H_{\text{eff}} = H_{\text{eff}}^{(\infty)}$, and satisfies

$$\tilde{H}_{\text{eff}} = \tilde{H}_{\text{BH}}(E) + \sum_{k=1}^{\infty} \hat{Q}_k(E)\{\tilde{H}_{\text{eff}}\}^k. \tag{3.8}$$

The effective interaction, V_{eff}, is then calculated by Eq. (2.36) as $V_{\text{eff}} = H_{\text{eff}} - PH_0P$. Here the definition of $\hat{Q}$-box is the same as KK method, that is,

$$\hat{Q}(E) = PVP + PVQ\frac{1}{E - QHQ}QVP, \tag{3.9}$$

and the derivative of $\hat{Q}$-box is

$$\hat{Q}_k(E) = \frac{1}{k!}\frac{\mathrm{d}^k\hat{Q}(E)}{\mathrm{d}E^k}. \tag{3.10}$$

Let us now compare the EKK and the KK methods. First, and most importantly, the above EKK method does not require that the model space is degenerate. It can, therefore, be applied naturally to a valence space composed of several shells. Second, Eq. (3.6) changes $\tilde{H}_{\text{eff}}$, while Eq. (2.46) changes only V_{eff} at each step of the iterative process. Third, in order to perform the iterative step of Eq. (3.6), we need to calculate $\hat{Q}_k(E)$ at the arbitrarily specified energy E, instead of at ϵ_0 for Eq. (2.46).

Equation (3.8) is interpreted as the Taylor series expansion of $\tilde{H}_{\text{eff}}$ around $\tilde{H}_{\text{BH}}(E)$, and changing E corresponds to shifting the origin of the expansion, and therefore to a re-summation of the series. This explains why the left hand side of Eq. (3.8) is independent of E, while each term on the right hand side depends on E. This in turn means that we can tune the parameter E in Eq. (3.8) to accelerate the convergence of the series on the right hand side, a feature which we will exploit in actual calculations.

3.2 Extended Kuo-Krenciglowa method in many-body system

Here we derive the effective Hamiltonian H_{eff} of the Extended Kuo-Krenciglowa (EKK) method, with an emphasis on its similarity with the KK method discussed in the Chap. 2.

3.2.1 Derivation of the Extended Kuo-Krenciglowa method

We consider first the general situation where the energies of the valence single-particle states in PH_0P are not necessarily degenerate. In this case, we have to apply the EKK formula Eq. (3.6) to our many-body systems.

We start from the Hamiltonian in many-body system,

$$
\begin{aligned}
H &= H_0 + V \\
&= \sum \epsilon_\alpha a_\alpha^\dagger a_\alpha + \frac{1}{2} \sum_{\alpha\beta,\gamma\delta} V_{\alpha\beta,\gamma\delta} a_\alpha^\dagger a_\beta^\dagger a_\delta a_\gamma,
\end{aligned} \tag{3.11}
$$

We can confirm that, in order to derive Eq. (3.6), we need to change the decomposition Eq. (2.53) of the Hamiltonian in the KK method. Suppose we decompose the total Hamiltonian into the following unperturbed Hamiltonian H_0' and the perturbation V'

$$
\begin{aligned}
H_0' &= PEP + QH_0Q \\
V' &= V - P(E - H_0)P,
\end{aligned} \tag{3.12}
$$

or in the matrix form,

$$
\begin{aligned}
H &= H_0' + V' \\
&= \begin{pmatrix} E & 0 \\ 0 & QH_0Q \end{pmatrix} + \begin{pmatrix} P\tilde{H}P & PVQ \\ QVP & QVQ \end{pmatrix},
\end{aligned} \tag{3.13}
$$

where $\tilde{H} \equiv H - E$. With the above unperturbed Hamiltonian H_0' in Eq. (3.12), we can treat the P-space as being degenerate at the energy E, and therefore we can follow the derivation of Eq. (2.86) in the KK method, to achieve

$$
\tilde{H}_{\text{eff}} = \tilde{H}_{\text{BH}}(E) - \hat{Q}'(E) \int \tilde{H}_{\text{BH}}(E) + \hat{Q}'(E) \int \tilde{H}_{\text{BH}}(E) \int \tilde{H}_{\text{BH}}(E) \cdots, \tag{3.14}
$$

which is then converted into

$$
\tilde{H}_{\text{eff}} = \tilde{H}_{\text{BH}}(E) + \frac{d\hat{Q}(E)}{dE} \tilde{H}_{\text{eff}} + \frac{1}{2!} \frac{d^2\hat{Q}(E)}{dE^2} \{\tilde{H}_{\text{eff}}\}^2 + \cdots . \tag{3.15}
$$

The point is that the derivative of $\hat{Q}$-box is the same as derivative of H_{BH}. Since the $\hat{Q}$-box include the interaction of QVP, PVQ and QVQ, all the interaction vertices are not affected by the shift of unperturbed Hamiltonian from H_0 to H_0'.

Note that Eqs. (3.14) and (3.15) are the EKK counterparts of Eqs. (2.86) and (2.87) of the KK method. We can solve Eq. (3.15) iteratively as done for Eq. (2.87).

Note that the above derivation of the EKK method is the same as that of the KK method apart from the decomposition of the Hamiltonian. However, for the application of EKK method to actual problems, there are several non-trivial questions.

The first question is, the diagram rules for EKK method. Since we have the different unperturbed Hamiltonian, the diagram rules have to be modified. Actually, as we will see in the next section, for our unperturbed Hamiltonian is defined for the two-body states, the energy denominator is not sum of all the single-particle energies in some cases.

Second question is the factorization theorem. In the derivation of Eqs. (3.14) and (3.15), we need to apply the factorization theorem to remove the divergences appearing in the theory. However, the straightforward application of the factorization theorem to EKK method might not be possible, because the diagram rules are slightly different.

As a consequence, we need to retain only the valence-linked $\hat{Q}$-box diagrams in Eqs. (3.14) and (3.15), as we do for the KK method. To summarize, all that we have to know is, as in the KK method, the $\hat{Q}$-box and its energy derivatives, except that now it is defined at the parameter E.

3.2.2   Perturbative expansion of the $\hat{Q}$-box

We discuss here how one can accommodate the perturbative expansion of the $\hat{Q}$-box in the EKK formalism. For the sake of simplicity, we will focus on a simple system composed of two particles on top of a closed-shell core in what follows, although the discussion is not restricted to this specific case. The projection operators P and Q are then given by

$$P = \sum_{a,b} a_a^\dagger a_b^\dagger |c\rangle\langle c| a_b a_a, \quad Q = 1 - P. \tag{3.16}$$

where $|c\rangle$ stands for the closed-shell core.

To become familiar with our new unperturbed Hamiltonian, H_0', we consider some selected examples; we show first the results from the operation of the new unperturbed Hamiltonian, H_0', on some selected many-particle states shown in Fig. 3.1:

$$
\begin{aligned}
\text{(i)} \quad & H_0' \, a_a^\dagger a_b^\dagger |c\rangle = E \, a_a^\dagger a_b^\dagger |c\rangle, \\
\text{(ii)} \quad & H_0' \, a_a^\dagger a_p^\dagger |c\rangle = (\epsilon_a + \epsilon_p) \, a_a^\dagger a_p^\dagger |c\rangle, \\
\text{(iii)} \quad & H_0' \, a_a^\dagger a_b^\dagger a_p^\dagger a_h |c\rangle = (\epsilon_a + \epsilon_b + \epsilon_p - \epsilon_h) \, a_a^\dagger a_b^\dagger a_p^\dagger a_h |c\rangle.
\end{aligned}
\tag{3.17}
$$

Here we denote the single particle states in the valence orbits by $a, b, \cdots$, the particle states outside of the valence orbits by $p, q, \cdots$ and the hole states by h. The first line is an example of a P-space state with two single-particle states on top of the closed-shell core, $|c\rangle$, while the second and third lines result in Q-space examples. The unperturbed energy of the P-space state $a_a^\dagger a_b^\dagger |c\rangle$ is E, while that of a Q-space state $a_a^\dagger a_p^\dagger |c\rangle$ results in $\epsilon_a + \epsilon_p$, a sum of unperturbed single-particle energies. It is important to
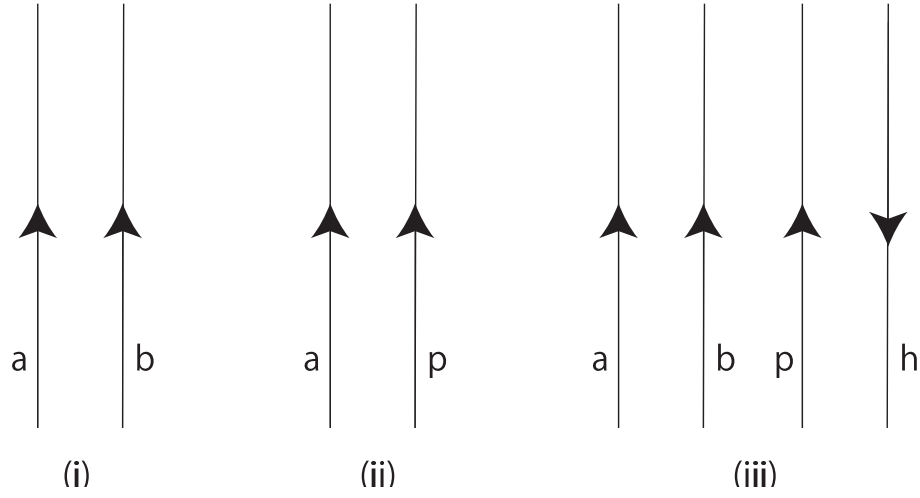
Figure 3.1: The examples of the states consist of core plus two particles. The diagram (i) is in P-space and (ii) and (iii) are in Q-space.

get convinced that in diagram (iii) contains the single particle states of diagram (i), but as a whole, the state is in Q-space. In diagram (ii), although the state a is in one of the valence orbits, the two-body state as a whole is not in P-space. Therefore ϵ_a appears only in the Q-space energy, while $a_a^\dagger$ appears in all of the above three states.

To implement the time dependent perturbation theory, we need to move onto the interaction picture. The interaction picture for those states are different from that of in KK method;

$$
\begin{aligned}
|\psi_i(t)\rangle &= e^{-iH_0' t}|\psi_i\rangle & &= e^{-iEt}|\psi_i\rangle \\
\{a_a^\dagger a_p^\dagger |c\rangle\}(t) &= e^{-iH_0' t}\{a_a^\dagger a_p^\dagger |c\rangle\} & &= e^{-i(\epsilon_a+\epsilon_p)t}a_a^\dagger a_p^\dagger |c\rangle, \\
\{a_a^\dagger a_b^\dagger a_p^\dagger a_h|c\rangle\}(t) &= e^{-iH_0' t}\{a_a^\dagger a_b^\dagger a_p^\dagger a_h|c\rangle\} & &= e^{-i(\epsilon_a+\epsilon_b+\epsilon_p-\epsilon_h)t}a_a^\dagger a_b^\dagger a_p^\dagger a_h|c\rangle,
\end{aligned}
\tag{3.18}
$$

where $|\psi_i\rangle$ is the state of P-space. It is important to notice that Eq. (2.59) is no longer valid for the Hamiltonian of EKK method. This is because the expression of H_0',

$$
H_0' = PEP + Q\sum \epsilon_\alpha a_i^\dagger a_i Q
\tag{3.19}
$$

includes projection operator to the core state wave function in the projection operator P and Q. The commutations $[H_0, a]$ and $[H_0, a^\dagger]$ are not as simple as that in KK method.

Nevertheless, because Eq. (3.18) holds, we can retain the diagrammatic approach of EKK method with a small modification of the evaluation of the diagram. The modification is that when we find the two-body states in the P-space, we replace the energy denominator of that point to E instead of the sum of single-particle energies. Corresponding to the fact that the diagram (iii) in Fig. 3.1 is in Q-space, the energy denominator for the diagram (iii) is not $E + \epsilon_p - \epsilon_h$, but $\epsilon_a + \epsilon_b + \epsilon_p - \epsilon_h$. In the perturbative expansion of $\hat{Q}(E)$ in Eq. (2.71), all the intermediate states are in the Q-space, and their unperturbed energies are given as in (ii) and (iii) of the above example. The general structure of $\hat{Q}(E)$

can then be given schematically by

$$\hat{Q}(E) = \prod \frac{V}{E - (\sum \epsilon_a + \sum \epsilon_p - \sum \epsilon_h)_{int}}, \tag{3.20}$$

where the subscript *int* indicates intermediate states between two interaction vertices. Note that the parameter E appears in all the denominators in the EKK method.

To make our diagram rules clear, let us see an example. The diagram shown in Fig. 3.2 is a
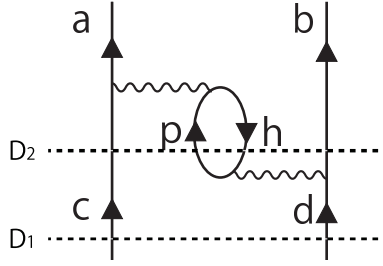

Figure 3.2: Core-polarization diagram as a second-order contribution to the $\hat{Q}$-box. The energy denominator is written as D_1 and D_2.

member of $\hat{Q}$-box diagram. The diagram is a contribution from the second-order term in Eq. (2.71). The energy denominator for the lower dashed line is denoted as D_1 and for the intermediate state we use D_2, and the energy denominator of this diagram should be calculated as $D_1 - D_2$. Therefore, it gives the following contribution to $\hat{Q}(E)$

$$\text{Fig. 3.2 (EKK)} \rightarrow \frac{V_{ah,cp}V_{pb,hd}}{E - \epsilon_c - \epsilon_b - \epsilon_p + \epsilon_h}. \tag{3.21}$$

If we on the other hand employ the KK method in order to calculate the contribution to $\hat{Q}(\epsilon_0)$ from Fig. 3.2, we would get

$$\begin{aligned} \text{Fig. 3.2 (KK)} \quad \rightarrow \quad & \frac{V_{ah,cp}V_{pb,hd}}{(\epsilon_c + \epsilon_d) - \epsilon_c - \epsilon_p + \epsilon_h - \epsilon_b} \\ = \quad & \frac{V_{ah,cp}V_{pb,hd}}{-\epsilon_p + \epsilon_h} \end{aligned} \tag{3.22}$$

where, in going to the second line, we have used the fact that the *P*-space is degenerate, and therefore $\epsilon_a = \epsilon_b = \epsilon_c = \epsilon_d$ and $\epsilon_c + \epsilon_d = \epsilon_0$.

Two points should be noted from the above example; first, in a degenerate model space, the EKK result Eq. (3.21) with $E = \epsilon_0$ coincides with the KK result Eq. (3.22). This is a direct consequence of the fact that the EKK formula contains the KK formula as a special case. Second, we can see the problem of divergence of the KK formula applied naively to a non-degenerate model space. Consider the case of ^{18}O as an example, and let the *P*-space consist of two major shells ($1s0d$ and $1p0f$-shells). The single particle states are taken as the eigenstates of harmonic oscillator potential. Then, the denominator of the first line in Eq. (3.22) vanishes for $b, c, p \in 1s0d$-shell, $a, d \in 1p0f$-shell, and

$h \in 0p$-shell, leading thereby to a divergence. The above mechanism is just one of many examples which show that we really need to use the EKK formalism in order to derive effective interactions for model spaces consisting of several shells.

For the next point, let us discuss the problem of factorization theorem. Factorization theorem in KK method is proved in the Appendix A to see the difference of KK method and EKK method better. The factorization theorem tells us that the diagram consist of disconnected pieces can be evaluated by the product of individual pieces. As we will discuss in Appendix A, in the proof of factorization theorem, we use the fact that the energy denominator is calculated by the sum of the energy denominators of individual disconnected pieces. However, in EKK method, for some cases this is not true.

Let us see the example shown in Fig. 3.3. The particle states a and b are in the valence orbits and
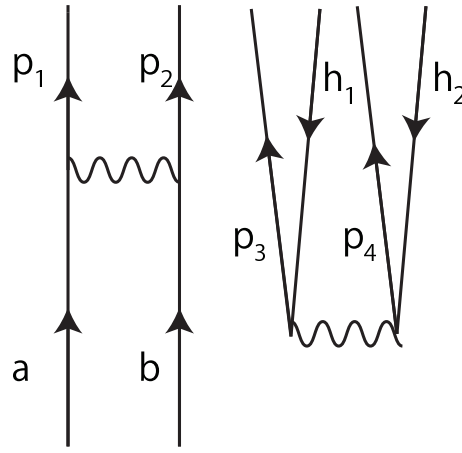
Figure 3.3: An example of the diagram consist of two disconnected pieces. The particle states a, b are in the model space and p_1, p_2, p_3, p_4 are in outside the model space. h_1, h_2 denote the hole states.

$p_1, \cdots, p_4$ are outside of the valence orbits and h_1, h_2 denote hole states. The energy denominator calculated with KK method is,

$$\text{Fig. 3.3 (KK)} \rightarrow \frac{1}{0 + \epsilon_{p3,p4}^{h1,h2}} \times \frac{1}{(\epsilon_a + \epsilon_b + \epsilon_{p1,p2} + \epsilon_{p3,p4}^{h1,h2})} \tag{3.23}$$

where $\epsilon_{\alpha,\beta}^{i,j}$ is the abbreviation of

$$\epsilon_{\alpha,\beta}^{i,j} = -\epsilon_\alpha - \epsilon_\beta + \epsilon_i + \epsilon_j. \tag{3.24}$$

As we mentioned, the energy denominator is obviously expressed as the sum of the denominator of left piece and right piece.

On the other hand, the energy denominator calculated in EKK method is,

$$\text{Fig. 3.3 (EKK)} \rightarrow \frac{1}{(E + \epsilon_{a,b} + \epsilon_{p3,p4}^{h1,h2})} \times \frac{1}{(E + \epsilon_{p1,p2} + \epsilon_{p3,p4}^{h1,h2})}. \tag{3.25}$$

The second denominator is actually the summation of the denominator of the left piece and the right piece. However, the first energy denominator is not. Without the right piece, the intermediate state of

the left piece is $a_a^\dagger a_b^\dagger |c\rangle \in P$. However, for the total state is $a_a^\dagger a_b^\dagger a_{p3}^\dagger a_{p4}^\dagger a_{h1} a_{h2} |c\rangle \in Q$, the denominator should be evaluated by the sum of single-particle energies present. The resultant denominator is no longer the sum of individual denominators.

With this diagram rule the factorization theorem is no longer valid. We saw in Chap. 2, that we need to factorize the divergence appearing in the perturbation theory (see Eqs. (2.68), (2.70), (2.74), (2.75)). For naive factorization theorem does not hold in EKK method, we need a further resummation to utilize the same equations in EKK method. We rewrite the Hamiltonian as follows:

$$
\begin{aligned}
H &= H_0 + V \\
&= H_0' + V' \\
&= H_0' - P(E - H_0)P + V \\
&= H_0' + V_1 + V,
\end{aligned}
\tag{3.26}
$$

where $V_1 = -P(E - H_0)P$ defined purely in P-space is to be regarded as perturbation as well. What we want to prove now is, for example, that the factorization like

$$
U(0, -\infty)|\psi_\alpha\rangle = U_V(0, -\infty)a_i^\dagger a_j^\dagger |c\rangle \times U(0, -\infty)|c\rangle
\tag{3.27}
$$

still hold in EKK method. We consider the following resummation ; once we find the state in P-space, we insert V_1 interaction up to infinite order. Explicitly, for a P-space state $|\psi_i\rangle = a_a^\dagger a_b^\dagger |c\rangle$ in interaction picture of EKK Hamiltonian,

$$
|\psi_i(t)\rangle = e^{-iEt}|\psi_i\rangle
\tag{3.28}
$$

is changed as follows,

$$
\begin{aligned}
Pe^{iV_1 t}P|\psi_i(t)\rangle &= Pe^{i(E-H_0)t}P|\psi_i(t)\rangle \\
&= e^{-iH_0 t}|\psi_i\rangle \\
&= e^{-i(\epsilon_a + \epsilon_b)t}|\psi_i\rangle.
\end{aligned}
\tag{3.29}
$$

With this transformation, the energy denominators are always the sum of individual pieces. Schematically, the factorization shown in Eq. (3.27) and the insertion of V_1 are shown in Fig. 3.4. The other necessary factorizations are also true with the same discussion. Once we know that the factorizations hold with the insertion of V_1 up to infinite order, we know that the factorization can be performed and we can remove the divergences in the same way as in KK method. Here we have to stress that in the actual calculation, however, we do not need to insert V_1 every time. After removing the divergence by use of folded diagrams, we calculate $\hat{Q}$-box with the Hamiltonian $H = H_0' + V'$, with the diagram rules we discussed.

Finally we obtain the following iterative formula,

$$
\tilde{H}_{\text{eff}}^{(n)} = \tilde{H}_{\text{BH}}(E) + \sum \hat{Q}_k(E)\{\tilde{H}_{\text{eff}}^{(n-1)}\}^k.
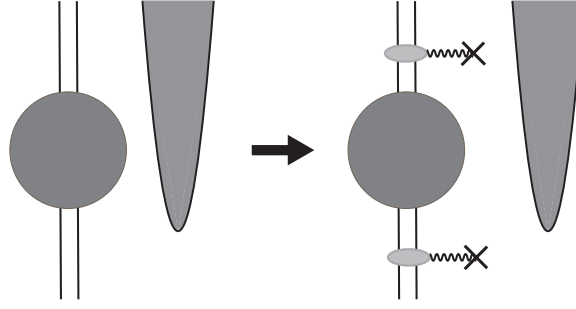\tag{3.30}
$$

Figure 3.4: Insertion of V_1 in EKK method. The wavy line and the cross indicate the insertion of V_1 interaction up to infinite order in perturbation. The pairs of lines indicate the two-body states in P-space and the gray circles and parabolas are the states in Q-space.

3.2.3 Poles of $\hat{Q}$-box

In this subsection, we analyze the positions of the poles of the $\hat{Q}$-box. It will be proved later that the poles of the $\hat{Q}$-box are not located at the energies no lower than certain point.
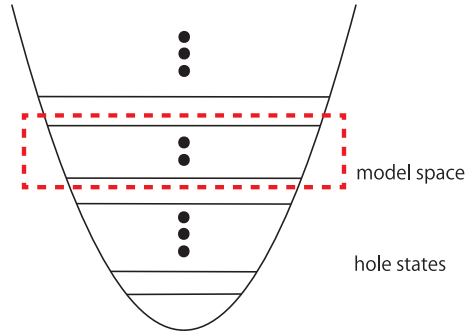

Figure 3.5: The harmonic oscillator potential. The red dashed square indicates the model space.

Figure 3.5 shows the schematic figure of unperturbed orbitals, which is often taken as the harmonic oscillator eigenstates, and the valence particle states. The red dashed square represent the position of P-space and the orbits below the box are the hole states and above the box are particle states outside the model space. The positions of the poles of $\hat{Q}$-box are easily extracted from Eq. (3.20),

$$E_{pole} = \sum_{int} (\epsilon_a + \epsilon_p - \epsilon_h). \tag{3.31}$$

Let us put the largest single particle energy of the hole state as ϵ_h^{max} and the smallest single particle energy of the particle state as ϵ_p^{min}. Now we are concerning is two-body states. Therefore, in any of intermediate states, the number of particles N_p and the number of holes N_h fulfill the following relation,

$$N_p - N_h = 2, \quad N_h \geq 0 \tag{3.32}$$

Therefore, the following inequality holds for positions of the poles of $\hat{Q}$-box for $N_h \neq 0$,

$$
\begin{aligned}
E_{pole} &\geq N_p \epsilon_p^{min} - N_h \epsilon_h^{max} \\
&= (N_h + 2)\epsilon_p^{min} - N_h \epsilon_h^{max} \\
&= N_h(\epsilon_p^{min} - \epsilon_h^{max}) + 2\epsilon_p^{min},
\end{aligned}
\tag{3.33}
$$

and if $N_h = 0$ and $N_p = 2$ the intermediate states are constructed only with particles and hence at least one particle should be outside of model space,

$$
E_{pole} \geq \epsilon_p^{min} + \epsilon_p^{min+1},
\tag{3.34}
$$

where ϵ_p^{min+1} is the smallest single particle energy of the particle state outside of the model space.

Suppose the single particle states are the eigenstates of harmonic oscillator potential. In this case, the single particle energies are located equal spacing of $\hbar\omega$, which means $\epsilon_p^{min} - \epsilon_h^{max} = \hbar\omega$. Then, combined Eq. 3.33 and Eq. 3.34, the lowest position of the pole can be determined with the following inequality of $N_h = 1$,

$$
E_{pole} \geq E_{pole}^{min} = 2\epsilon_p^{min} + \hbar\omega.
\tag{3.35}
$$

Therefore, the parameter E should be at least less than E_{pole}^{min}. Actually, if E is too close to E_{pole}^{min}, the energy denominator is too small and the iteration does not converge and the perturbation also does not work. On the other hand, if E is too small and far from E_{pole}^{min}, the contribution to $\hat{Q}$-box is too small and we need to include intractably large $n\hbar\omega$ excitations.

3.3   The energy parameter E

Here we make several points in connection with the new parameter E in the EKK theory.

First, by virtue of the arbitrariness of the parameter E, we can get around the problems of the poles of the $\hat{Q}$-box. As explained with the example in Fig. 3.2, the $\hat{Q}$-box contribution, (3.22), is divergent in the KK formula when we work in a non-degenerate model space. On the other hand, the EKK counterpart, (3.21), becomes divergent only for specific values of E. This means that we can always select a parameter E that makes the $\hat{Q}$-box to behave smoothly as a function of E.

Second, the parameter E provides us with a reasonable test of the calculation. Equation (3.8) shows that the resulting effective Hamiltonian H_{eff}, does not depend on the value of E, provided that we have the exact $\hat{Q}$-box in Eq. (3.8). Any approximation may spoil the E-independence of H_{eff}, and thereby of other physical quantities described by H_{eff}. This may in turn imply that a $\hat{Q}$-box that gives E-independent physical quantities is a good approximation to the exact $\hat{Q}$-box. In the most sophisticated calculations up to date, we can evaluate the $\hat{Q}$-box diagrams only up to third order in the perturbation V at most, and we can include only a limited number of excitations in the intermediate states (typically including up to $10-20$ oscillator quanta excitations), because of practical computational limitations. In Chap. 4, we shall present numerical tests of the above E-independence.

Here we explain how to fix the value of E in the actual calculations. If there are no intruder states in the target states $\{|\phi_i\rangle, \ i = 1, \cdots, d\}$ that are to be described by H_{eff}, it can be shown that there is a finite range of E values that make the series in Eq. (3.15) convergent [2]. The convergence is usually at its fastest when E is fixed around the mean value of the target energies, $\{E_i, \ i = 1, \cdots, d\}$. Let us come back to our specific case of two particles on top of a core, and employ a single-particle basis of the harmonic oscillator. Let ϵ_a^{min} be the minimum energy of active (valence) particle states. We then expect that our target states are distributed around $E \sim 2\epsilon_a^{\text{min}}$, which serve as the first guess for E. It is also clear that the lowest energy of the Q-space states is $2\epsilon_a^{\text{min}} + 1\hbar\omega$, which gives the lowest position of the poles of $\hat{Q}(E)$.

In actual calculations, the allowed range of E, which is limited both from above and from below, can be estimated as follows. Let us increase E from the above "*optimal*" value $2\epsilon_a^{\text{min}}$. As E approaches the lowest pole $2\epsilon_a^{\text{min}} + 1\hbar\omega$ of $\hat{Q}(E)$, $\hat{Q}(E)$ and its derivatives in Eq. (3.15) would diverge. On the other hand, if we choose too low a value of $E \ll 2\epsilon_a^{\text{min}}$, the resultant energy denominators in the $\hat{Q}(E)$ would be dominated by E, but not by the unperturbed energies of the intermediate states. In this situation, we have to expect that our approximation, truncation of the intermediate states at some unperturbed energies, cannot be justified.

In the next section, we present numerical examples where E is varied in some range around $E \sim 2\epsilon_a^{\text{min}}$.

Chapter 4

Application based on realistic interactions

In this chapter, we apply the EKK method to nuclear systems, starting from the realistic interactions. In order to apply the EKK formalism to nuclear systems, we consider simple nuclei composed of two nucleons on top of a given closed-shell core, ^{18}O, ^{18}F and ^{42}Ca, ^{42}Sc, employing a single-particle basis defined by the harmonic oscillator unperturbed Hamiltonian. As the P-space for ^{18}O and ^{18}F, we employ the sd-shell (degenerate case), and the $sdf_{7/2}p_{3/2}$-shell (non-degenerate case) composed of the sd-shell and the $0f_{7/2}$ and the $1p_{3/2}$ single-particle states. The P-space for ^{42}Ca, ^{42}Sc is the pf-shell (degenerate case), and the $pfg_{9/2}$-shell (non-degenerate case) composed of all the pf-shell single-particle states and the $0g_{9/2}$ single-particle state. In the degenerate P-space, both the KK and the EKK methods can be used, while in the non-degenerate P-space only the EKK method is applicable.

Our input interaction V in the Hamiltonian Eq. (3.11) is the low-momentum interaction $V_{\text{low}k}$ with a sharp cutoff $\Lambda = 2.5$ fm^{-1}, derived from the chiral χN^{3}LO interaction of Entem and Machleidt [43, 44]. Calculations with the different cutoffs Λ are presented in Sec. 4.6. Our total $(P + Q)$ Hilbert space is composed of the harmonic oscillator basis states in the lowest nine major shells. The Q-space degrees of freedom come into play either by the KK method or the EKK method through the $\hat{Q}$-box that is calculated to third order in the interaction V. The final effective interactions are thus obtained in the P-space of one or two major shells.

We ought to mention two points. First, the amount of oscillator quanta excitations in each term in perturbation theory, may not be fully adequate if one is interested in final shell-model energies that are converged with respect to the number of intermediate excitations in the $\hat{Q}$-box diagrams. We discuss the convergence of the $\hat{Q}$-box in Sec. 4.7 more in detail. Second, neglected many-body correlations, like those arising from three-body forces are not taken into account. Such effects, together with other many-body correlations not included here are expected to play important roles, see for example the recent studies of neutron-rich oxygen and calcium isotopes [45, 46, 47, 48, 49]. However, the main purpose here is to study the effective interactions that arise from the KK and the EKK methods in one and two major shells. The application to the various isotopic chains will be presented in Chap. 5, but the results are thus preliminary.

In the actual calculation of the $\hat{Q}$-box using the harmonic oscillator basis functions, we drop the Hartree-Fock diagram contributions, assuming that it is well simulated by the harmonic oscillator

potential, as in many of the former works [29].

In order to show how the EKK method works, we present separate studies of (i) the two-body matrix elements (TBMEs) of the effective interaction V_{eff}, and (ii) several low-lying energy levels obtained by shell model calculations. In particular, we focus on the E-independence of the numerical results; as discussed in Sec. 3.3, the effective Hamiltonian H_{eff} obtained with the exact $\hat{Q}$-box is independent on the energy parameter E, and so are physical quantities calculated with H_{eff}. In other words, the explicit E-dependence of the first term $H_{\text{BH}}(E)$ (or equivalently $\hat{Q}(E)$) in Eq. (3.15) is canceled by other terms that represent the folded diagram contributions, making thereby H_{eff} (and therefore V_{eff}) energy independent. In actual calculations, however, we can calculate the $\hat{Q}$-box only up to third order in V, and we have to examine the E-dependence of the right hand side of Eq. (3.8). In what follows, we shall see clearly that the $\hat{Q}$-box up to third order is sufficient to achieve an almost E-independent effective interaction V_{eff} (or H_{eff}).

The rest of this chapter is devoted to the detailed analysis of the V_{eff}. In Sec. 4.4, we analyze the spin-tensor decomposition of the effective interaction focusing on the property of the tensor force. The tensor force is of great importance particularly when we explore the neutron-rich nuclei, for example. The tensor force has the special property that the monopole interaction between $j_>$ orbit and j' orbit and that of between $j_<$ orbit and j' orbit have opposite sign. Here we define $j_>$ and $j_<$ to represent the spin-orbit partners, that is, $j_> = l + 1/2$ and $j_< = l - 1/2$, where l stands for the orbital momentum of a given single-particle state. This special feature of tensor force changes the spin-orbit splitting between $j_>$ and $j_<$ and therefore the shell structure as well. In particular, when we have a sizable number of neutrons in the single-particle state j', the effects play the important roles.

In Sec. 4.5, we compare the effective interaction obtained by EKK method with the phenomenological interactions. We compare both in degenerate and non-degenerate model spaces. In particular, the effective interaction in non-degenerate model space is only obtained via the phenomenological fitting to experimental data, while the EKK method enable us to derive them from the realistic interaction and the microscopic theories.

As the supplemental analyses, we discuss the above-mentioned points last two sections in this chapter. In Sec. 4.6, we repeat the calculation with the various cutoff Λ appearing in $V_{\text{low}k}$ interactions to see how the results depends on the cutoff parameter. Finally, in Sec. 4.7, the convergences with respect to the inclusion of the higher intermediate excitations are discussed.

4.1   EKK method in sd-shell and $sdf_{7/2}p_{3/2}$-shell

In this section, we consider ^{18}O and ^{18}F as two-nucleon systems on top of the ^{16}O closed-shell core. We calculate the effective interactions V_{eff} in the degenerate sd-shell, and in the non-degenerate $sdf_{7/2}p_{3/2}$-shell model spaces. The input of the EKK method is the $\hat{Q}$-box calculated up to third order in V with the harmonic oscillator basis of $\hbar\omega = 14$ MeV. We set the origin of the energy as $\epsilon_{sd} = 0$, which suggests that the optimal choice of E is $E \sim 0$.
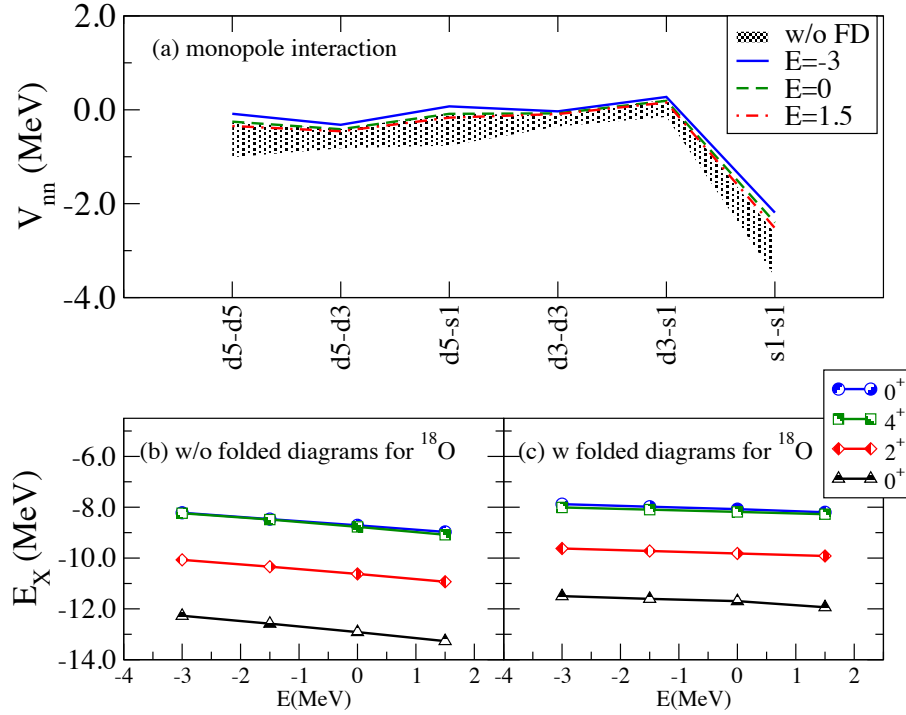
4.1.1 Degenerate *sd*-shell model space

Figure 4.1: (Color online) *E*-dependence of the EKK results of neutron-neutron channel in the *sd*-shell (degenerate model space). The figure shows the monopole part, of V_{eff} (denoted by V_{nn}), see Eq. (4.1), and the level energies of ^{18}O with respect to ^{16}O. In panel (a), the monopole panel, dotted lines (which make the shaded area) show the results without the folded diagram contributions for $-3 \leq E \leq 1.5$ MeV. The full line, dashed line and dot-dash line show the V_{nn} for $E = -3$, 0, 1.5 MeV, respectively. In the lower panels (b) and (c), energy levels are calculated for $E = -3$, -1.5, 0, 1.5 MeV (b) without and (c) with the folded diagram contribution. Triangles, diamonds, squares and circles show the energy levels of the ground, the first excited, the second and third excited states, respectively.

In Fig. 4.1, we show our numerical results for the two-body matrix elements and level energies calculated in the degenerate *sd*-shell model space for the neutron-neutron channel (^{18}O) and in Fig. 4.2 the proton-neutron channel (^{18}F).

To see the *E*-independence of the numerical results for V_{eff}, calculations are performed for several values of *E*. As explained before, the optimal value of *E* may be estimated as $E \sim 2\epsilon_{sd} = 0$. Note also that $E = 0$ is far from the lowest pole of $\hat{Q}(E)$, $E = E_{\text{pole}}^{min} = 1\,\hbar\omega = 14$ MeV, and the calculation is free from the divergence problem of the $\hat{Q}$-box. We have thus varied *E* in the range of $-3 \leq E \leq 1.5$ MeV in Fig. 4.1 and 4.2. Obviously, the EKK method with $E = 0$ coincides exactly with the KK method because our *P*-space is degenerate now (compare Eqs. (3.21) and (3.22)).

In order to study the effect on the various matrix elements, we analyze the monopole term in the
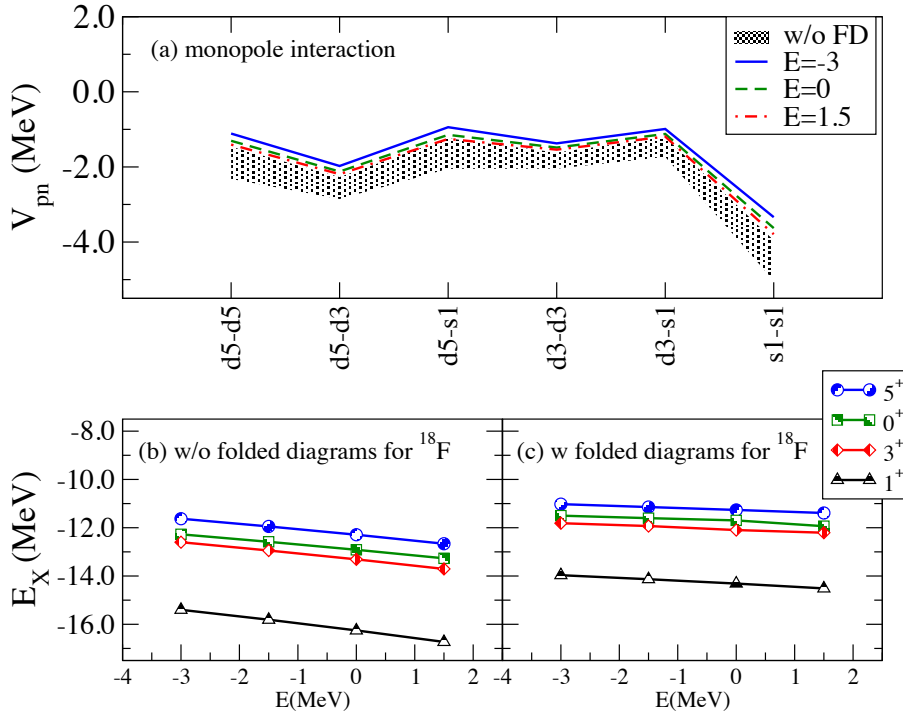
Figure 4.2: (Color online) E-dependence of the EKK results of proton-neutron channel in the sd-shell (degenerate model space). (a) monopole part of the interaction, (b) level energies of ^{18}F without folded diagrams and (c) with folded diagrams. Else, we use the same notation as in Fig. 4.1.

neutron-neutron channel in Fig. 4.1 (a). The monopole part of V_{eff}, is defined as

$$V_{\text{eff}}{}_{j,j'}^{T} = \frac{\sum_J (2J+1)\langle jj'|V_{\text{eff}}|jj'\rangle_{JT}}{\sum_J (2J+1)}. \tag{4.1}$$

Let us look at the dotted lines (which make a shaded band in the figure) that are calculated by dropping the folded diagram contributions, i.e., by replacing V_{eff} simply by $\hat{Q}(E)$. We can see clearly that $\hat{Q}(E)$ depends strongly on E. Next, let us turn to the EKK results that include all the folded diagram contributions in the right hand side of Eq. (3.15). They are shown by solid lines for $E = -3$, 0, 1.5 MeV, whose difference can hardly be seen. The above observation suggests that the folded diagrams cancel the E-dependence of $\hat{Q}(E)$ and yield an almost E-independent $\tilde{H}_{\text{eff}}$ (and V_{eff}) in Eq. (3.15).

In the lower panels (b) and (c) of Fig. 4.1, we show several energy levels of ^{18}O with respect to ^{16}O obtained by shell-model calculations with our effective interaction V_{eff}. Here the single particle energies in the shell-model diagonalization are taken from the USD interaction [50, 13]; the single-particle energies of the states (in the isospin formalism) $\epsilon_{d_{5/2}}$, $\epsilon_{s_{1/2}}$, and $\epsilon_{d_{3/2}}$ are -3.9478 MeV, -3.1635 MeV and 1.6466 MeV, respectively.

Panels (b) and (c) show the results without and with folded diagram contributions, respectively. We note that in panel (b) the energy levels are decreasing functions of E, which is explained by the E-dependence of $\hat{Q}(E)$. On the other hand, in panel (c), we see that the energy levels are almost independent of the parameter E, as they should.

The above observation also implies that the evaluation of the $\hat{Q}$-box up to third order in V is sufficient to establish a seemingly E-independence of the right hand side of Eq. (3.15), and therefore of V_{eff} in the left hand side.

Figure 4.2 shows the results for V_{eff} in the proton-neutron channel and level energies for ^{18}F with the same setting as for ^{18}O. We can repeat exactly the same arguments as we did for ^{18}O and realize that the folded diagram contribution eliminates the E-dependence, to a large extent, of $\hat{Q}(E)$ to give, almost, an E-independent V_{eff} and energy levels.

4.1.2 Non-degenerate $sdf_{7/2}p_{3/2}$-shell

Here we examine ^{18}O and ^{18}F in the non-degenerate P-space, labelled the $sdf_{7/2}p_{3/2}$-shell here, composed of the sd-shell and the $0f_{7/2}$ and $1p_{3/2}$ single-particle states. In this non-degenerate model space, the standard KK method cannot be applied, since it leads to divergences, as discussed above. The EKK method offers however a viable approach to this system. To date, therefore, there have been only empirical interactions in this model space, see for example the effective interaction employed in Ref. [51]. A comparison between empirical and our effective interaction is given in Sec. 4.5.
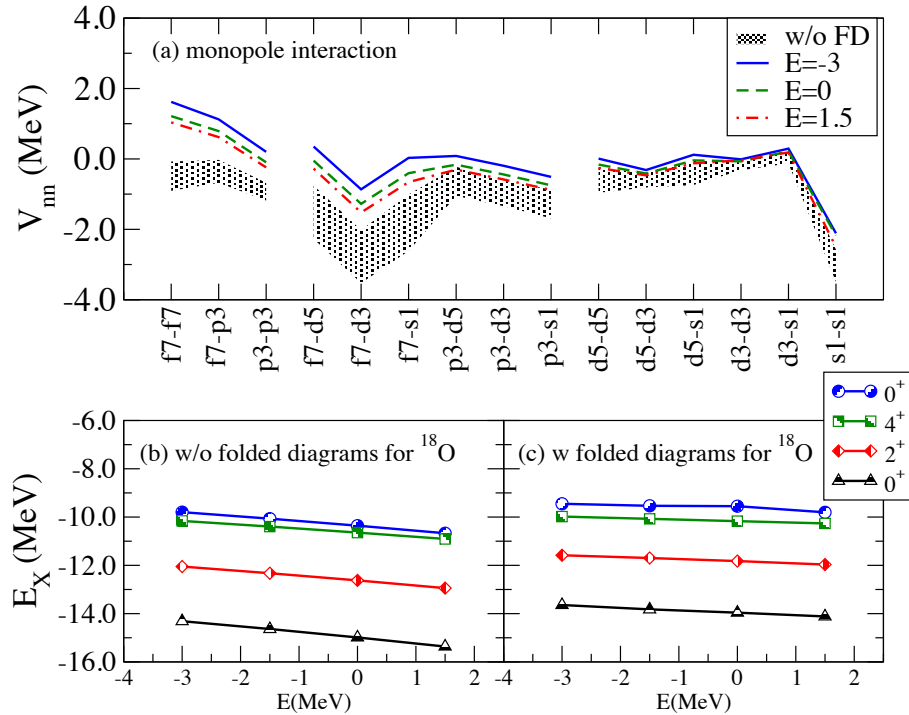

Figure 4.3: (Color online) E-dependence of the EKK results of neutron-neutron channel in the $sdf_{7/2}p_{3/2}$-shell (non-degenerate model space). (a) monopole part of the interaction, (b) level energies of ^{18}O without folded diagrams and (c) with folded diagrams. Else, we use the same notation as in Fig. 4.1.
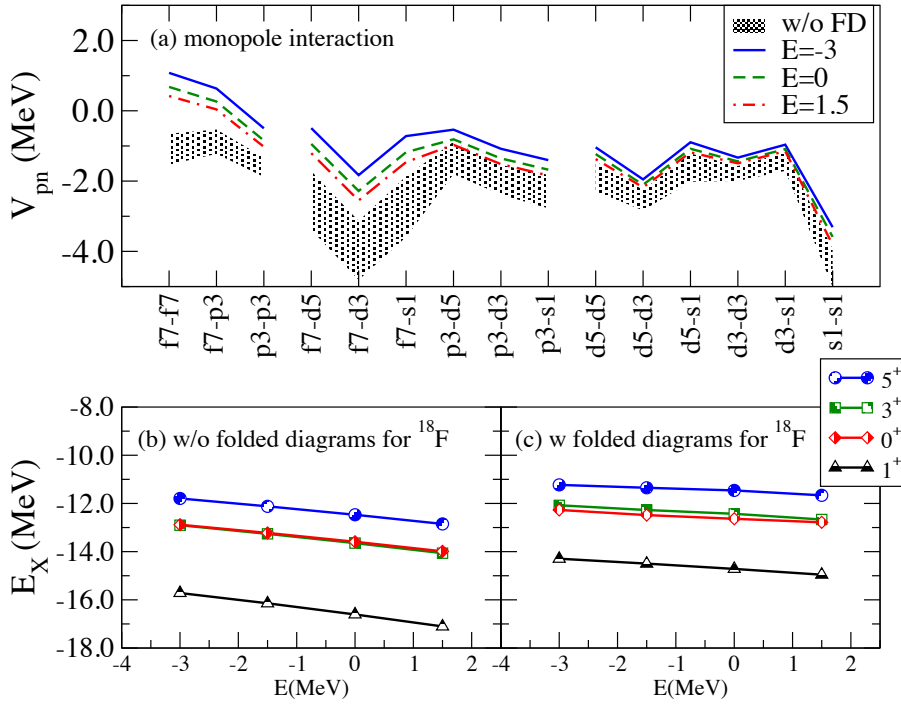
Figure 4.4: (Color online) *E*-dependence of the EKK results of proton-neutron channel in the $sdf_{7/2}p_{3/2}$-shell (non-degenerate model space). (a) monopole part of the interaction, (b) level energies of ^{18}F without folded diagrams and (c) with folded diagrams. Else, we use the same notation as in Fig. 4.2.

Figures 4.3 and 4.4 show the numerical results of the EKK method in the $sdf_{7/2}p_{3/2}$-shell model space, in the same way as Figs. 4.1 and 4.2 for the degenerate *sd*-shell. In what follows, we will introduce the wording inter-shell interaction for the interaction between particles in different major shells, for example we can have one particle in the *sd*-shell and the other one in the *pf*-shell. Similarly, we will use the naming intra-shell interaction for interactions between particles within a single major shell.

Let us first study the the monopole part of the TBMEs of V_{eff} (Fig. 4.3 (a) for neutron-neutron channel and Fig. 4.4 (a) for proton-neutron channel). Here we have inter-shell interactions in addition to the intra-shell interactions within the *sd*-shell and within the *pf*-shell. We see that the inter-shell interactions depend more strongly on *E* without the folded diagrams than the intra-shell interaction within the *sd*-shell. This feature is due to the fact that $\hat{Q}(E)$ for the inter-shell interaction has intermediate states with small energy denominators. This figure clearly shows that the folded diagram contributions cancel the strong *E*-dependence of the $\hat{Q}(E)$, and the resulting V_{eff} becomes almost independent of *E*, showing that the EKK method is stable and useful also in the non-degenerate $sdf_{7/2}p_{3/2}$-shell.

From the panels of the energy levels of ^{18}O and ^{18}F, we can draw the same conclusion for the degenerate *sd*-shell; the folded diagram contribution makes the energy levels independent of the pa-

rameter E.

4.1.3   Comparison of KK and EKK methods

The main advantage of our EKK method is that it allows for a fully consistent treatment of the non-degenerate model space. On the other hand, in the KK method, the naive perturbative calculation of $\hat{Q}$-box by Eq. (2.86) leads to divergence in non-degenerate $sdf_{7/2}p_{3/2}$-shell, as discussed in Sec. 3.2.

   One possible *ad hoc* way to avoid this divergence is to artificially force the $sdf_{7/2}p_{3/2}$-shell to be degenerate in energy by shifting the single-particle energies [46]. Although there is no physical justification for this artificial shift, it removes the poles which arise in the various $\hat{Q}$-box diagrams.

   Note, however, that the obtained V_{eff} is defined with artificially degenerate single-particle energies. Furthermore, in actual calculations, this method dose not necessarily lead to a convergent result even with all the folded diagrams in Eq. (2.86).

   For the purpose of comparing the EKK method with the *ad hoc* treatment of the non-degeneracy in the KK method, we apply the EKK method to both sets of unperturbed Hamiltonians; one with the artificially degenerate $sdf_{7/2}p_{3/2}$-shell, and the other with the non-degenerate $sdf_{7/2}p_{3/2}$-shell. Note that the EKK method in the artificially degenerate $sdf_{7/2}p_{3/2}$-shell simulates the *ad hoc* KK method explained above. In this calculation, in order to obtain the convergent result, we set $E = -1.5$ MeV in both cases.
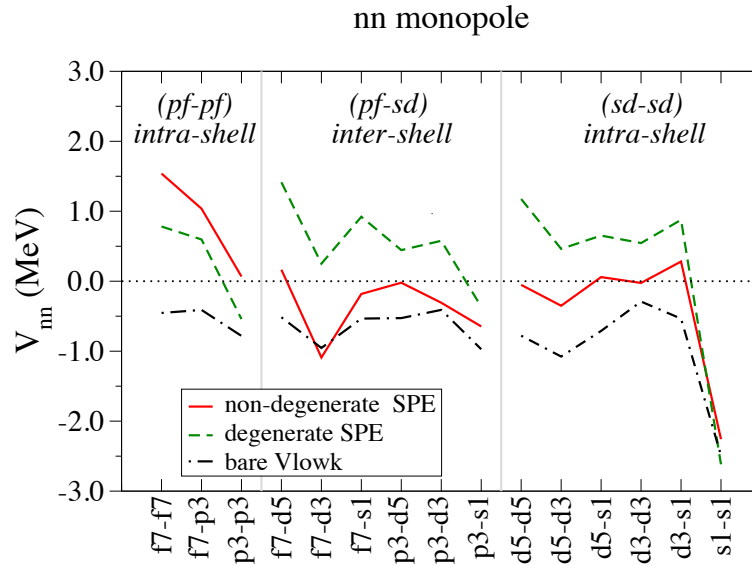

Figure 4.5: (Color online) The monopole part of V_{eff} in the $sdf_{7/2}p_{3/2}$-shell model space, obtained via the physical (non-degenerate) single particle energies (full line) and via the *ad hoc* (degenerate) single particle energies (dashed line). Both calculations are performed in the neutron-neutron channel. As a reference, the monopole part of the first-order effective is shown with dash-dotted line.

   Figure 4.5 shows the monopole part of the effective interaction V_{eff} in the $sdf_{7/2}p_{3/2}$-shell interac-

tion for the neutron-neutron channel. The dashed lines show the results with the *ad hoc* modification of the unperturbed Hamiltonian as explained above. The full lines display the results in the non-degenerate model space. To show the contribution of the $\hat{Q}$-box and folded diagrams, we display also the monopole part of the first-order term of the $\hat{Q}$-box. This term is energy independent.

It is interesting to note that the inter-shell *(pf-sd)* interaction and the intra-shell *(sd-sd)* interaction are more attractive in the EKK method than in the *ad hoc* KK method. This discrepancy clearly comes from the difference in the energy denominator in the $\hat{Q}$-box. Suppose we have two particles within $f_{7/2}$ or $p_{3/2}$ states. The magnitude of the energy denominator shown in Eq. (3.20) is larger, making thereby the $\hat{Q}$-box smaller in the EKK method than in the *ad hoc* KK method. For the inter-shell *(pf-sd)* interaction and the intra-shell *(sd-sd)* interaction, this difference makes the interaction for the artificially degenerate single-particle states more repulsive. On the other hand in the intra-shell *(pf-pf)* interaction, the EKK results are more repulsive than the *ad hoc* KK results. This can be understood as follows; the effect of the folded diagram contribution is quite large in the EKK method since we use $P\tilde{H}P$ in the folding procedure instead of PVP. This difference makes the contribution of the folded diagrams larger.

The above comparison shows that there is a sizable difference between the effective interaction in the EKK method and in the *ad hoc* KK method, and the difference affects mostly the inter-shell interaction.

4.2   EKK method in pf-shell and $pfg_{9/2}$-shell

We apply the EKK method to the nuclei ^{42}Ca and ^{42}Sc as well. These nuclei can be described as two nucleons on top of a ^{40}Ca core. Here the degenerate model space is composed of the single-particle states of the pf-shell, while our non-degenerate model space is defined by the single-particle states of the pf-shell and the single-particle state $0g_{9/2}$. We have performed the calculation in the same way as in Sec. 4.1.2, but with an oscillator parameter $\hbar\omega = 11$ MeV, which is appropriate for ^{40}Ca region. We have taken $\epsilon_{pf} = 0$ and therefore our first guess for the energy parameter is $E = 0$.

4.2.1   Results for pf-shell

Figure 4.6, 4.7 shows the effective interaction V_{eff} defined in the degenerate pf-shell. In Fig. 4.6, the panel (a) shows the neutron-neutron monopole interactions and the panels (b) and (c) display the energy levels of ^{42}Ca. Figure 4.7 shows the results for ^{42}Sc, the proton-neutron channel, in the same manner. In the shell-model diagonalization, the single particle energies are taken from the GXPF1 interaction [16]; the particle energies (in the isospin formalism) of $\epsilon_{f_{7/2}}$, $\epsilon_{p_{3/2}}$, $\epsilon_{p_{1/2}}$ and $\epsilon_{f_{5/2}}$ are equal to -8.6240 MeV, -5.6793 MeV, -4.1370 MeV and -1.3829 MeV, respectively.

We have carried out the calculation by varying E in the range of $-3 \leq E \leq 1.5$ MeV. Clearly, we can make the same observation as in Sec. 4.1.1; the shaded bands in the monopole panels shrink when we include folded diagrams, making the monopole part of V_{eff} almost independent of E. Moreover,
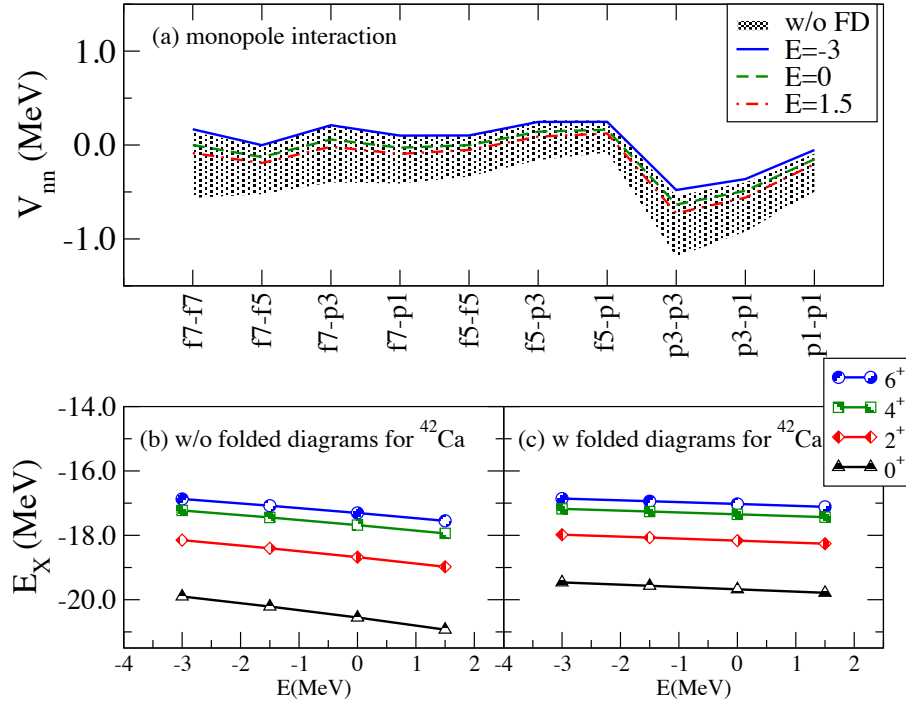
Figure 4.6: (Color online) E-dependence of the EKK results of neutron-neutron channel in the pf-shell (degenerate model space). (a) monopole part of the interaction, (b) level energies of ^{42}Ca without folded diagrams and (c) with folded diagrams. Else, we use the same notation as in Fig. 4.1.

from the energies levels of ^{42}Ca (Fig. 4.6 (b) and (c)) and ^{42}Sc(Fig. 4.7 (b) and (c)), we observe that the folded diagrams restore nicely the E-independence of all the lowest-lying levels, which is a natural consequence expected by the theory.

4.2.2   Results for $pfg_{9/2}$-shell

As our final example, we present the results for the $pfg_{9/2}$-shell in Fig. 4.8 for the neutron-neutron channel and Fig. 4.9 for the proton-neutron channel. The parameter E is varied in the range of $-3 \leq E \leq 1.5$ MeV. The particle energies (in the isospin formalism) of $\epsilon_{f_{7/2}}$, $\epsilon_{p_{3/2}}$, $\epsilon_{p_{1/2}}$, $\epsilon_{f_{5/2}}$ and $\epsilon_{g_{9/2}}$ are equal to -8.6240 MeV, -5.6793 MeV, -4.1370 MeV, -1.3829 MeV and 2.1000 MeV, respectively. We note again the role played by folded diagrams; they remove the E-dependence of the $\hat{Q}(E)$, resulting in an almost E-independent effective interaction V_{eff} and energy levels of ^{42}Ca (Fig. 4.8 (b) and (c)) and ^{42}Sc (Fig. 4.9 (b) and (c)).

4.3   Application of the EKK method to shell-model calculations

With effective Hamiltonians derived by the EKK method, we can study the role of such Hamiltonians in actual shell-model calculations. Here we focus on the previously discussed systems, with at most
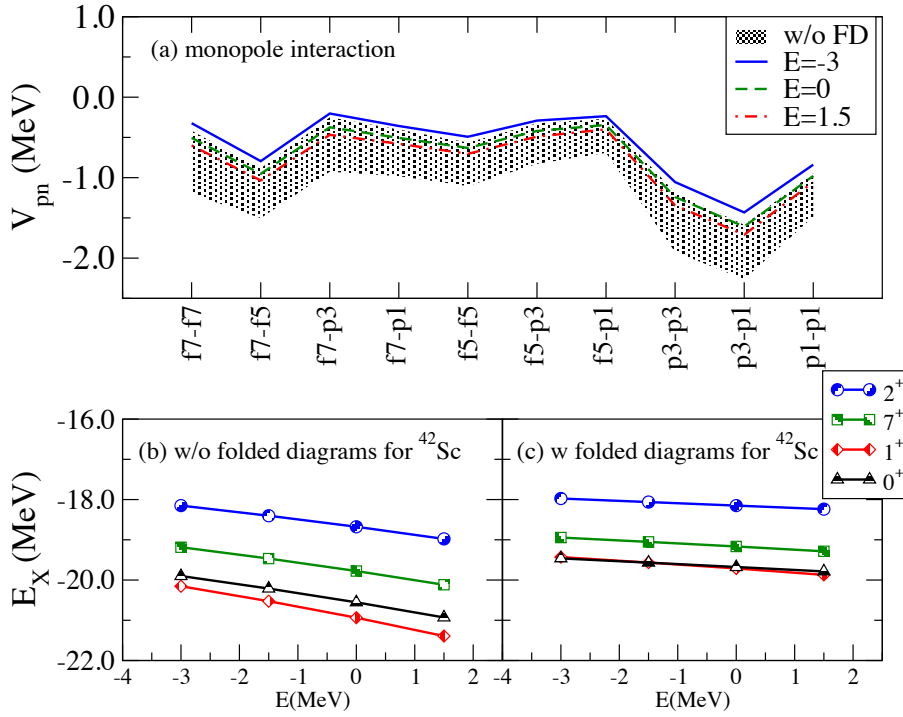
Figure 4.7: (Color online) E-dependence of the EKK results of proton-neutron channel in the pf-shell (degenerate model space). (a) monopole part of the interaction, (b) level energies of ^{42}Sc without folded diagrams and (c) with folded diagrams. Else, we use the same notation as in Fig. 4.2.

two valence nucleons outside a closed-shell core. Results from large-scale shell model calculations will be presented in Chap. 5.

For this purpose, Fig. 4.10 shows the low-lying energy levels for ^{42}Ca obtained by the shell-model calculation with the same setting as in Sec. 4.2.1. The TBMEs are derived by the EKK method, with the $\hat{Q}$-box calculated to first, second and third order in the interaction V. The parameter E is varied in the range of $-3 \leq E \leq 0$ MeV in the calculation of the second-order and the third-order $\hat{Q}$-box. Note that the first-order $\hat{Q}$-box is V itself, and is independent of E. The leftmost levels show the result with the first-order $\hat{Q}$-box. The middle two levels represent the results with the second-order and third-order $\hat{Q}$-box, where the shaded bands show the range of the energy levels corresponding to $-3 \leq E \leq 0$ MeV. The rightmost levels are the experimental data.

As discussed above, by construction, all the physical results are independent of E if our $\hat{Q}$-box is calculated without any approximation. In other words, the weaker dependence on E implies a better approximation to the $\hat{Q}$-box (see Figs. 4.1-4.4, 4.6-4.9). This means that the width of the shaded band may be taken as a measure of the size of the error.

In Fig. 4.10, independently of the comparison to experiment, two types of convergence can be seen; the first one is (i) the convergence of the energy levels with respect to the order of the perturbation, and the second one is (ii) the convergence of the band widths (E-dependence of the energy levels) with respect to the order of the perturbation.
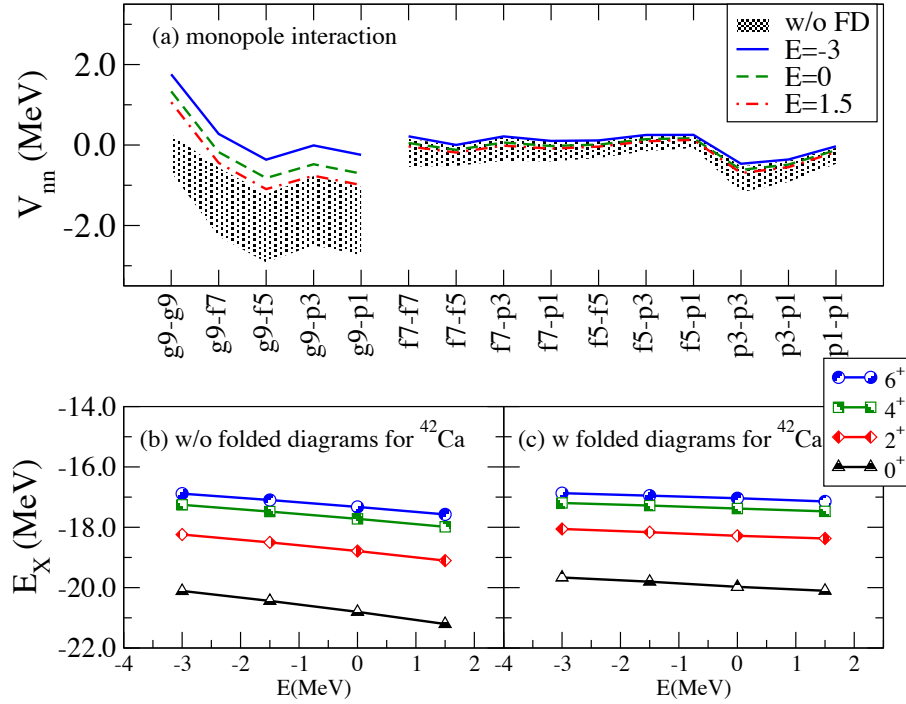
Figure 4.8: (Color online) E-dependence of the EKK results of neutron-neutron channel in the $pfg_{9/2}$-shell (non-degenerate model space). (a) monopole part of the interaction, (b) level energies of ^{42}Ca without folded diagrams and (c) with folded diagrams. Else, we use the same notation as in Fig. 4.1.

Let us start with discussions on the convergence issue (i). Figure 4.10 shows that the magnitude of the third-order contribution is approximately 30% as large as that of the second-order contribution. A simple estimate from these observations tells us that the perturbation series make a geometric series with common ratio ~ 0.3. We can then expect that the fourth-order correction to the $\hat{Q}$-box are small.

Let us turn to the convergence case (ii). Figure 4.10 exhibits also that, compared with the second-order $\hat{Q}$-box, the band widths are smaller for the third-order $\hat{Q}$-box, as we would expect. Besides these theoretical features, the agreement with experiment is acceptable.

Next we examine the proton-neutron channel using ^{42}Sc as our testcase. The results are shown in Fig. 4.11. The experimental values (right-most levels) are shifted by -7.2 MeV so that the 0^+ state forms the $T = 1$ triplet state with corresponding 0^+ ground state of ^{42}Ca, since we presently do not take into account any isospin dependence of the nuclear force or the Coulomb interaction.

Here we observe similar patterns to those seen in the neutron-neutron channel of Fig. 4.10. However, we notice that as far as the convergence case (i) is concerned, the contribution of third-order terms is not necessarily smaller than second-order contributions.

On the other hand, for the convergence case (ii), we observe smaller band widths for the third-order $\hat{Q}$-box results as compared with those obtained with the second-order $\hat{Q}$-box. This may indicate that the third-order $\hat{Q}$-box represents a better approximation than the second-order $\hat{Q}$-box.

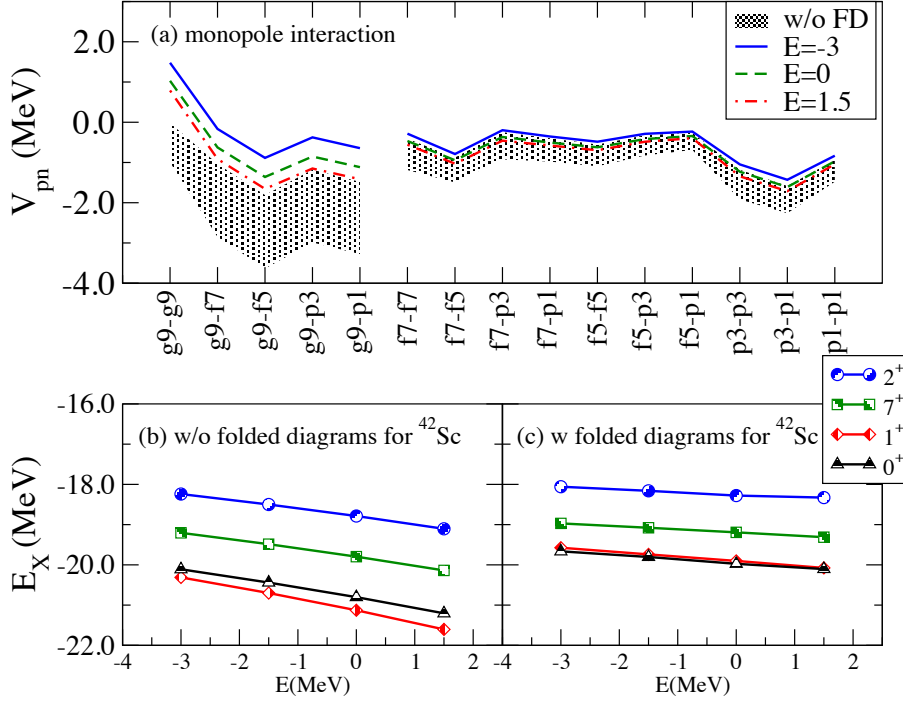The agreement with experimental data is rather nice for the $0^+, 7^+, 3^+$ states, but we observe a

Figure 4.9: (Color online) E-dependence of the EKK results of proton-neutron channel in the $pfg_{9/2}$-shell (non-degenerate model space). (a) monopole part of the interaction, (b) level energies of ^{42}Sc without folded diagrams and (c) with folded diagrams. Else, we use the same notation as in Fig. 4.2.
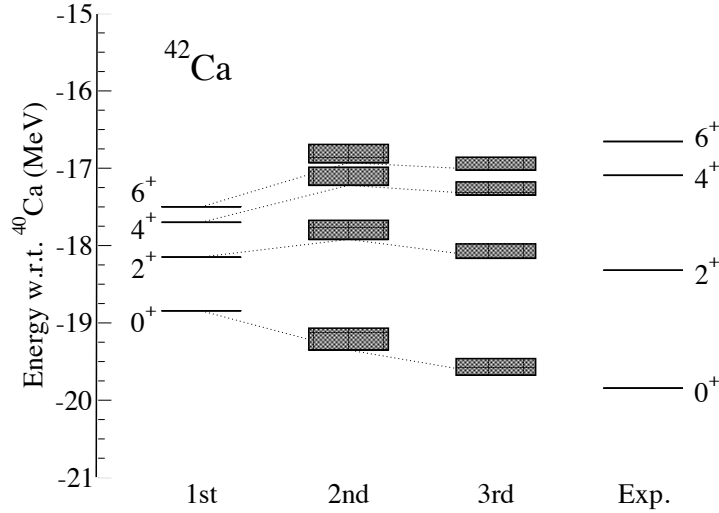

Figure 4.10: Energy levels of the ground state and low-lying states of ^{42}Ca using the $\hat{Q}$-box to first, second, and third order in the interaction. The right most levels represent the experimental values. Energies are measured from the closed-shell core, ^{40}Ca. The TBMEs (neutron-neutron channel) are obtained by the EKK method, with the parameter E in the range $-3 \leq E \leq 0$ MeV. The shaded bands indicate the variation of calculated energy levels for $-3 \leq E \leq 0$ MeV.
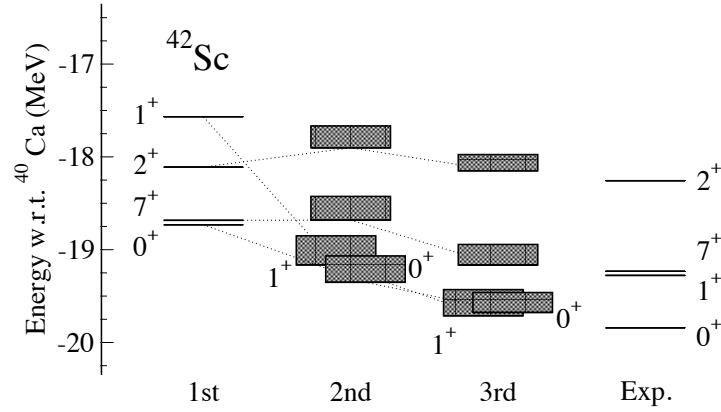
Figure 4.11: Energy levels of the ground state and low-lying states of ^{42}Sc with respect to ^{40}Ca core. The TBMEs (proton-neutron channel) are obtained via EKK method with parameter $-3 \leq E \leq 0$ MeV. Since we do not include Coulomb effects throughout the calculation, the absolute values are shifted by -7.2 MeV, so that the 0^+ state forms the $T = 1$ triplet state with the corresponding 0^+ ground state of ^{42}Ca. Other notation is the same as for Fig. 4.10

slight overbinding for the 1^+ state. From the convergence property of the 1^+ state, it is unlikely that fourth-order contributions to the $\hat{Q}$-box could play an important role. Several explanations for this discrepancy are possible. One possibility for this overbinding is that the single particle energies presently used are not fully adequate. As mentioned above, we have employed the single-particle energies determined from the GXPF1 [16] interaction. These energies are the results of a fit together with the two-body interaction to reproduce experimental data. The experimental data that enter the fitting procedure consist of selected observables from pf-shell nuclei. Since the GXPF1 interaction differs from those derived here, other sets of single-particle energies could have been more appropriate. Another possibility is that our Q-space and order in perturbation theory may not be large enough. Thus, there may be missing many-body correlations which could play an important role. Three-body forces [45, 46, 47, 48, 49] are examples of many-body contributions not studied here. However, the aim of this work has been to study the recently developed EKK formalism for deriving effective interactions for more than one major shell. The role of more complicated many-body correlations are the scope of future works.

4.4 Spin-tensor decomposition of the effective interaction

Spin tensor decomposition of V_{eff} is presented in this section. In previous studies [52], the tensor-force component in effective interactions for shell-model calculations was, for the sake of simplicity, modeled via the exchange of π and ρ mesons only. To a large extent, this yields results close to the tensor force in realistic NN interactions. In fact, this model describes rather well the experimental data in several mass regions [53]. However, it is far from trivial that the tensor force in effective interactions

for the shell-model can be considered to be given by the exchange of π and ρ mesons only. In this section, we show that the tensor force is in a large extent unchanged from the original interaction. This special property of the tensor force is referred as Renormalization-persistency, in ref. [54], and shown in the framework of KK method, Here we show the same with EKK method, therefore, not only in degenerate model spaces but also in non-degenerate model spaces. The decomposition of the effective interaction is accomplished as follows,

$$\langle ABLS|V_p|CDL'S'\rangle_{J'T} = (-1)^{J'}(2p+1) \left\{ \begin{array}{ccc} L & S & J' \\ S' & L' & p \end{array} \right\} \sum_J (-1)^J (2J+1)$$

$$\left\{ \begin{array}{ccc} L & S & J \\ S' & L' & p \end{array} \right\} \langle ABLS|V|CDL'S'\rangle_{JT}, \tag{4.2}$$

where the subscript p represent the rank of the operator. When $p = 0$, V_p is central and $p = 1, 2$, the contributions have LS and tensor force spin-tensor property. The matrix elements are written by LS-coupled form, which is given by the following relation to ordinary jj-coupled matrix elements,

$$\langle ABLS\,JT|V|CDL'S'\,JT\rangle$$

$$= [(1 + \delta_{AB})(1 + \delta_{CD})]^{1/2} \sum_{j_a, j_b, j_c, j_d} \left[\begin{array}{ccc} l_a & \frac{1}{2} & j_a \\ l_b & \frac{1}{2} & j_b \\ L & S & J \end{array} \right] \left[\begin{array}{ccc} l_c & \frac{1}{2} & j_c \\ l_d & \frac{1}{2} & j_d \\ L' & S' & J \end{array} \right]$$

$$\times [(1 + \delta_{ab})(1 + \delta_{cd})]^{1/2} \langle abJT|V|cdJT\rangle \tag{4.3}$$

where parentheses represent transformation bracket and defined by

$$\left[\begin{array}{ccc} j_1 & j_2 & J_{12} \\ j_3 & j_4 & J_{34} \\ J_{13} & J_{24} & J \end{array} \right] = (\hat{J}_{12}\hat{J}_{34}\hat{J}_{13}\hat{J}_{24})^{\frac{1}{2}} \left\{ \begin{array}{ccc} j_1 & j_2 & J_{12} \\ j_3 & j_4 & J_{34} \\ J_{13} & J_{24} & J \end{array} \right\}. \tag{4.4}$$

The hat $\hat{J} = 2J + 1$ and the parentheses are the ordinary $9j$ coefficients. Note that this decomposition uniquely determine the central, the spin-orbit and the tensor component of the given interaction. Note also that to obtain the reasonable results we need to choose the model space which fully include the spin-orbit partners, that is, $j_>$ and $j_<$ spontaneously. Therefore, for the example of the effective interaction in two-major shell, full $sdpf$-shell is adequate, while $sdf_{7/2}p_{3/2}$-shell is not.

Sections 4.4.1 and 4.4.2 are devoted to make it sure that the Renormalization-Persistency in degenerate model space, and the Sec. 4.4.3 is for that of full $sdpf$-shell. As a result, we will see that the Renormalization-Persistency is the common feature of both degenerate and non-degenerate model spaces.

Throughout this section, the word "bare tensor" indicates the tensor force in $V_{\text{low}k}$. By the previous work of the author and collaborators [54], it is already known that the tensor force is not changed by the renormalization of the strong short-range repulsion, in other word, the tensor force in $V_{\text{low}k}$ is almost the same as that of bare nuclear force. This is because the matrix element of the tensor force is

mainly reflect the property of the long-range part of the tensor force, and short-range renormalization produce mainly the central and LS force only. Tensor force, which has rank 2 angular-momentum structure, is hardly happen to be produced by the complexity of the short-range renormalization. In this thesis, we do not repeat those calculations, regarding bare tensor force is almost the same as tensor force in $V_{\text{low}k}$.

4.4.1 Results for *sd*-shell

Figure 4.12 shows the monopole part of the tensor force in degenerate *sd*-shell. Because of the angular momentum restriction, the monopole parts of the tensor force which include $s_{1/2}$ orbit are equal to zero. The circle and the solid line is that of bare NN interaction, the square and the dashed line is V_{eff}
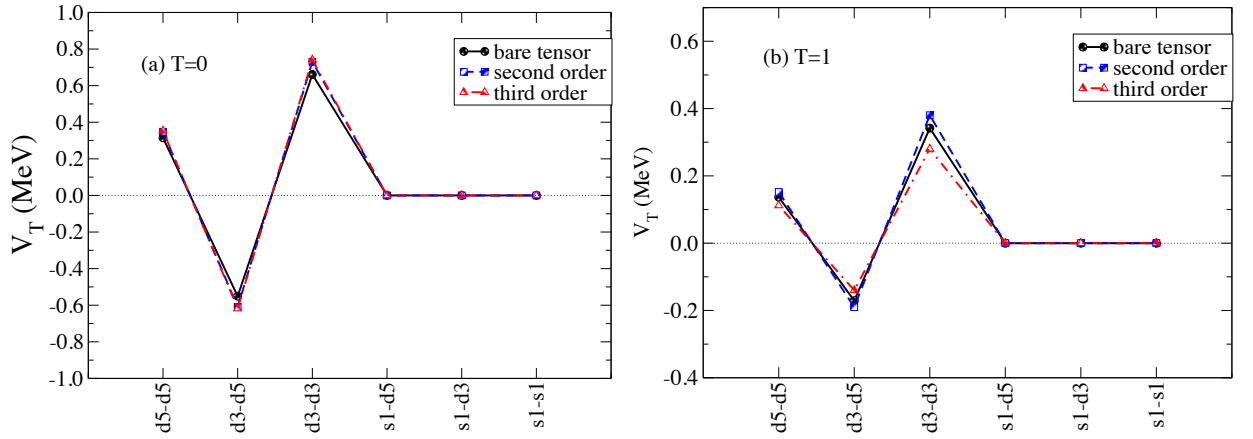
Figure 4.12: Monopole part of the tensor force in *sd*-shell (a) T=0 channel and (b) T=1 channel. The circles and the solid lines are that of bare NN interaction, the squares and the dashed lines are V_{eff} with second order $\hat{Q}$-box and the triangles and dot-dashed lines are V_{eff} with third order $\hat{Q}$-box.

with second order $\hat{Q}$-box and the triangular and dot-dashed line is V_{eff} with third order $\hat{Q}$-box. In both $T = 0$ and $T = 1$ channel, we observe that the renormalization persistency of the tensor force under the inclusion of the medium effects.

4.4.2 Results for *pf*-shell

In this section, we show the spin-tensor decomposition of V_{eff} in degenerate *pf*-shell.

Figure 4.13 shows the monopole part of the tensor force in degenerate *pf*-shell. The renormalization persistency of the tensor force is maintained to a large extent but less than *sd*-shell case. Except for $p_{1/2}$ channel, the renormalization persistency is almost perfect. For $p_{1/2}$ channel, only 2 nucleons can fill the orbit, and therefore the influences to nuclear structure are not as significant as the other orbits.
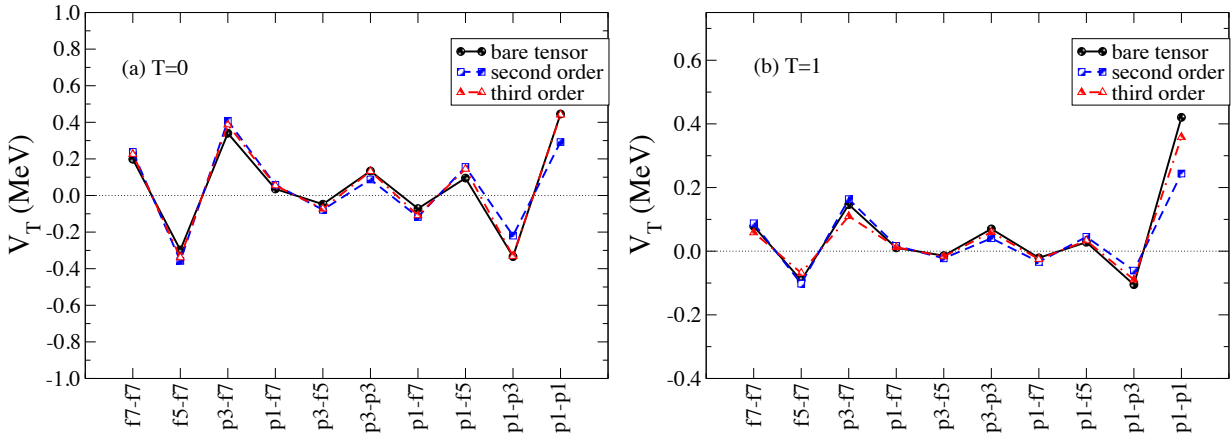
Figure 4.13: Monopole part of the tensor force in pf-shell (a) T=0 channel and (b) T=1 channel. The other notations are the same as Fig. 4.12.

4.4.3   Results for $sdpf$-shell

Finally, we present the result of $sdpf$-shell. Figures 4.14 and 4.15 shows the monopole part of the tensor force in bare tensor force, V_{eff} calculated using $\hat{Q}$-box up to second order, and that of third order. The left 6 channels are for intra-shell sd-sd interaction, the middle 12 channels are for inter-shell sd-pf interaction, and the right 10 channels are for again intra-shell pf-pf interaction.
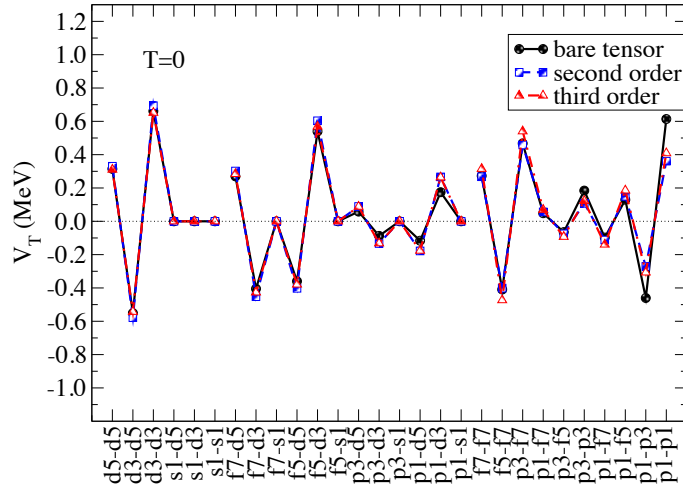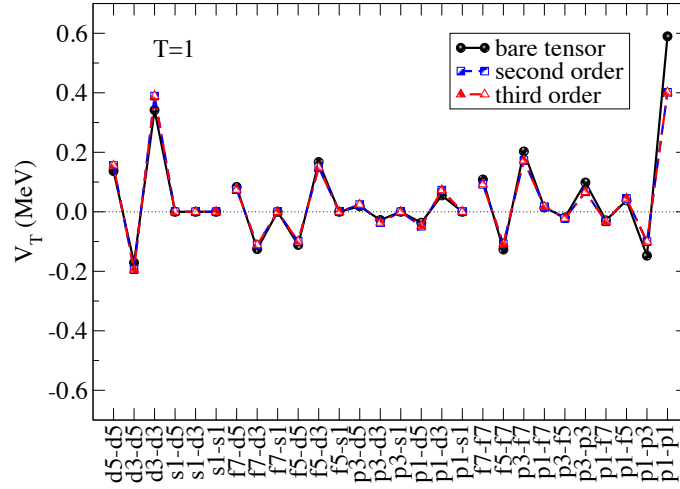

Figure 4.14: Monopole part of the tensor force in $sdpf$-shell ($T = 0$).

What is interesting and important is that the renormalization persistency of the tensor force is, to a amazingly large extent, maintained even for the inter-shell interactions. For effective interaction for the inter-shell interaction has been only determined empirically, the renormalization persistency of the inter-shell interaction derived by the microscopic theory has a great importance. This feature can be one of the guide when we consider the effective interaction in this model space.

Figure 4.15: Monopole part of the tensor force in *sdpf*-shell ($T = 1$).

4.4.4 Renormalization persistency

We saw the results that the renormalization persistency of the tensor force is observed in *sd*-shell, *pf*-shell for degenerate model space and *sdpf*-shell for non-degenerate model space. The results mean that the monopole part of the tensor force is dominated by the first-order term in the $\hat{Q}$-box and the contributions from second or higher-order terms are remarkably small. These results can be understood by considering the specific angular momentum structure of the tensor force, which is a scalar product of two rank 2 tensors in spin and coordinate spaces. In a perturbative correction to second or higher-order, such a complicated structure is smeared out and the resulting interaction consists mainly of a central force contribution. Therefore, as for the tensor-force component in the monopole interaction, it is the first-order contribution which is the dominant one.

To elucidate why higher-order terms in many-body perturbation theory are small, we consider as an example a contribution from second order in the interaction, by far the largest higher-order term.

The Hamiltonian causing the present second-order perturbation can be written as

$$H_1 = \sum_{p=0,1,2} w_p (U^{(p)} \cdot X^{(p)}), \tag{4.5}$$

where w_p represents an interaction strength, $U^{(p)}$ and $X^{(p)}$ are operators of rank p in spin space and coordinate space, respectively. A contribution from second-order in perturbation theory to a state ϕ can then be written as

$$\eta(\phi) = -\sum_j \frac{\langle \phi | H_1 | \psi_j \rangle \langle \psi_j | H_1 | \phi \rangle}{\Delta E_j}, \tag{4.6}$$

where ψ_j defines an intermediate state with energy denominator ΔE_j. The summation is done over all intermediate states ψ_j. As far as ψ_j varies in this summation, within a fixed configuration with respect to harmonic-oscillator (HO) shells, ΔE_j remains constant due to the degeneracy of single-particle energies in a given HO shell. We mention that the usage of non-degenerate perturbation theory yields only small changes.

Such a configuration for a given HO shell is denoted by S. As ΔE_j is a constant within a fixed shell S, we label it as ΔE_S. Note that S corresponds to a part of the Q-space, while ϕ is in the P-space. The term $\eta(\phi)$ can then be decomposed into contributions from individual S's as

$$\eta(\phi) = -\sum_S \frac{\zeta(\phi, S)}{\Delta E_S}, \tag{4.7}$$

where

$$\zeta(\phi, S) = \sum_{j \in S} \langle \phi|H_1|\psi_j\rangle\langle\psi_j|H_1|\phi\rangle. \tag{4.8}$$

For a given S, all ψ_js are included, and the summation can be replaced by the closure relation as

$$\zeta(\phi, S) = \langle\phi|\{H_1 H_1\}_S|\phi\rangle, \tag{4.9}$$

where the parentheses $\{\ \}_S$ are introduced to indicate that the second H_1 changes ϕ to an S-configuration state in the Q-space and the first H_1 moves it back to state ϕ in the P-space. In other words, $H_1 H_1$ in this equation cannot be a simple product, but a certain contraction is needed as we shall show soon.

By utilizing Eq. (4.5), we obtain

$$\{H_1 H_1\}_S = \sum_{p_1,p_2} w_{p_1} w_{p_2} \{(U^{(p_1)} \cdot X^{(p_1)})(U^{(p_2)} \cdot X^{(p_2)})\}_S$$

$$= \sum_{k=0,1,2} (2k+1) \left(\sum_{p_1,p_2} w_{p_1} w_{p_2} \begin{Bmatrix} p_1 & p_2 & k \\ p_1 & p_2 & k \\ 0 & 0 & 0 \end{Bmatrix} \{[[U^{(p_1)} \times U^{(p_2)}]^{(k)} \times [X^{(p_1)} \times X^{(p_2)}]^{(k)}]^{(0)}\}_S \right), \tag{4.10}$$

where the terms in curly brackets are $9j$ symbols and k implies the rank of the recoupling. The operator $\{[U^{(p_1)} \times U^{(p_2)}]^{(k)}\}_S$ acts in the P-space as a rank-k two-body operator in spin space, while $\{[X^{(p_1)} \times X^{(p_2)}]^{(k)}\}_S$ acts as a rank-k two-body operator in coordinate space. Because the contraction due to the elimination of the Q-space does not affect the angular momentum properties, the variable $k = 0, 1, 2$ represents induced central, spin-orbit and tensor forces in the P-space, respectively.

Since we are mainly interested in the tensor component, we focus on the case of $k = 2$, with the obvious restriction $p_1 + p_2 \geq 2$. Since the above $9j$ symbols is proportional to $1/\sqrt{(2p_1 + 1)(2p_2 + 1)}$, it is easy to convince oneself that the central force component receives the largest contribution from the $9j$ symbol. Furthermore, for our analyses it is important to keep in mind that the expectation value of the central component is the largest in absolute value, the tensor component the second largest and the spin-orbit term gives rise to the smallest contribution to the renormalized $V_{\text{low}k}$ interaction.

From these considerations, for $k = 2$ the largest contribution comes from the combination $p_1 = 0$, $p_2 = 2$ or $p_1 = 2$, $p_2 = 0$ in Eq. (4.5), that is either a central-tensor or a tensor-central combination. Let us now discuss this case. We assume without loss of generality that the tensor component of H_1 acts on the ket state of the matrix element being considered. While the central component of H_1 acts afterward on this state, we can also consider that this central force acts to the left on the bra state.

We then take the overlap between these two states by considering one by the tensor on the ket side, and the other by the central on the bra side. These two states are sum-rule states for the two forces within the S-configuration space. As the central force and the tensor force are very different in nature, such sum-rule states are very different from each other in general, leading to a very small overlap. This is the main reason why the combination of the central force and the tensor force produces small contributions.

This argument does not hold for the case where the tensor component of H_1 acts twice in the term to second-order in perturbation theory. However, due to the angular momentum coupling, the product of two tensor forces ($p_1 = p_2 = 2$ in Eq. (4.5)) yield small contributions to the $k = 2$ terms of Eq. (4.5). For higher orders, other tensor-force components may show up, but there is no mechanism to enhance their contributions.

The small contribution of the tensor force in MBPT can be viewed to be reasonable also under the following intuitive picture: after multiple actions of the forces, the spin dependence is smeared out, and only the distance between two interacting nucleons becomes the primary factor to the whole processes. This results in the dominance of the induced effective interaction by the central components and yields only a minor change in the tensor component.

It is instructive to study in more detail the contributions to second-order in perturbation theory. To do so, we single out the by far largest second-order term, namely the so-called core-polarization term, depicted in Fig. 2.3. For the core-polarization diagram we can show that the contribution to the tensor force vanishes by simple angular momentum algebra arguments. The contribution to a specific core-polarization matrix element can then be written as

$$
\begin{aligned}
\langle am_a bm_b | V_T^{\text{cp--eff}} | cm_c dm_d \rangle &= \sum_{p,m_p,h,m_h} \langle am_a pm_p | V_C | cm_c hm_h \rangle \langle hm_h bm_b | V_T | pm_p dm_d \rangle / \Delta E \\
&= \sum_{n_p,l_p,n_h,l_h} \Big(\sum_{j_p,m_p,j_h,m_h} \langle am_a pm_p | V_C | cm_c hm_h \rangle \langle hm_h bm_b | V_T | pm_p dm_d \rangle \Big) / \Delta E_S \\
&= \sum_{n_p,l_p,n_h,l_h} \Big(\sum_{m_{lp},m_{sp},m_{lh},m_{sh}} \langle am_a n_p l_p m_{lp} m_{sp} | V_C | cm_c n_h l_h m_{lh} m_{sh} \rangle \\
&\quad \times \langle n_h l_h m_{lh} m_{sh} bm_b | V_T | n_p l_p m_{lp} m_{sp} dm_d \rangle \Big) / \Delta E_S,
\end{aligned}
\tag{4.11}
$$

where $V_T^{\text{cp--eff}}$ is the induced tensor force, V_T and V_C are the tensor force and central force components from H_1, respectively. With a harmonic oscillator basis, the term ΔE_S represents an energy denominator which is constant for a given set of quantum numbers n_p, n_h, l_p and l_h, as discussed above. Here $a = (n_a, l_a, j_a)$, and m_a denotes magnetic substate of l_a. Note that the two-body states are not anti-symmetrized. The states p and h represent particle and hole states, respectively. In the third line of the equation, only particle and hole states are transformed to the ls coupling scheme. Note that the intermediate states are summed up to fulfill spin-saturation within each HO major shell.

We can divide the contribution into two different types according to the spin dependence of the central force. One comes from the terms whose central force part V_C includes $\sigma \cdot \sigma$ (type I) and the other does not (type II). With our summation tailored to a spin-saturated core or an excluded Q-space

with all spin-orbit partners, we can prove that type II contributions always vanish because the first factor is diagonal with respect to spin, that is $m_{sp} = m_{sh}$, and the second factor is zero when we sum over spin-saturated contributions. Therefore, only a spin-dependent central force results in non-vanishing contributions to the tensor force for higher-order terms in $V_{\mathrm{eff}}^{\mathrm{SM}}$. Finally, the contribution to the tensor force from the spin-dependent central force is quite small because the spin-dependent central force is generally by far smaller than the spin-independent central force in modern realistic NN potentials.

In conclusion, medium effects produce minor contributions to the tensor-force component, resulting in a tensor-force component that is dominated by the bare NN interaction. Our hypothesis about Renormalization Persistency is fulfilled to a good extent by the tensor force.

4.5   Comparison with phenomenological interactions

In this section, we compare our effective interaction V_{eff} to the phenomenological interactions. As the phenomenological interactions, we take USD as sd-shell interaction [12, 13], GXPF1 as pf-shell interaction [16] and SDPF-M as $sdf_{7/2}p_{3/2}$-shell interaction [19].

Since in the phenomenological interactions they fix the matrix element one by one, the reproduction ability of the experimental data is much better than the interaction derived by the microscopic theories. Moreover, our method does not include the effect of three-body force, the continuum states, the difference of wave function from harmonic oscillator basis, which sometimes are crucial to explain the physics in extreme cases.

In this sense, it is interesting to see how our method reproduce and does not reproduce the phenomenological interactions in each mass region.

When we find the differences between the interactions derived via the EKK method and the phenomenological interactions, we can consider two aspects of the fact.

For phenomenological interaction reproduce the experimental data well by construction, such an interaction is kind of "answer" of the effective interaction for the shell model. From this standpoint, the deviation from the "answer" of the microscopic effective interaction should be corrected in some way. The major points we can improve are the better approximations in the evaluation of $\hat{Q}$-box and including the physics we did not consider in the EKK method. For the first point, we will see the $V_{\mathrm{low}k}$ cutoff Λ dependence of the results and the convergence property of the V_{eff}. The E-dependence of the results also tells us how the approximation works. For the second point, for example, what is convincing is that we do not include the effect from the genuine three-body force at the beginning of the calculation. The perturbative treatment of three-body force is considered to be sometimes crucial when we consider the physics far from the stability line.

On the other hand, since the effective interaction derived by EKK method is originated in bare realistic NN interaction, the interaction is expected to include such rich features of the realistic NN interaction as it is, for example, the spin-tensor structures. Those features appear as a channel dependence

of the monopole interaction. The phenomenological interactions are fit to tremendous experimental data in the corresponding region. By construction, they reproduce the experimental data in a great precision. However, one should be careful with this fitting, because the experimental data include every configuration of the nuclei, meaning that some of those states are not adequate to express the states within the shell-model framework. For example, for the physics of dripline, the continuum degrees of freedom is important. It is known that there exist the cluster-like structures in some nuclei. On the other hand, the shell model should not reproduce those states. Although most of phenomenological interaction is designed to be reproduce only shell-model like states, the one of the role of effective interaction derived from microscopic theory is to clarify which states are shell-model like and which states are not. Therefore, the deviation between EKK method and phenomenological force should not be always considered negatively, but especially the difference of channel dependence might imply the interesting physics, which is not described only by phenomenological theories.

4.5.1 Comparison with USD interaction in *sd*-shell

As our first example, we calculated the effective interaction in *sd*-shell and compare it to phenomenological interaction. Figure 4.16 shows the comparison of V_{eff} obtained by EKK method and USD
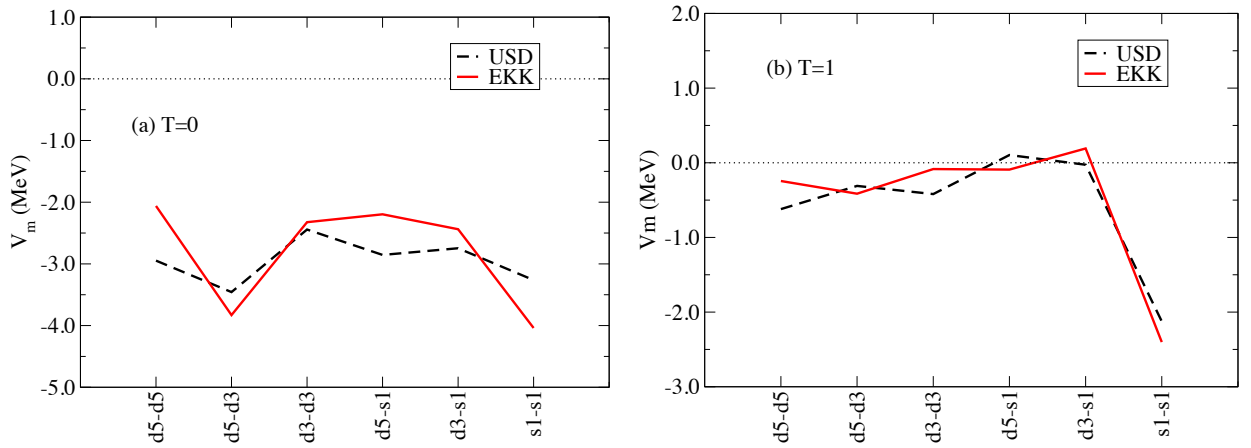

Figure 4.16: Comparison of monopole part of the interaction between USD and V_{eff} (a) $T = 0$ channel and (b) $T = 1$ channel. Dashed lines are USD interaction and the solid lines are V_{eff} derived via the EKK method.

interaction. The left is the comparison in $T = 0$ channel and the right is $T = 1$ channel. Considering the fact that we do not have any adjustment in EKK method, the agreement is generally no so bad. However, more precisely watching the graphs, there are some differences between two interactions. In $T = 0$ channel, V_{eff} by EKK has more channel dependence and the monopole related to $d_{5/2}$ orbit is repulsive and inversely $s1 - s1$ channel is more attractive.
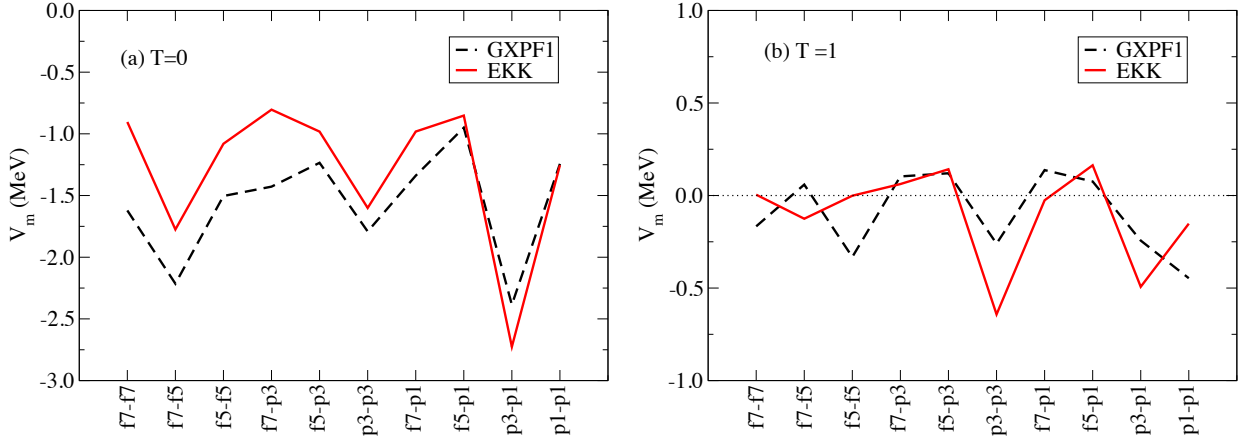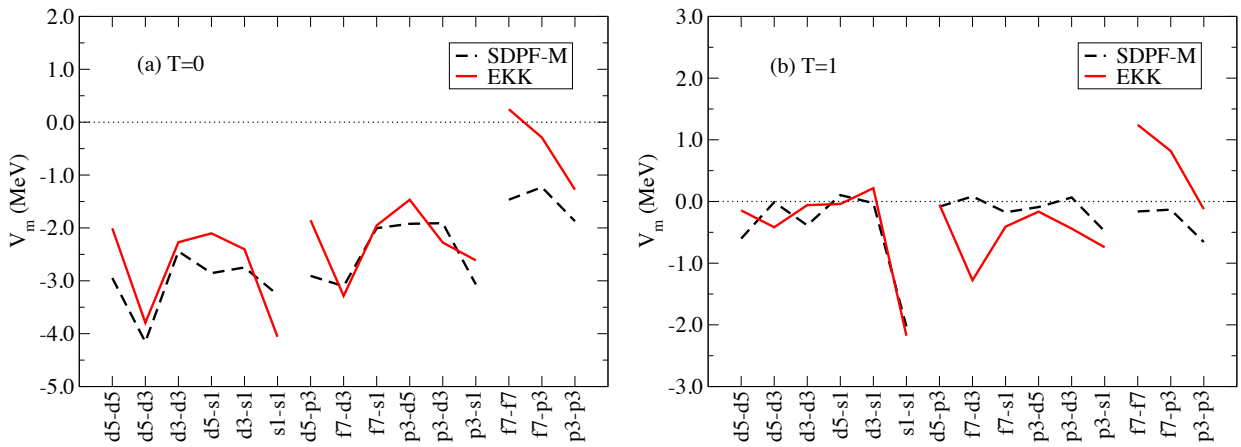
Figure 4.17: Comparison of monopole part of the interaction between GXPF1 and V_{eff} (a) $T = 0$ channel and (b) $T = 1$ channel. Dashed lines are GXPF1 interaction and the solid lines are V_{eff} derived via the EKK method.

4.5.2 Comparison with GXPF1 interaction in pf-shell

Figure 4.17 shows the comparison of V_{eff} obtained by EKK method and GXPF1 interaction [16]. As a general trend, the monopoles of EKK in $T = 0$ channel is less attractive than GXPF1 interaction, but the relative channel dependence is similar. On the other hand, however, the channel dependence in $T = 1$ channel are quite different in EKK and GXPF1, while the averages of this two interactions agree better than $T = 0$ case.

4.5.3 Comparison with SDPF-M interaction in $sdf_{7/2}p_{3/2}$-shell

Figure 4.18: Comparison of monopole part of the interaction between SDPF-M and V_{eff} (a) $T = 0$ channel and (b) $T = 1$ channel. Dashed lines are SDPF-M interaction and the solid lines are V_{eff} derived via the EKK method. Model space is $sdf_{7/2}p_{3/2}$-shell, non-degenerate model space.

Figure 4.18 shows the comparison of V_{eff} obtained by EKK method and SDPF-M interaction. In $T = 0$ channel, both SDPF-M and EKK interactions have the feature that the hierarchy of the strength of monopole. The monopoles of *sd-sd* shell are the most attractive, those of *sd-pf* inter-shell interaction are the next, and those of *pf-pf* shell are the least attractive. It is worth noticing that in *pf-pf* channel two interactions are very much different. In $T = 1$ channel, the monopole of *sd-sd* shell interaction is similar in strength, but the monopole of *sd-pf* inter-shell interaction is more attractive in EKK method than SDPF-M.

4.6 Dependence on $V_{\text{low}k}$ cutoff

As we stated before, the nuclear force has strong short-range repulsion and we need to renormalize those degrees of freedom to low-momentum interaction. The $V_{\text{low}k}$ cutoff is often refereed as the Greeks Λ, which is the resolution of obtained low-momentum interaction. The physics with higher momentum is not seen with this low-momentum interaction. In the nuclear many-body problem, those degrees of freedom is not needed. The typical value of cutoff of $V_{\text{low}k}$ is $\Lambda \approx 2.0 - 2.5 \text{fm}^{-1}$, where the $V_{\text{low}k}$ is almost seems to be model independent [40, 38]. By the study of ^{3}He and ^{4}He with exact solution within two-body interaction of three-body and four-body problem, the $V_{\text{low}k}$ reproduce those binding energies the best with the same cutoff $\Lambda \approx 2.0 \text{fm}^{-1}$ [42].

This fact can be explained as follows: the nuclear force includes three-body force because the nucleons themselves are composite particles. The renormalization to a low-momentum space of the nuclear force inevitably produces the "induced" three-body forces as well. If we can reproduce the binding energy of ^{3}He and ^{4}He with two-body $V_{\text{low}k}$ interaction only, we can expect that the three-body force happen to be canceled out, and we do not need to think about the three-body force in whole mass region.

However, things is not that simple. This ansatz might only valid in three and four-body system, because the spin-tensor property of three-body force can differ between "induced" three-body force and genuine three-body force. Actually, there are many works where three-body force play a crucial role in considering the neutron-rich isotopes [45, 46, 47, 48, 49].

In this section, we will explore the cutoff Λ dependence of V_{eff}, varying the Λ in the region of $\Lambda \approx 2.1 - 2.5 \text{ fm}^{-1}$.

Figure 4.19 shows the cutoff Λ dependence of monopole part of the interaction in neutron-neutron channel and proton-neutron channel. Model space is chosen as *sd*-shell as an example. The Λ dependence in neutron-neutron channel is not large. The similar observation is in reference [40] as well, they claim that the results are insensitive to cutoff Λ around $\Lambda = 2.0 \text{ fm}^{-1}$. On the other hand, the Λ dependence in proton-neutron channel is relatively large.

To see how it affects the level energies of atomic nuclei, we performed shell-model calculations with the same interaction, varying the cutoff Λ in the same region. The single particle energies are taken from USD interaction, that is, $\epsilon_{d5/2} = -3.94780$ MeV, $\epsilon_{d3/2} = -3.16354$ MeV and $s1/2 =$
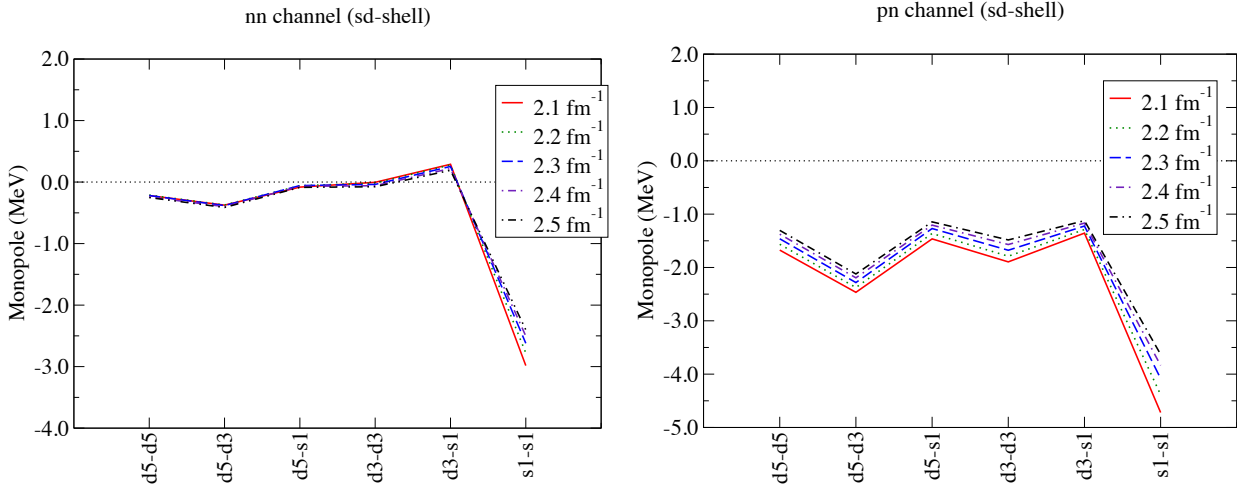
Figure 4.19: Cutoff dependence of the monopole part of the effective interaction V_{eff}. The cutoff is taken from 2.1 fm^{-1} to 2.5 fm^{-1}.

1.64658 MeV. In Fig. 4.20, the cutoff dependencies of the level scheme of ^{18}O and ^{18}F are presented,

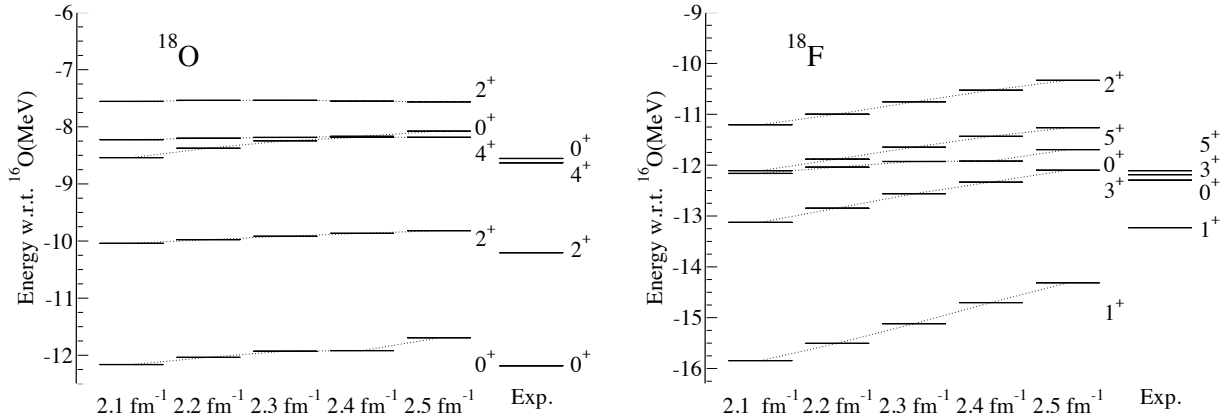Figure 4.20: Cutoff dependence of the level scheme of ^{18}O and ^{18}F. The cutoff Λ is varied from 2.1 fm^{-1} to 2.5 fm^{-1} and the experimental data is listed at the right-most levels.

as an example to examine the neutron-neutron interaction and the proton-neutron interaction. For the calculation of ^{18}O, considering the energy scale and the fact that we do not have any adjustment in EKK method, the agreement to experimental data is nice in general. Although we still see the Λ dependence, especially for two 0+ states, the results looks stable.

On the other hand, the results for ^{18}F depend on Λ. This dependence can be interpreted by two reasons. One is that the effects of induced higher-body force. If we calculate the effective interaction including all the induced higher-body force, results should be completely invariant under the change of cutoff Λ, although practically it is not possible. The other reason is that our truncation of the Q-space. The whole Hilbert should be theoretically infinite, while in the practical calculation we need to truncate. In general, in the harmonic oscillator potential, the large $(2n + l)$ value corresponds to higher

energy and therefore higher momentum. Therefore, the larger the cutoff Λ is, the larger Hilbert space we need to include as Q-space. We included only nine major shells throughout these calculations, independently of cutoff Λ. Therefore, the effective interaction and the resultant level energies depend on Λ, but when we include larger shells as Q-space, it is expected that the dependence is suppressed. We discuss those convergence properties of V_{eff} in the next section with an example.

Therefore the issue that which cutoff we have to choose is non-trivial. It should be discussed with full consideration with sufficiently large whole Hilbert space, and this is one of the important future works. In this thesis, to save the computational time, we use the nine major shell as the whole Hilbert space for most cases. Simultaneously, we used the cutoff of $\Lambda = 2.5$ fm^{-1}, for this seems to reproduce the experimental values the best. This choice of Λ does not contradict to the consideration by Nogga and his collaborators [42]. Since their case for 3N and 4N system and ours is 18N system, with inert core of ^{16}O. It is no less logical to choose the $V_{\text{low}k}$ cutoff Λ to reproduce the level energies of ^{18}O and ^{18}F, than choose the Λ to reproduce the biding energies of ^{3}He and ^{4}He the best. We have to note that the effective two-body interaction originated from three-body force in $T = 1$ channel is also non-negligible, and therefore we have to include this effect before finally fix the cutoff Λ. This point will be the future work.

4.7 Convergence property of V_{eff}

The $\hat{Q}$-box expansion is exact if all the excitations are included as Q-space degrees of freedom and infinite degrees of perturbation. Obviously, numerical calculation does not allow to include everything exactly.

The perturbation can only be performed at most up to third order in V, and it seems fairly well converged as we saw before. We also truncate Q-space. In the preceding sections, we only include $9\,\hbar\omega$ shell space as whole $(P + Q)$-space, that means, the Q-space intermediate states consist of the particles whose $2n + l$ value are less than $9\,\hbar\omega$ are only included for the evaluation of the $\hat{Q}$-box.

In this section, we will see how this truncation works. As a test, we calculated the sd-shell interactions with the total $(P + Q)$-space with $7\,\hbar\omega$, $9\,\hbar\omega$ (our preceding calculations), $11\,\hbar\omega$ and $13\,\hbar\omega$.

Up to date, the largest calculations include $13\hbar\omega$ [55, 56]. The necessary inclusion of $n\hbar\omega$ relate to the cutoff of the $V_{\text{low}k}$. The smaller the cutoff is, the less $n\hbar\omega$ have to be included. It is explained as follows: in $V_{\text{low}k}$, the interactions above the certain cutoff Λ is not defined at all. The relative momentum k is related to the kinetic energy of the colliding two particles by $E = 2k^2$ in the scattering unit ($\hbar = c = m = 1$). Therefore, $\Lambda = 2.0$ fm^{-1} corresponds to the energy in MeV by

$$E_{rel} = \frac{2\hbar^2 k^2}{m} = 2k^2 \frac{(\hbar c)^2}{mc^2} \approx 2 \times (2.0)^2 \times \frac{200^2}{1000} = 320 \text{ MeV} \tag{4.12}$$

In the case of V_{eff} for sd-shell, we took the harmonic oscillator of $\hbar\omega = 14$ MeV. Relating this relative energy between two nucleons directly to the eigenenergies of harmonic oscillator states, considering

the fact that we have two nucleons, the necessary inclusion of $n\hbar\omega$ is typically the order of $15-20\,\hbar\omega$. When the cutoff is raised to 2.5 fm^{-1}, $E_{rel} \approx 500$ MeV, the typical $n\hbar\omega$ is $20-30\,\hbar\omega$. Of course, because the interaction in momentum space is not completely transformed to harmonic oscillator space with finite number of basis, this is not a mathematically rigorous estimation.
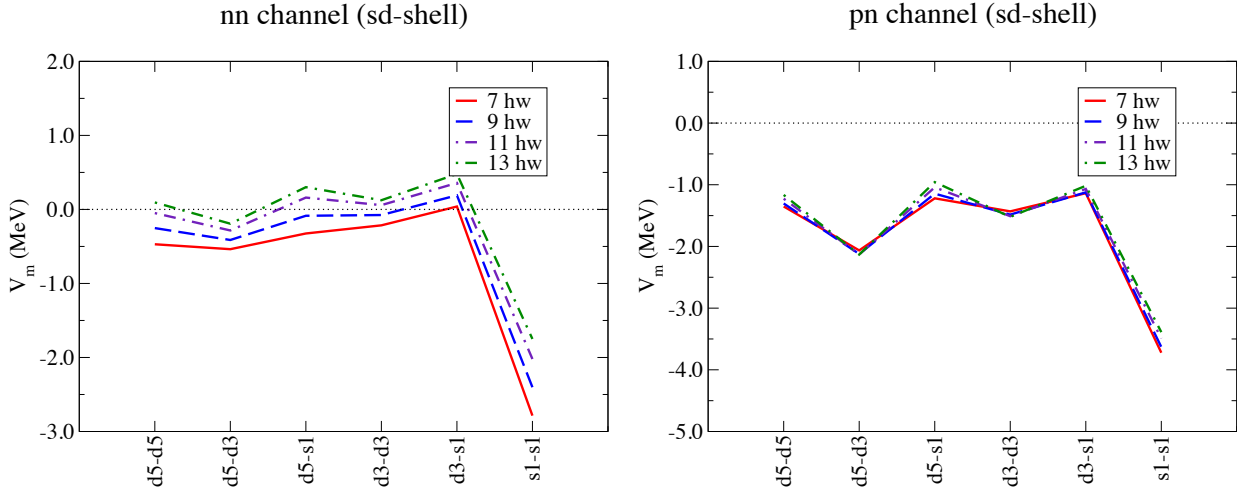

Figure 4.21:   Convergence property of the monopole part of the matrix element of V_{eff}. The total $P + Q$ space is shown by $n\hbar\omega$, $7, 9, 11, 13\,\hbar\omega$.

Figure 4.21 shows the convergence property of the matrix elements of V_{eff} obtained by EKK method, by showing the monopole part. Both in neutron-neutron channel and the proton-neutron channel the convergences are not perfect even for $13\hbar\omega$, unfortunately. For proton-neutron channel, however, the matrix elements looks enough well converged already 9 or 11 $\hbar\omega$, which is the same as our truncation in the most of this thesis. For neutron-neutron channel, on the other hand, the monopole part of the matrix element seems not to be converged yet even at 13 $\hbar\omega$. The calculation done in 13 $\hbar\omega$ is the best calculation up to date, and the indicate that more precise exploration about the convergence property is important.

One should also note that the monopole reflect the matrix elements which have the large angular momentum. To see the low angular momentum matrix elements, we also show the level schemes of ^{18}O and ^{18}N, in Fig. 4.22. Let us start from ^{18}O. All the levels are nearly convergent, but are not fully converged yet. The calculation in 15 $\hbar\omega$ is expected. Next, we move to ^{18}F. The general convergence is better than ^{18}O. However, the ground state 1^+ state is only converged at 11 or 13 $\hbar\omega$, which is different from our expectation from Fig. 4.21.

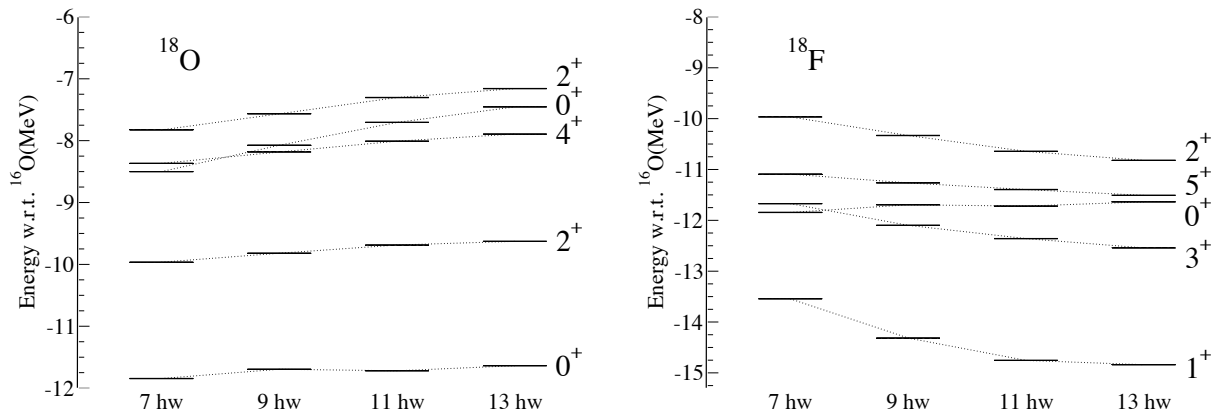Figure 4.22: Convergence property of the level schemes of ^{18}O and ^{18}F, respectively. The total $P + Q$ space is shown by $n\hbar\omega$, $7, 9, 11, 13\ \hbar\omega$.

Chapter 5

Shell-model calculation with the effective interaction based on EKK method

In this chapter, we discuss the possible applications to calculate the various kinds of atomic nuclei using newly derived interaction V_{eff} by EKK method. Although the results are preliminary, it is useful to present the future direction to proceed and show the utility of the EKK method.

The main purpose of EKK method is, of course, deriving the effective interaction defined with more than one-major shell. We actually obtained the effective interaction for sd-shell and pf-shell for degenerate model spaces, $sdf_{7/2}p_{3/2}$-shell and $pfg_{9/2}$-shell for non-degenerate model spaces. Then, we can now move to calculate the physics of atomic nuclei with appropriate model space. When we calculate the properties of the nuclei away from the stability line, the inclusion of two-major shell degrees of freedom is essential. For example, the $N = 20$ magic number is known to be broken in the wide region of the nuclear chart, where $sdpf$-shell or $sdf_{7/2}p_{3/2}$-shell degrees of freedom is essential [51]. The inclusion of $g_{9/2}$ orbit to pf-shell is also interesting [55].

In Sec. 5.1, a specific nuclei ^{16}N is studied. This nucleus has one neutron and one proton hole with respect to ^{16}O core, and therefore have a characteristic structure of the level scheme. In Sec. 5.2, Fluorine isotope is studied in the model spaces of $sdf_{7/2}p_{3/2}$-shell and $sdpf$-shell. The shell-model calculation in this Chapter is performed using "KSHELL", which enable us the massively parallel computation, and is developed by N. Shimizu recently [57].

5.1   Shell-model calculation of ^{16}N

The nucleus ^{16}N is consist of seven protons and nine neutrons. When we consider the normal configuration, it has one proton hole in $p_{1/2}$ orbit and one neutron in $d_{5/2}$ orbit of $s_{1/2}$, with respect to ^{16}O core.

Figure. 5.1 is the schematic picture of ^{16}N. Because of the large shell gap between p-shell and sd-shell, the low-lying levels of ^{16}N should be explained with the degrees of freedom of one proton hole in $p_{1/2}$ orbit and one neutron in $d_{5/2}$ or $s_{1/2}$ orbit, respectively.

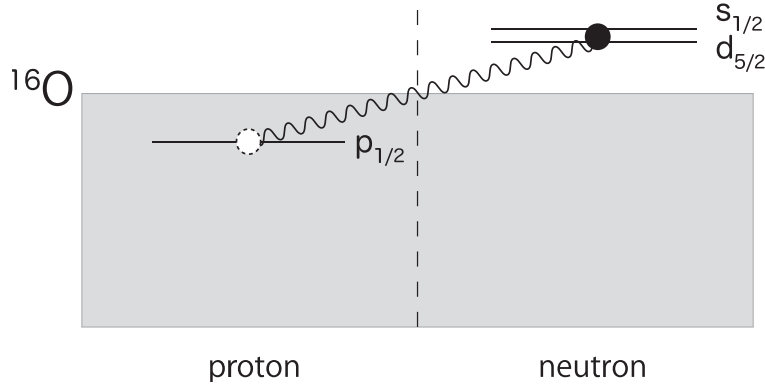When we explore this nucleus with the shell-model, the inter-shell matrix elements are essential.

Figure 5.1: Schematic image of ^{16}N. Because of large shell gap between p-shell and sd-shell, the low-lying levels of ^{16}N should be explained with the degrees of freedom of one proton hole in $p_{1/2}$ orbit and one neutron in $d_{5/2}$ or $s_{1/2}$ orbit, respectively.

The low-lying levels of ^{16}N are expected to have negative parity reflecting the fact that the hole state in $0p_{1/2}$ orbit has negative parity and the particle in the $0d_{5/2}$ has the positive parity. The possible spin-parities are 3^-, 2^-, 1^-. The particle state can also be $1s_{1/2}$, for the difference of single-particle energies of $0d_{5/2}$ and $1s_{1/2}$ are just around 500 keV. For the particle state $1s_{1/2}$ the possible angular momentum is 1^-, 0^-. Therefore, we expect that those states are nearly degenerate and low-lying and there should be gap between the other states.

In the actual calculation, we prepared the effective interaction defined in psd-shell using EKK method, and calculate the several low-lying states of ^{16}N by shell-model calculations. The $\hbar\omega =$ 14 MeV is designed appropriate for mass number $A = 16$. The single-particle energies are taken to reproduce the low-lying states of ^{15}O and ^{17}O.

Figure 5.2 shows the result of shell model calculation of ^{16}N with $V_{\rm eff}$ by EKK method and the experimental data. As we saw in Fig. 5.1, the natural configuration is one neutron and one proton hole with respect to ^{16}O core. Since the single particle energy of $s_{1/2}$ orbit is near from that of $d_{5/2}$, the neutron can excite to $s_{1/2}$ orbit as well. Then, the allowed angular momentum configurations are $J = 3, 2, 1, 0$ and the allowed parity is negative. Beyond those natural configuration, the more complex configuration which need the excitation beyond the shell gap between p-shell and sd-shell are placed above the red filled circle as shown in Fig. 5.2. This structure in which the negative parity states are placed as low-lying states and form a kind of multiplet is the characteristic feature of ^{16}N or ^{40}K. In those nuclei, one neutron (proton) above the shell gap and one proton (neutron) below the shell gap interact.

5.2   Application to $sdf_{7/2}p_{3/2}$-shell nuclei

In this section, the preliminary results of the isotopic chains of several nuclei above the Oxygen are presented. The model space is $sdf_{7/2}p_{3/2}$-shell.
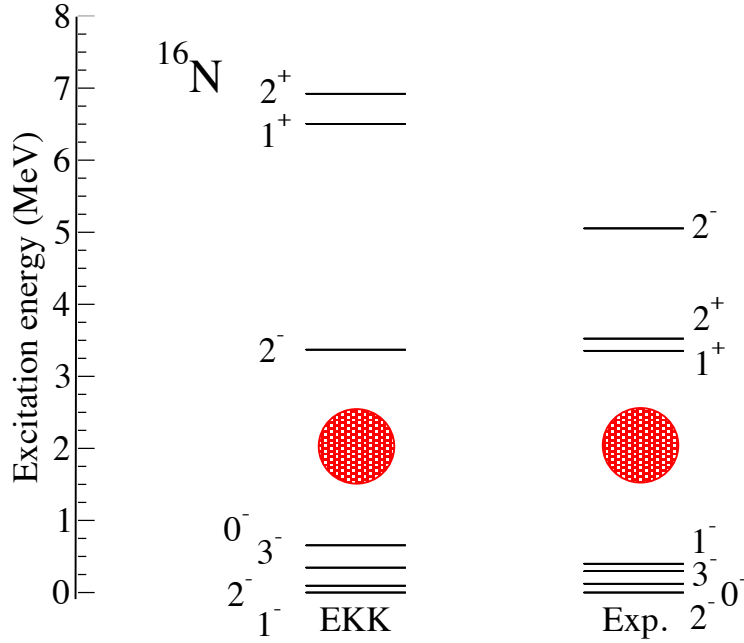
Figure 5.2: Level scheme of ^{16}N calculated in psd-shell model space with EKK method. Below the red filled circles are the states with natural configuration, where one neutron and one proton hole are added to ^{16}O core.

Throughout this section, we adapt a two-body effective interactions obtained via the EKK method, starting from the $V_{\text{low}k}$ interaction with cutoff Λ = 2.5 fm^{-1} starting from the χN3LO realistic NN interaction. We adapted, on the other hand, the single-particle energies (SPEs) of SDPF-M interaction, after slightly modify them. Theoretically, the SPEs can also be calculated via the EKK method, but the convergence with respect to higher $\hbar\omega$ excitation is rather slow for SPEs and the contribution from the three-body force is known to be sizable, order of MeV. Then, as in most of these studies, we adapted the SPEs of phenomenological interaction basically. Modification is done in the manner that we can reproduce the spin-parity of selected nuclei. The SPEs are shown in Table. 5.1.

orbit	SPE (EKK)	SPE (SDPF-M)
$d_{5/2}$	-4.50000	-3.94780
$s_{1/2}$	-2.16354	-3.16354
$d_{3/2}$	1.64658	1.64658
$f_{7/2}$	7.10000	3.10000
$p_{3/2}$	7.10000	3.10000

Table 5.1: Single-particle energies defined in the model space $sd f_{7/2}p_{3/2}$-shell. The energies given as SPE (EKK) are adapted in the shell-model calculations. SPE (SDPF-M) is the single-particle energies of the SDPF-M interaction, shown as a reference.

The major modification is that the SPEs of the particles in pf-shell. From SDPF-M, the $\epsilon_{f7/2}$ and

$\epsilon_{p3/2}$ are raised by 4 MeV each, reflecting the fact that our inter-shell interaction is more attractive than SDPF-M. Actually, the energy gap between *sd*-shell and *pf*-shell is 14 MeV, when we consider the harmonic oscillator potential appropriate for ^{18}O. Therefore, the values we adapted can be considered as reasonable. The other modifications in $\epsilon_{d5/2}$ and $\epsilon_{s1/2}$ are to reproduce the spin-parities of odd-even nuclei in the Fluorine isotopes and Sodium isotopes.

Note that we do not include the contribution of three-body force in these calculations. It is known that the for the single particle energies the contribution of three-body force is order of MeV. The contribution to two-body force is not also negligible, order of several hundred keV.
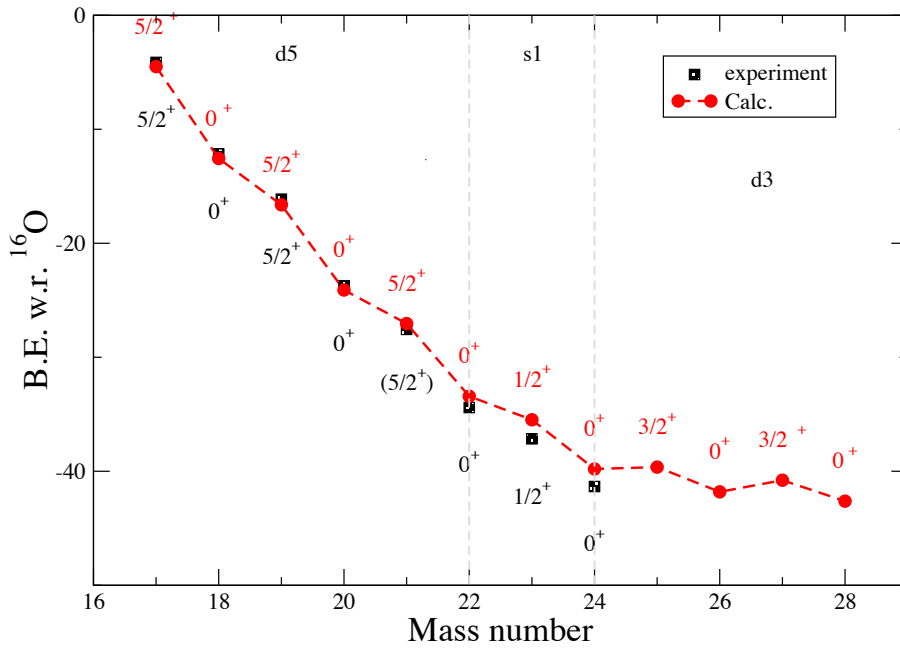

Figure 5.3: The binding energies for Oxygen isotopes. The squares shows the experimental values and the circles and lines show the theoretical values.

Figure 5.3 shows the results of the shell-model calculation of Oxygen isotopes. The ground state energies are presented, with squares the experimental data and the circles and dashed line are the results of the shell-model calculation done with the effective interaction derived via EKK method. The general agreement of the binding energies are rather good. The dripline of Oxygen is experimentally determined as ^{24}O, which is not reproduced in our calculations. This is not a surprise because it is also known that this dripline is well described by including the effective two-body force coming from the three-body force, in which $\Delta(1232)$ is excited as an intermediate states [45, 46, 47, 48, 49]. This effective two-body force originated in three-body force has repulsive contribution and makes the ^{26}O and ^{28}O less bound.

Figure 5.4 shows the results of Fluorine isotopes. The Fluorine dripline is far longer than that of Oxygen isotopes. A proton added to Oxygen changes the structure of effective single particle energies. We do not consider neither the Coulomb force nor the charge symmetry breaking of the effective interaction. Then we restrict ourselves to consider the binding energy with respect to ^{18}F,
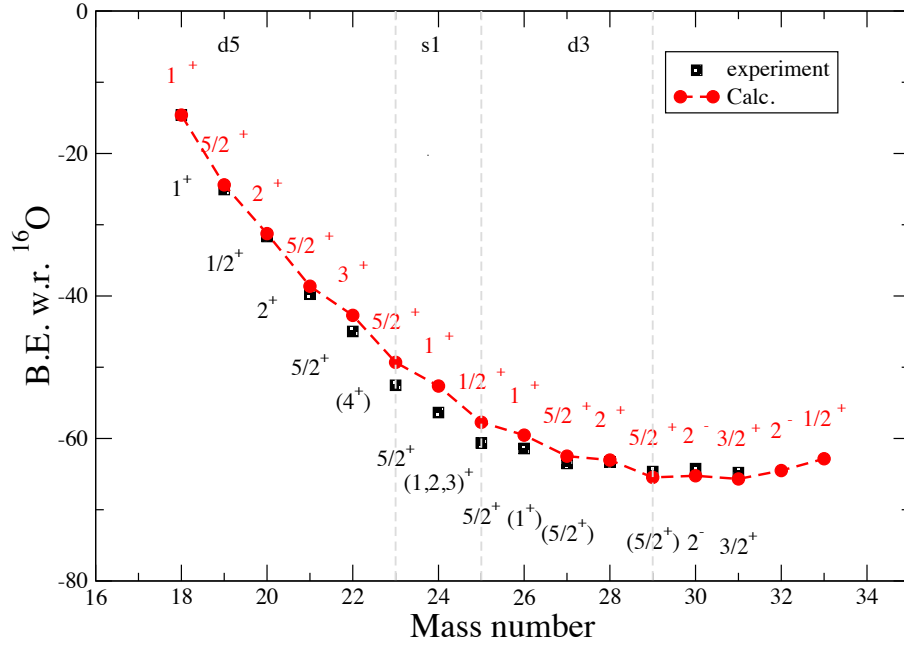
Figure 5.4: The binding energies for Fluorine isotopes. The squares shows the experimental values and the circles and lines show the theoretical values.

for we can expect that the effect of Coulomb force is nearly constant along the isotopic chain. In Fig. 5.4, the experimental values are subtracted by constant, to make the binding energies of ^{18}F by experimental data and the calculation equal.

In the isotopic chain, the nuclei above the ^{29}F can only calculated with the model space consist of more than one major shell. In particular, it is striking that we can reproduce the experimental dripline of ^{31}F. We can interpret this by the following mechanism. If we assume natural occupation, ^{31}F has two neutrons in the $f_{7/2}$ orbit. Knowing the fact that the curve of ground state energy around $N = 29$ is flat, the effective single particle energy of $f_{7/2}$ at $N = 29$ should be nearly zero. Once neutrons begin to fill the $f_{7/2}$ orbit, the effective single particle energies of $f_{7/2}$ gets higher, and at ^{31}F, it reaches the dripline.

For just a glance at the physics including island of inversion, we quickly see the results of Ne and Na isotopes, as those nuclei have three and four protons outside the ^{16}O core, respectively. In Figs. 5.5 and 5.6, the ground state energies of Neon and Sodium isotopes are presented. The squares are experimental values and the circles and the line are theoretical calculation. The subtractions of the Coulomb force are the same as in the case of Fluorine isotope, that is, the ground state energies of ^{20}Ne and ^{22}Na are adjusted. Looking at the figure, the ground state spin-parities and binding energies of Ne isotopes and the binding energies of Na isotopes are reasonably well described.

As a summary, we will mention the future work about the calculations. There results are preliminary in several reasons. First, we should think about the convergence problem as discussed in Sec. 4.3. Our calculation now is restricted to the $P + Q$-space of nine major shells, which is not fully sufficient. Second, we need to include effective two-body force derived from the three-body force.
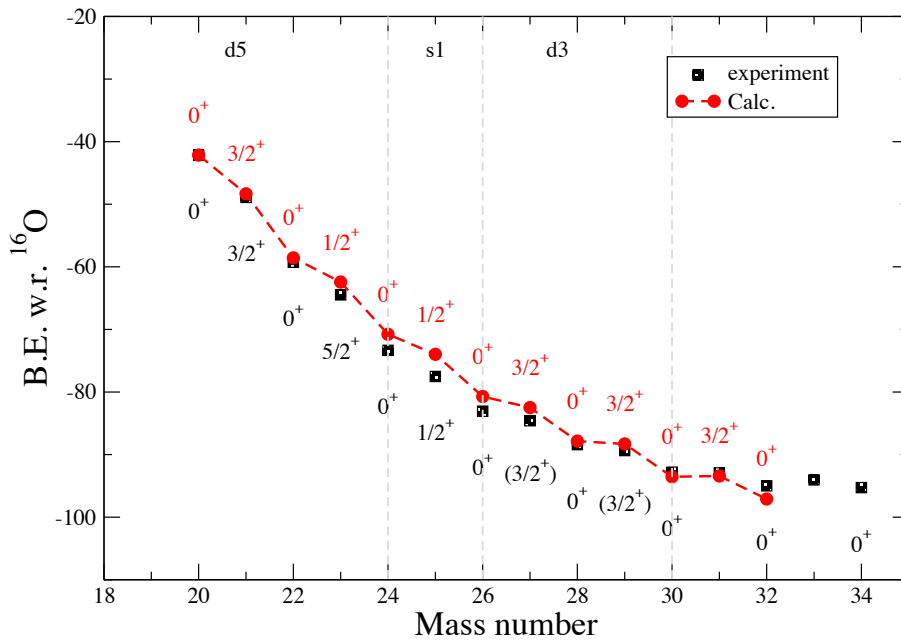
Figure 5.5: The binding energies for Neon isotopes. The squares show the experimental values and the circles and line show the theoretical values.
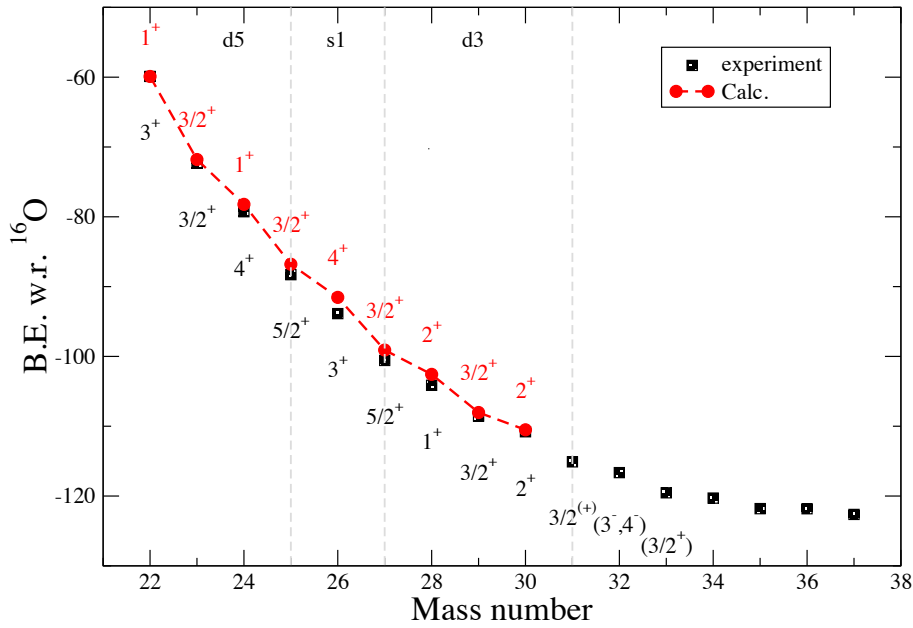

Figure 5.6: The binding energies for Sodium isotopes. The squares show the experimental values and the circles and line show the theoretical values.

Third, we still have the possibility to calculate SPEs by EKK method. For the SPEs, we need quite larger $P + Q$-space for the convergence than those of two-body interaction. The effect of three-body force is also large. Nevertheless, seeing from the results shown in Figs. 5.3 - 5.6, this line of work is promising. We are then quite sure that we can access to the physics of island inversion, for example, in near future.

Chapter 6

Summary and Concluding Remarks

We have presented a novel many-body theory (the so-called EKK method) to calculate the effective interaction V_{eff} for the shell-model calculation that is applicable not only to degenerate model spaces, but also to non-degenerate model spaces.

In Chapter 1, the introduction is given. The former half of Chap. 2 is devoted to the brief review of the history of the nuclear shell model and the nuclear force, including the theory to renormalize the strong short-range repulsion. In the latter half, we reviewed the theory of effective interaction, with the special emphasis on the Kuo-Krenciglowa method and Lee-Suzuki method. Chapter 3 is the theoretical explanation of EKK method. In Sec. 3.1, we presented the formal theory of EKK method, which is a summary of references [1, 2]. From Sec. 3.2 to the end of this thesis, we presented our original work. The method is based on a re-interpretation of the unperturbed Hamiltonian and the interacting part. A few non-trivial questions arise when applying the perturbation theory based on the re-interpreted Hamiltonian of EKK method, but we presented that we can still formulate the EKK method in the framework of many-body perturbation theory. We constructed the diagrammatic rules for EKK method and proved that the factorization can be achieved also in EKK method. The final expressions for the effective interactions can be understood as a Taylor series expansion of the Bloch-Horowitz Hamiltonian around a newly introduced parameter E. Since the change in E should not affect the effective interactions V_{eff}, the E-independence of the numerical results provides us with a sensible test of our framework and the approximations we make in the actual calculations.

In Chap. 4, we have presented numerical results for the effective two-body nucleon-nucleon interactions V_{eff}, with applications to shell-model calculations of selected nuclei, with and without the contribution from the folded diagrams. The degenerate model spaces are the sd-shell for the nuclei ^{18}O and ^{18}F, and the pf-shell for the nuclei ^{42}Ca and ^{42}Sc. Our non-degenerate model spaces consist of the single-particle states from the $sdf_{7/2}p_{3/2}$-shell and the $pfg_{9/2}$-shell. Based on our numerical results, we have found that our method works well in practical situations. For degenerate model spaces, our method gives the same results as the conventional KK method. In the non-degenerate model space, which is beyond the applicability of the KK method, we have shown that our method works nicely.

We have shown that our V_{eff} and therefore the energy levels are almost independent of the pa-

rameter E, as they should, if we calculate the $\hat{Q}$-box up to third order. This in turn suggests that the perturbative expansion of the $\hat{Q}$-box through third order gives almost converged results.

In Sec. 4.1.3, the difference between the EKK method and the KK method with an *ad hoc* modification of the unperturbed Hamiltonian is significant, especially for inter-shell interactions. This can have a large impact, for example, on the investigation of neutron-rich nuclei where the degrees of freedom defined by two or more major oscillator shells are important.

In Sec. 4.4, the renormalization persistency of the tensor force in EKK method is presented. Not only for degenerate model spaces, but also for non-degenerate model space, the tensor force has the property of renormalization persistency.

Sections. 4.6 and 4.7 are devoted to the detailed verification of the robustness of the results shown in EKK method. We still cannot say the results get converged completely, and we saw the dependence on the $V_{\text{low}k}$ cutoff Λ. We should note that our work is the first attempt to construct a robust way to derive the multi-shell effective interactions for the shell model starting from realistic nuclear interaction. Therefore, for our purpose, our calculation is not necessarily completely converged. The complete analysis on the convergence or cutoff dependence of the results is one of the important future works.

In Chap. 5, we selected a few applications of our new interaction obtained via EKK method, though the results are still preliminary. We prepared the effective interaction defined in *psd*-shell and *sd*$f_{7/2}p_{3/2}$-shell, and calculate ^{16}N and O, F, Ne, Na isotopes, respectively. In particular, the characteristic gap structure of the level scheme of the ^{16}N, and dripline of the F isotopes are amazingly well reproduced. We still need to work on these calculation to obtain the robust results, but we can say that this line of work is really interesting and promising.

Finally, we stress that our method has established a robust way to calculate microscopically the effective interaction in non-degenerate model spaces. These spaces involve typically more than one major oscillator shell. We believe that this is an indispensable step to make the nuclear shell model a reliable theory, in particular for exotic nuclei, based on a microscopic effective interaction derived from the realistic *NN* interactions.

Acknowledgments

Appendix A

Time-dependent formalism of Extended Kuo-Krenciglowa method

In Secs. 2.4 and 3.2, we reviewed and presented the time-dependent theory of the KK method and EKK method. To make the explanation clearer, in this appendix, we show here examples of the evaluation of the diagrams appearing in the $\hat{Q}$-box via the time-dependent formalism of KK and EKK method.

A.1   Time-dependent formalism of Kuo-Krenciglowa method

First, we start from the evaluation of the diagrams in KK method. As we saw in Eq. 2.76, what we need to evaluate is in the form of

$$\langle \psi_\alpha | H U(0, -\infty) | \psi_\beta \rangle. \tag{A.1}$$

As the minimal example, let us focus on a second-order contribution and set $\langle \psi_\alpha | = \langle c | a_a a_b$ and $| \psi_\beta \rangle = a_c^\dagger a_d^\dagger | c \rangle$. Combined with Eq. (2.61), the second-order contribution is written as, apart from the numerical factors,

$$
\begin{aligned}
&\lim_{\epsilon \to 0} \lim_{t' \to -\infty(1+i\epsilon)} \int_{t'}^{0} dt_1 \langle \psi_\alpha | H_1 H_1(t_1) | \psi_\beta \rangle \\
&= \lim_{\epsilon \to 0} \lim_{t' \to -\infty(1+i\epsilon)} \sum_{i,j,k,l} \sum_{i',j',k',l'} V_{ij,kl} V_{i'j',k'l'} \langle c | a_a a_b a_i^\dagger a_j^\dagger a_l a_k a_{i'}^\dagger a_{j'}^\dagger a_{l'} a_{k'} a_c^\dagger a_d^\dagger | c \rangle \\
&\quad \times \int_{t'}^{t} dt_1 e^{i(\epsilon_c + \epsilon_d - \epsilon_{l'} - \epsilon_{k'} \epsilon_{i'} + \epsilon_{j'} - \epsilon_a - \epsilon_b)t_1}.9
\end{aligned}
\tag{A.2}
$$

The bracket should be calculated by the Fock's theorem and a way to contract the creation and annihilation operators corresponds to a diagram. One possible diagram is presented in fig. A.1. In this case, Eq. (A.2) reads

$$\frac{V_{ah,cp} V_{pb,hd}}{\epsilon_c + \epsilon_d - \epsilon_c - \epsilon_p + \epsilon_h - \epsilon_b} = \frac{V_{ah,cp} V_{pb,hd}}{\epsilon_d - \epsilon_p + \epsilon_h - \epsilon_b} \tag{A.3}$$

where we used the notation of hole states, $b_i^\dagger = a_i$ when the state i is below the closed core.

In the next section, we will discuss the difference between KK method and EKK method.
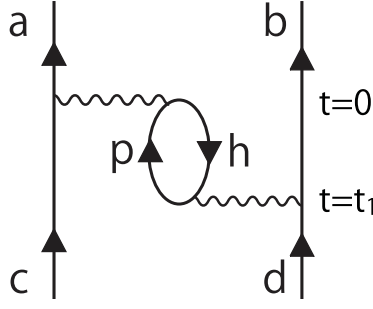
Figure A.1: core-polarization diagram.

A.2   Time-dependent formalism of Extended Kuo-Krenciglowa method

In EKK method, we start from the same Hamiltonian.

$$
\begin{aligned}
H &= H_0 + V \\
&= \sum \epsilon_\alpha a_\alpha^\dagger a_\alpha + \frac{1}{2} \sum V_{\alpha\beta,\gamma\delta} a_\alpha^\dagger a_\beta^\dagger a_\delta a_\gamma,
\end{aligned}
\tag{A.4}
$$

As we presented in sec. 3.2.1, in EKK method we change the unperturbed Hamiltonian and perturbation as follows,

$$
\begin{aligned}
H_0' &= PEP + QH_0Q \\
V' &= V - P(E - H_0)P,
\end{aligned}
\tag{A.5}
$$

Note that in this case, H_0' does not commute with single creation or annihilation operators. The definition of P-space is the same as KK method, Eq. (2.55). But in the interaction picture, the following equations are slightly different,

$$
\begin{aligned}
H_0' \, a_a^\dagger a_b^\dagger |c\rangle &= E \, a_a^\dagger a_b^\dagger |c\rangle, \\
H_0' \, a_a^\dagger a_p^\dagger |c\rangle &= (\epsilon_a + \epsilon_p) \, a_a^\dagger a_p^\dagger |c\rangle, \\
H_0' \, a_a^\dagger a_b^\dagger a_p^\dagger a_h |c\rangle &= (\epsilon_a + \epsilon_b + \epsilon_p - \epsilon_h) \, a_a^\dagger a_b^\dagger a_p^\dagger a_h |c\rangle.
\end{aligned}
\tag{A.6}
$$

Therefore, the interaction picture is a little complicated and should be defined within core plus two-body states.

$$
\begin{aligned}
|\psi_i(t)\rangle &= e^{-iH_0 t} |\psi_i\rangle & &= e^{-iEt} |\psi_i\rangle \\
\{a_a^\dagger a_p^\dagger |c\rangle\}(t) &= e^{-iH_0 t} \{a_a^\dagger a_p^\dagger |c\rangle\} & &= e^{-i(\epsilon_a + \epsilon_p)t} a_a^\dagger a_p^\dagger |c\rangle, \\
\{a_a^\dagger a_b^\dagger a_p^\dagger a_h |c\rangle\}(t) &= e^{-iH_0 t} \{a_a^\dagger a_b^\dagger a_p^\dagger a_h |c\rangle\} & &= e^{-i(\epsilon_a + \epsilon_b + \epsilon_p - \epsilon_h)t} a_a^\dagger a_b^\dagger a_p^\dagger a_h |c\rangle.
\end{aligned}
\tag{A.7}
$$

Then, Eq. (A.2) is changed as follows,

$$\lim_{\epsilon \to 0} \lim_{t' \to -\infty(1+i\epsilon)} \int_{t'}^{t} dt_1 \langle \psi_\alpha | H_1 H_1(t_1) | \psi_\beta \rangle$$

$$= \lim_{\epsilon \to 0} \lim_{t' \to -\infty(1+i\epsilon)} \sum_{i,j,k,l} \sum_{i',j',k',l'} V_{ij,kl} V_{i'j',k'l'} \int_{t'}^{0} dt_1 \langle c | a_a a_b a_i^\dagger a_j^\dagger a_l a_k e^{-iH_0' t_1} a_{i'}^\dagger a_{j'}^\dagger a_{l'} a_{k'} e^{iH_0' t_1} a_c^\dagger a_d^\dagger | c \rangle \qquad (A.8)$$

We will take the same example as in the previous section, that is, take the contraction corresponding to fig. A.1. In this case, Eq. (A.8) is written as,

$$\lim_{\epsilon \to 0} \lim_{t' \to -\infty(1+i\epsilon)} \sum_{p,h} V_{dh,bp} V_{hc,pa} \int_{t'}^{0} dt_1 \langle c | a_a a_b a_a^\dagger a_h^\dagger a_p a_c \, e^{-iH_0' t_1} \, a_p^\dagger a_b^\dagger a_d a_h \, (P e^{iEt} P + Q e^{iH_0 t} Q) \, a_c^\dagger a_d^\dagger | c \rangle$$

$$= \lim_{\epsilon \to 0} \lim_{t' \to -\infty(1+i\epsilon)} \sum_{p,h} V_{dh,bp} V_{hc,pa} \int_{t'}^{0} dt_1 \langle c | a_a a_b a_a^\dagger a_h^\dagger a_p a_c \, e^{-iH_0' t_1} \, a_p^\dagger a_b^\dagger a_d a_h a_c^\dagger a_d^\dagger | c \rangle e^{iEt} \langle c | a_d a_c a_c^\dagger a_d^\dagger | c \rangle$$

$$= \lim_{\epsilon \to 0} \lim_{t' \to -\infty(1+i\epsilon)} \sum_{p,h} V_{dh,bp} V_{hc,pa} \int_{t'}^{0} dt_1 \, e^{iEt} \, \langle c | a_a a_b a_a^\dagger a_h^\dagger a_p a_c \, Q e^{-iH_0 t} Q \, a_p^\dagger a_b^\dagger a_h a_c^\dagger | c \rangle$$

$$= \lim_{\epsilon \to 0} \lim_{t' \to -\infty(1+i\epsilon)} \sum_{p,h} V_{dh,bp} V_{hc,pa} \int_{t'}^{0} dt_1 \, e^{iEt} \, \langle c | a_a a_b a_a^\dagger a_h^\dagger a_p a_c \, e^{-i(\epsilon_c + \epsilon_p + \epsilon_b - \epsilon_h) t_1} \, a_p^\dagger a_b^\dagger a_h a_c^\dagger | c \rangle$$

$$= \frac{V_{ah,bp} V_{hc,pa}}{E - (\epsilon_c + \epsilon_p + \epsilon_b - \epsilon_h)}. \qquad (A.9)$$

Note that we used the fact that

$$P = \sum_i^d |\phi_i\rangle\langle\phi_i| = \sum_{i,j}^{\text{valence}} a_i^\dagger a_j^\dagger |c\rangle\langle c| a_j a_i$$

$$Q = 1 - P$$

$$(P + Q) e^{iH_0' t} (P + Q) = P e^{iEt} P + Q e^{iH_0 t} Q. \qquad (A.10)$$

Appendix B

Linked Cluster Theory in Extended Kuo-Krenciglowa method

We presented the theory of EKK method in Chap. 3. The EKK method has been expressed as the re-interpretation of the unperturbed Hamiltonian and the perturbation.

and we pointed out a few non-trivial issue to In this appendix,

B.1 Factorization theorem

First, we prove the factorization theorem briefly.

The factorization theorem insists that the unlinked pieces can be calculated independently and the final answer results in the product of those pieces. Let us consider the unlinked diagram consist of two pieces. Once the case of two pieces is proved, the cases of more than two pieces are also proved. In general, however, the denominator for the evaluation of the diagram is changed by the presence of the other disconnected pieces. Therefore, the fact that the disconnected pieces can be calculated independently helps us much and also is not trivial. We restrict ourselves to the case all the diagrams terminate at $t = 0$, because it is sufficient to prove it for our purpose.
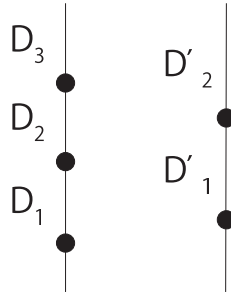

Figure B.1: The example for the factorization theorem.

Figure B.1 shows the typical example of the usage of factorization theorem. The diagram is consist of two disconnected pieces. The lines correspond to the states, which can be arbitrary many-particle states, and the black circles indicate the interaction vertices. Energy denominators of the

left disconnected piece are D_1, D_2, D_3 and those of the right are D'_1, D'_2. The left one includes three interaction vertices and the right one has two. The denominator is determined by the the ordering of the interactions. For example, in the case of Fig. B.1, the denominator is

$$D = D_1(D_1 + D'_1)(D_2 + D'_1)(D_2 + D'_2)(D_3 + D'_2). \tag{B.1}$$

Factorization theorem tells us that when we add up all the diagrams, finally we obtain the energy denominator of $D_1 D_2 D_3 D'_1 D'_2$.

We prove this factorization theory by the induction. Before move to the proof, let us make the notation clear. Since the numerator is not affected by the ordering of the interaction, we only have to consider the denominator. We denote the sum of the denominator factors for all the possible relative ordering, by $S_{n,m}$. The indices n and m is the number of vertices included the left and the right disconnected pieces, respectively. The D's are the energy denominators between vertices, $D_1, D_2, \cdots$ are for left piece and D'_1, D'_2 are for right piece. For each diagrams, we write the products of energy denominators in short by S_n and S'_m, that is,

$$S_n = \prod_{i=1}^{n} \frac{1}{D_i}, \qquad S'_m = \prod_{i=1}^{m} \frac{1}{D'_i}. \tag{B.2}$$

First, we start from the case both of the two pieces have only one interaction line. The contribution is written as $S_{1,1}$ Figure B.1 shows the possible ordering of the interactions appearing in the evaluation of $S_{1,1}$.
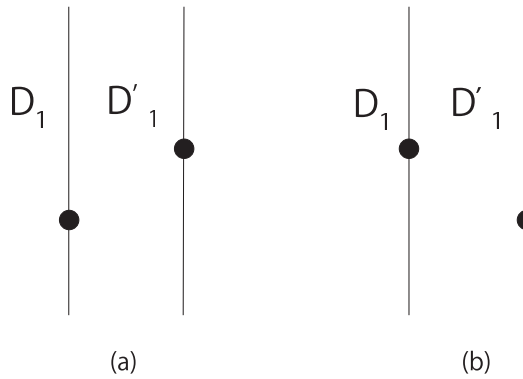

Figure B.2: The diagrams appearing in the evaluation of $S_{1,1}$.

In the diagram (a), the left interaction is earlier than the right interaction, and in the diagram (b), the right is earlier. In total, $S_{1,1}$ can be calculated as follows:

$$
\begin{aligned}
S_{1,1} &= (a) + (b) \\
&= \frac{1}{D_1} \frac{1}{D_1 + D'_1} + \frac{1}{D'_1} \frac{1}{D_1 + D'_1} \\
&= \frac{1}{D_1} \frac{1}{D'_1} \\
&= S_1 \cdot S'_1.
\end{aligned}
\tag{B.3}
$$

As the assumption of the induction, we assume that the value can be calculated by the product of two pieces, that is,

$$S_{k,l} = S_k \cdot S'_l \qquad (k \leq n, \; l \leq m). \tag{B.4}$$

Now we consider the quantity $S_{n,m+1}$, that is, the second piece has $m + 1$ vertices. Depending on the position of the last $m + 1$-th vertex, the sum of the denominator factors can be written as follows:

$$S_{n,m+1} = S_{n,m} \frac{1}{D_n + D'_{m+1}} + S_{n-1,m} \frac{1}{D_n + D'_{m+1}} \frac{1}{D_{n-1} + D'_{m+1}} + \cdots. \tag{B.5}$$

Let us label the time of the vertex as $(t_1, t_2, \cdots, t_n)$ and $(t'_1, t'_2, \cdots, t'_m, t'_{m+1})$. Then, the first term of Eq. (B.5) is for $t_n \leq t_{m+1} < 0$, and the second term is for $t_{n-1} \leq t_{m+1} < t_n$, and so on. Using the assumption of the induction Eq. (B.4), $S_{n,m+1}$ can be calculated as follows:

$$
\begin{aligned}
S_{n,m+1} &= S_n \cdot S'_m \frac{1}{D_n + D'_{m+1}} + S_{n-1} \cdot S_m \frac{1}{D_n + D'_{m+1}} \frac{1}{D_{n-1} + D'_{m+1}} + \cdots \\
&= S_n \cdot S'_m \left(\frac{1}{D_n + D'_{m+1}} \left(1 + \frac{D_n}{D_{n-1} + D'_{m+1}} \left(1 + \frac{D_{n-1}}{D_{n-2} + D'_{m+1}} \left(1 + \cdots \right. \right. \right. \right. \\
&\qquad \left. \left. \left. \left. + \frac{D_2}{D_1 + D'_{m+1}} \left(1 + \frac{D_1}{D'_{m+1}} \right) \cdots \right) \right. \right. \right) \\
&= S_n \cdot S'_m \cdot \frac{1}{D'_{m+1}} \\
&= S_n \cdot S'_{m+1}.
\end{aligned}
\tag{B.6}
$$

This indicates that the Eq. (B.4) is also valid for the case of $S_{n,m+1}$. The case of $S_{n+1,m}$ is the same. Therefore, it is proved that Eq. (B.4) is valid for all the n and m.

B.2 The evaluation of folded diagrams

To show how the folded diagram is calculated, we show the minimal example of the folded diagram in Fig. B.2. The railed line represents the state γ is in Q-space. The diagram Fig. B.2 is calculated as
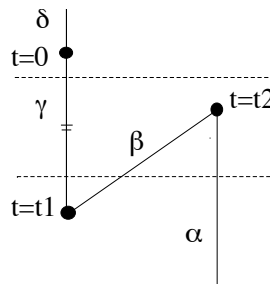

Figure B.3: folded diagram differentiation

$$(B.2) = \frac{V_{\alpha\beta}V_{\beta\gamma}V_{\gamma\delta}}{(\epsilon_\alpha - \epsilon_\gamma - (\epsilon_\alpha - \epsilon_\beta))(\epsilon_\alpha - \epsilon_\gamma)}$$

$$= V_{\alpha\beta}V_{\beta\gamma}V_{\gamma\delta} \frac{\left((\epsilon_\alpha - \epsilon_\gamma) - (\epsilon_\alpha - \epsilon_\beta)\right)^{-1} - (\epsilon_\alpha - \epsilon_\gamma)^{-1}}{\epsilon_\alpha - \epsilon_\beta} \tag{B.7}$$

since P-space is degenerate, we should take the limit of $\epsilon_\beta \to \epsilon_\alpha$ and obtain

$$= \frac{d}{d\omega}\left(\frac{V_{\beta\gamma}V_{\gamma\delta}}{\omega - \epsilon_\gamma}\right)_{\omega=\alpha} \times V_{\alpha\beta} \tag{B.8}$$

In the general case, the folded diagram including of the $\hat{Q}$-box is calculated as the derivative of $\hat{Q}$-box with respect to energy parameter.

Using the expression of $\hat{Q}$-box,

$$H_{\text{eff}} = \hat{Q} - \hat{Q}\int\hat{Q} + \hat{Q}\int\hat{Q}\int\hat{Q} - \cdots. \tag{B.9}$$

Knowing the fact that the $\hat{Q}$-box can be written as follows,

$$\hat{Q}(\omega)_{\alpha\beta} = V_{\alpha\beta} + \sum_i \frac{V_{\alpha i}V_{i\beta}}{\omega - \epsilon_i} + \sum_{ij}\frac{V_{\alpha i}V_{ij}V_{j\beta}}{(\omega - \epsilon_i)(\omega - \epsilon_j)} + \cdots \tag{B.10}$$

it is straight-forward to prove that the folded diagram can be calculated by derivatives with respect to ω. After all, we reached the expression to calculate the effective interaction V_{eff} in the iterative formula,

$$V_{\text{eff}}^{(n)} = \hat{Q} + \sum_{m=1}^{\infty}\frac{1}{m!}\frac{d^m\hat{Q}}{dE_0^m}\{V_{\text{eff}}^{(n-1)}\}^m. \tag{B.11}$$

B.3   Linked Cluster Theory in Extended Kuo-Krenciglowa method

With the knowledge of Secs. B.1 and B.2, we summarize the folded-diagram method in EKK method here in this section. As a consequence, what we need to evaluate is only valence-linked irreducible diagrams and its derivatives for folded diagrams, as we claimed in Chap. 3.

First, we briefly repeat the proof of the factorization theorem in EKK method. The naive application of the factorization theorem to the diagrams appearing in the diagrams of EKK method fails, because the total energy denominator of the diagram consist of disconnected pieces is not equal to the sum of the denominators of the individual pieces, when we have the states within P-space. This problem is cured by the rewritten of the Hamiltonian of EKK method as follows:

$$\begin{aligned}
H &= H_0 + V \\
&= H_0' + V' \\
&= H_0' - P(E - H_0)P + V \\
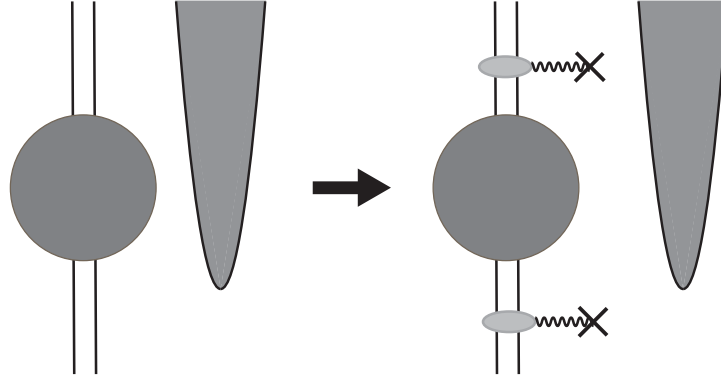&= H_0' + V_1 + V, \tag{B.12}
\end{aligned}$$

Figure B.4: Example of factorization theorem in EKK method.

where $V_1 = -P(E - H_0)P$ defined purely in P-space is to be regarded as another perturbation. As far as we include the contribution up to all order in perturbation, we can freely change the order of the interaction V and V_1, without changing the final result. Therefore, only before we prove the factorization theorem, we change the order as follows: whenever we find a line consist of two particles both in valence space, we insert the V_1 interaction up to infinite order. Then, the states are changed to

$$
\begin{aligned}
P e^{i V_1 t} P |\psi_i(t)\rangle &= P e^{i(E - H_0)t} P |\psi_i(t)\rangle \\
&= e^{-i H_0 t} |\psi_i\rangle \\
&= e^{-i(\epsilon_a + \epsilon_b)t} |\psi_i\rangle .
\end{aligned}
\tag{B.13}
$$

The wavy lines and the crosses represent the insertion of V_1 in Fig. B.4. After the insertion, the energy denominators for the states is calculated by the summations of single-particle energies. With this insertion of V_1 potential, we can apply the factorization theorem in exactly the same as Sec. B.1. Once we can factorize and cancel out the divergences, we obtain the relation of Eq. 2.85. After obtaining this equation, we can evaluate the diagrams as in the usual manner of EKK method without the insertion of V_1 interaction any more. Then we have achieved Eq. 3.14.

Next, we demonstrated that the folded diagrams can be calculated via the derivatives of the $\hat{Q}$-box. In Sec. B.2 we saw that the folded diagrams can be evaluated by the energy derivatives, using the minimal example. We used the fact that the model space is degenerate in Eq. B.7. In our case of EKK method, on the other hand, regarding that the states α, β and γ are two-body states and α and β are in the P-space, we obtain $\epsilon_\alpha = \epsilon_\beta = E$. Therefore, we can calculate the folded diagrams can be obtained by the derivatives with respect to E. One should note that this holds because we already factorize out the disconnected pieces, as we discussed above. With the presence of extra particles and holes states, the states no longer included in P-space.

Then we finally achieved our equation to derive the effective interaction for the shell model studies,

$$
\tilde{H}_{\text{eff}} = \tilde{H}_{\text{BH}}(E) + \frac{d\hat{Q}(E)}{dE} \tilde{H}_{\text{eff}} + \frac{1}{2!} \frac{d^2 \hat{Q}(E)}{dE^2} \{\tilde{H}_{\text{eff}}\}^2 + \cdots .
\tag{B.14}
$$

Bibliography

[1] K. Takayanagi: Nucl. Phys. A **852** (1), 61 (2011).

[2] K. Takayanagi: Nucl. Phys. A **864** (1), 91 (2011).

[3] M. Mayer: Phys. Rev. **78** (1), 16 (1950).

[4] M. Mayer: Phys. Rev. **78** (1), 22 (1950).

[5] M. Mayer: Nobel lecture (1963).

[6] L. Talmi and I. Unna: Annu. Rev. Nucl. Sci. **10** (1), 353 (1960).

[7] J. McCullen, B. Bayman and L. Zamick: Phys. Rev. **134** (3B), B515 (1964).

[8] T. T. S. Kuo and G. E. Brown: Nucl. Phys. **85** (1), 40 (1966).

[9] K. Brueckner, J. Gammel and H. Weitzner: Phys. Rev. **110** (2), 431 (1958).

[10] T. T. S. Kuo, S. Y. Lee and K. F. Ratcliff: Nucl. Phys. A **176** (1), 65 (1971).

[11] T. Kuo and E. Osnes: Lecture Notes in Physics **364**, 1 (1990).

[12] B. H. Wildenthal: Prog. Part. Nucl. Phys. **11**, 5 (1984).

[13] B. A. Brown, W. A. Richter, R. E. Julies and B. H. Wildenthal: Annals of Physics **182** (2), 191 (1988).

[14] B. Brown and W. Richter: Phys. Rev. C **72** (5), 057301 (2005).

[15] B. A. Brown and W. A. Richter: Phys. Rev. C **74** (3), 034315 (2006).

[16] M. Honma, T. Otsuka, B. A. Brown and T. Mizusaki: Phys. Rev. C **65** (6), 061301 (2002).

[17] A. Poves and A. Zuker: Phys. Rep. **70** (4), 235 (1981).

[18] A. Poves, J. Sánchez-Solano, E. Caurier and F. Nowacki: Nucl. Phys. A **694** (1-2), 157 (2001).

[19] Y. Utsuno, T. Otsuka, T. Glasmacher, T. Mizusaki and M. Honma: Phys. Rev. C **70** (4), 044307 (2004).

[20] P. Navratil, S. Quaglioni, I. Stetcu and B. R. Barrett: J. Phys. G **36** (8), 083101 (2009).

[21] B. R. Barrett, P. Navratil and J. P. Vary: Prog. Part. Nucl. Phys. **69**, 131 (2013).

[22] E. D. Jurgenson, P. Maris, R. J. Furnstahl, P. Navratil, W. E. Ormand et al.: Phys. Rev. C **87** (5), 054312 (2013).

[23] B. H. BRANDOW: Rev. Mod. Phys. **39** (4), 771 (1967).

[24] P. J. Ellis and E. Osnes: Rev. Mod. Phys. **49** (4), 777 (1977).

[25] D. J. Klein: The Journal of chemical physics **61** (3), 786 (1974).

[26] T. H. Schucan and H. A. Weidenmüller: Annals of Physics **73** (1), 108 (1972).

[27] P. A. Schaefer: Annals of Physics **87** (2), 375 (1974).

[28] K. Suzuki: Prog. Theor. Phys. **68**, 1999 (1982).

[29] M. Hjorth-Jensen, T. T. S. Kuo and E. Osnes: Phys. Rep. **261** (3-4), 125 (1995).

[30] E. M. Krenciglowa and T. T. S. Kuo: Nucl. Phys. A **235** (1), 171 (1974).

[31] K. Suzuki and S. Y. Lee: Prog. Theor. Phys. **64** (6), 2091 (1980).

[32] N. Tsunoda, K. Takayanagi, M. Hjorth-Jensen and T. Otsuka: Phys. Rev. C accepted (2014).

[33] H. Yukawa: Proc.Phys.Math.Soc.Jap. **17**, 48 (1935).

[34] M. Taketani, S. Nakamura and M. Sasaki: Prog. Theor. Phys. **6** (4), 581 (1951).

[35] R. B. Wiringa and S. C. Pieper: Phys. Rev. Lett. **89** (18), 182501 (2002).

[36] R. B. Wiringa, V. G. J. Stoks and R. Schiavilla: Phys. Rev. C **51** (1), 38 (1995).

[37] M. C. Birse, J. A. McGovern and K. G. Richardson: Phys. Lett. B **464** (3-4), 169 (1999).

[38] S. K. Bogner, T. T. S. Kuo and A. Schwenk: Phys. Rep. **386** (1), 1 (2003).

[39] S. K. Bogner, T. T. S. Kuo, A. Schwenk, D. R. Entem and R. Machleidt: Phys. Lett. B **576** (3-4), 265 (2003).

[40] S. Bogner, T. T. S. Kuo, L. Coraggio, A. Covello and N. Itaco: Phys. Rev. C **65** (5), 051301 (2002).

[41] F. Andreozzi: Phys. Rev. C **54** (2), 684 (1996).

[42] A. Nogga, S. K. Bogner and A. Schwenk: Phys. Rev. C **70** (6), 061002 (2004).

[43] D. R. Entem and R. Machleidt: Phys. Rev. C **68** (4), 041001 (2003).

[44] R. Machleidt and D. R. Entem: Phys. Rep. **503** (1), 1 (2011).

[45] T. Otsuka, T. Suzuki, J. D. Holt, A. Schwenk and Y. Akaishi: Phys. Rev. Lett. **105** (3), 032501 (2010).

[46] J. D. Holt, T. Otsuka, A. Schwenk and T. Suzuki: arXiv (2010). 1009.5984v2.

[47] T. Otsuka and T. Suzuki: Few-Body Syst. **54** (7-10), 891 (2013).

[48] G. Hagen, M. Hjorth-Jensen, G. R. Jansen, R. Machleidt and T. Papenbrock: Phys. Rev. Lett. **108** (24), 242501 (2012).

[49] G. Hagen, M. Hjorth-Jensen, G. R. Jansen, R. Machleidt and T. Papenbrock: Phys. Rev. Lett. **109** (3), 032502 (2012).

[50] B. A. Brown and B. H. Wildenthal: Annu. Rev. Nucl. Part. Sci. **38** (1), 29 (1988).

[51] Y. Utsuno, T. Otsuka, T. Mizusaki and M. Honma: Phys. Rev. C **60** (5), 054315 (1999).

[52] T. Otsuka, T. Suzuki, R. Fujimoto, H. Grawe and Y. Akaishi: Phys. Rev. Lett. **95** (23), 232502 (2005).

[53] T. Otsuka, T. Suzuki, M. Honma, Y. Utsuno, N. Tsunoda et al.: Phys. Rev. Lett. **104** (1), 012501 (2010).

[54] N. Tsunoda, T. Otsuka, K. Tsukiyama and M. Hjorth-Jensen: Phys. Rev. C **84** (4), 044322 (2011).

[55] J. D. Holt, T. Otsuka, A. Schwenk and T. Suzuki: J. Phys. G **39** (8), 085111 (2012).

[56] J. D. Holt, J. Menéndez and A. Schwenk: Eur. Phys. J. A **49** (3), 39 (2013).

[57] N. Shimizu: arXiv (2013). 1310.5431.